Master´s thesis

NTNU
Norwegian University of
Science and Technology
Faculty of Engineering, Scieme and Technology
Department of Marine Technology

Stefan Hjønnevåg Karlsen

Barge transportation of heavy objects

Trondheim, 14th of June, 2010

NTNU
Norwegian University of
Science and Technology

1 Preface

This M.Sc. thesis has been produced at Department of Marine Technology, NTNU in the period from February 4th to June 14th, 2010.

The subject of the project was proposed by Aker Solutions after I worked there as a summer intern the summer of 2009. I found the subject interesting and relevant for learning more about hydrodynamics, statistics and calculation methods used in marine operations.

At first, the plan was to use only SESAM Software, Genie and HydroD for modelling and hydrodynamics and Postresp for postprocessing. However, it turned out that Postresp could not produce the final design accelerations, only its components. Thus, further processing was performed in Matlab to avoid time-consuming manual calculations. This proved an advantage with respect to workload as there were many cases to be analysed and it proved a more flexible tool for representing results.

Introducing viscous roll damping required that a large amount of data had to be processed and combined, thus this would probably not have been possible without Matlab. The creation of the Matlab code however, and some numerical problems with the viscous roll damping in WADAM, delayed the work and thus viscous roll damping was only included for one case.

In the theoretical review, the subjects that I already had a good insight in were less emphasized as opposed to the newer areas i.e. source technique and understanding the software.

I would like to thank Professors Dag Myrhaug, Bernt J. Leira and Asle Natskår at NTNU and Eirik Engevik and Gunnar Gjerde at Aker Solutions for guidance.

Kristiansand, June 12th 2010

Stefan Hjønnevåg Karlsen

2 Index

Figure list

Table list

3 Nomenclature

(x, y, z)	Orthogonal axes in the Cartesian coordinate system
ϕ	Fluid velocity potential
ϕ_I, ϕ_D, ϕ_R	Incident-, Diffraction- and Radiation velocity potentials
$\vec{V}$ = [u, v, w]	Fluid velocity vector
$\vec{a}$	Fluid acceleration vector
t	Time variable
$\left(\vec{i}, \vec{j}, \vec{k}\right)$	Unit vectors along (x, y, z)
p	Pressure variable
p_a	Atmospheric pressure
ρ	Water density
g	Gravity constant
ω	circular frequency
$\vec{n}$	Unit normal vector
S_B	Wetted body surface
ζ	Free-surface elevation
ζ_a	Free-surface elevation amplitude
$\vec{V}_s$	Local velocity of wetted surface
h	Water depth
ε_j	Phase angle of *j*th wave component
A_j	Wave amplitude of *j*th wave component
k_j	Wave number of *j*th wave component
$S(\omega)$	Wave spectrum
E	Wave energy per square meter
$f(\theta)$	Wave spreading function
θ	Wave spreading angle
Q	Source strength
r	radial distance
dS	Surface element
$FR(\omega)$	Complex Frequency-Response function
$H(\omega)$	Hydrodynamic transfer function (RAO)
q	Source density
$\overline{q}$	Normalised source density
$\overline{\phi}$	Normalised velocity potential
ξ,η,ζ	Coordinates on the body surface (source technique)
s	integration variable along the body surface
S	Body surface
n_3	Vertical normal vector component
η_i	Motion in mode *i*
$\dot{\eta}_i$	Velocity in mode *i*
$\ddot{\eta}_i$	Acceleration in mode *i*
$\eta_{i,a}$	Motion amplitude in mode *i*
G	Green function
J_0	Bessel function of first kind and 0^{th} order

Y_0	Bessel function of second kind and 0^{th} order
K_0	Modified Bessel function of 0^{th} order
i	Complex unit
A	Added mass(inertia) matrix
B	Damping matrix
C	Restoring matrix
F_j	Complex amplitude of exciting force/moment in mode *j*
F_i^{ex}	Excitation force in mode *i*
F_i^D	Diffraction force in mode *i*
F_i^{FK}	Froude-Kriloff force in mode *i*
ϕ_0	Complex incident wave potential
ϕ_7	Complex diffraction wave potential
ϕ_k	Complex radiation potential
M	Mass
I	Inertia moment
dV	Volume element
ξ	Damping ratio
ω_n	Natural circular frequency
F_{VD}	Viscous damping force
B_{44}^*	Linearised viscous damping coefficient
s	Vertical motion of a point
a	Vertical acceleration of a point
F^R	Restoring force/moment
$\overline{GM_L}$	Longitudinal metacentric height
GZ_L	Longitudinal righting arm
$\overline{GM_T}$	Transverse metacentric height
GZ_i	Initial (linear) righting arm
f	Factor for linearization of roll restoring
Δ	Mass displacement
∇	Volume displacement
ω_P	Peak frequency
T_p	Peak period
T_z	Mean zero-crossing period
U	Wind velocity
X	Wind fetch
A, B	Constants in the Pierson-Moskowitz wave spectrum
α, σ	JONSWAP parameters
γ	JONSWAP peakedness parameter
H_s	Significant wave height
X_s	Significant response
m_n	wave spectral moment of n^{th} order
m_n^x	Spectral moment of n^{th} order for response x
S_x	Response spectrum for response x
σ_x	Standard deviation of response x
T_{m02}	Wave zero-crossing period approximated from wave spectrum

ω_{m02}	Wave zero-crossing frequency approximated from wave spectrum
F_s	Rice cumulative distribution function
Φ	Cumulative probability function for normal distribution
P	Probability
Lpp	Length between perpendiculars
B	Beam
D	Depth/height
d	draught

Abbreviations

COG – Center of gravity
COB – Center of buoyancy
LCF – Longitudinal flotation centre
GM – Distance from centre of gravity to metacentre
RAO – Response Amplitude Operator
STR – Short Term Response
STS – Short Term Statistics
VRD – Viscous Roll Damping

4 Summary

The topic for this master thesis is transportation of heavy platform modules on barges. The goal is to find the short-term extreme accelerations, or design accelerations, that are limiting for the feasibility of the transportation operation. Motion response analyses have been performed for six different combinations of barges and module weights as follows:

Barge	Module
300 feet	1000 tonnes
300 feet	3000 tonnes
400 feet	1000 tonnes
400 feet	5000 tonnes
600 feet	5000 tonnes
600 feet	8000 tonnes

It has been observed that the roll acceleration is overestimated in non-viscous motion analyses of barge type vessels. Thus for the first case an additional analysis including viscous roll damping has been performed.

The software used to perform the analyses and the theory used has been reviewed. The following programs are described:

- Genie – modelling of the barge (hull, ballast tanks)
- HydroD (WADAM) – modelling of environment, hydrodynamic analysis by source technique
- Postresp – combination and printing of motion characteristics
- Matlab – statistical postprocessing, calculation of design accelerations

The founding theories are linear potential wave theory and source technique. The viscous roll damping, which in reality is non-linear, was estimated in a linearised form using strip theory and empirical data. Based on the calculated motion characteristics, the design accelerations are estimated by short-term statistics, meaning the extreme accelerations are estimated in 3 hour seastates. This was performed for four different significant wave heights and all relevant wave periods.

The accelerations are calculated in the system centre of gravity, module centre of gravity and top and bottom corners of the module. The limiting criterion of a barge transportation is normally the forces the seafastening can withstand, thus the acceleration on the seafastening has been examined closer. Aker Solutions have roughly defined the seafastening capacity by setting absolute limits for the accelerations in the longitudinal, transverse and vertical direction.

Compared to the criteria for accelerations given by Aker Solutions, the results proved that the acceleration in the transverse direction is the limiting factor. Beam seas close to the roll eigenperiod gave the highest accelerations on the seafastening both in the transverse and vertical direction, suggesting that these accelerations are governed by the roll motion. When viscous roll damping was included, there was a significant reduction in the transverse acceleration, and a slightly smaller reduction in the vertical acceleration on the seafastening compared to the non-viscous case. However, the transverse acceleration was still the most

critical with respect to the given criteria. There was little or no effect of viscous roll damping on longitudinal design accelerations.

Design accelerations for a 1000 tonne module were found for two different barges, a 300 feet barge and a 400 feet barge. The accelerations proved significantly smaller on the 400 feet barge, especially in the transverse direction. A 5000 tonne module was also tested on two different barges, a 400 feet barge and a 600 feet barge. As in the preceding comparison, the accelerations were significantly larger on the smaller barge. Thus, for a given load, switching to a larger barge can give a large reduction in the acceleration.

There are indications that the results achieved are conservative, including the case with viscous roll damping. However, this is only an indication. The viscous roll damping is difficult to estimate correctly and therefore a suggestion could be to investigate the validity of the viscous roll damping model through model tests.

A certain reduction in the roll acceleration was observed when the load was increased for the 300 feet barge, without giving an increase in the roll angle extremes. This indicates that for some cases a decrease in the metacentric height can, provided that the stability is sufficient, contribute to a decrease in the roll acceleration without increasing the extreme roll angle.

In high sea states, non-linear effects can become significant. The resulting effect on roll acceleration is unknown. Hence, it could be advantageous to investigate the extent of these effects using a non-linear calculation model.

5 Introduction

Both with respect to installation and decommissioning of topside installations, barge transport of heavy objects, such as platform modules, is an important part. The problem of this M.Sc. thesis is to find the short-term design accelerations, i.e. on the seafastening, for a selection of barges, stretching from 300 feet to 600 feet length, transporting platform modules reaching from 1000 tonnes to 8000 tonnes. The goal is to find the short-term extreme accelerations, and thus the design forces on the seafastening. Hence, the limiting seastate for a transportation operation can be found.

In addition, design accelerations for a given module placed on different barges are to be compared and one of the cases is to be analysed including viscous roll damping.

The software used in the hydrodynamic and statistic analyses will be described, and the theory used will be reviewed.

Thus, the scope for the present work include

- A general description of the software applied
- An outline of the theory used by the programs for establishing and solving the equation of motion and finding extreme responses from short-term statistics
- Non-viscous motion response analyses for six cases
- Motion response analysis for one case including viscous roll damping
- Comparison of responses for a given module placed on different barges
- Comparison of responses with and without viscous roll damping

The numerical methods used by the computer programs can be very complex, thus the main focus will be on the founding hydrodynamic and statistical theory.

The absolute design accelerations for a transport depend on the loading condition. For future similar motion response analyses, the loading conditions will probably differ. Still, this work can present an approximation of the expected design accelerations, and the relative variation in response due to change in load or barge size.

6 Theoretical review

6.1 Response analysis software

In the present section follows a general description of the software used in this work. For more details about the tasks performed by each programme and the connection between them, see section 8.

6.1.1 Genie

Genie is a platform tool for structural analysis and design of offshore and maritime structures made of beams and plates. Modelling, analysis and results processing are performed in the same graphical user interface. Hydrodynamic analysis, strength calculations and evaluation of results can be done within Genie for fixed structures.

Genie can perform static and dynamic linear analysis for structures subjected to wave, wind, current and the equipment layout. It is also possible to include the effects from non-linear pile/soil behaviour.

The wind and wave loads create input to fatigue assessments that can be based on a deterministic or stochastic approach. The analyses may also be performed based on user defined source concentration factors from local analysis. It is also possible to perform progressive collapse analysis considering the effect of residual strength in the structure.

Genie can be used to produce the panel model and the structural model that are input in HydroD for hydrodynamic analysis. For the panel model, this includes creating the geometry of the structure as well as creating the panel mesh and assigning hydro pressure. The structural model is in principle the same as the panel model but it includes tank walls with defined specific hydro pressure on the surfaces of each tank.

6.1.2 HydroD(Wadam)

HydroD is a platform combining the different SESAM programs for hydrostatic/stability analysis and hydrodynamic analysis. Earlier, there were one pre-processor for each program, but with HydroD one can perform the pre-processing interactively and then run the relevant program through HydroD.

The possible applications are stability and hydrodynamic response of floating structures and loads on fixed structures. Using the loads calculated one can transfer these to a structural model and perform structural analyses with respect to strength or fatigue. To determine the floating position, trim and draught, one can use the actual mass and buoyancy or one can define the desired floating position and then automatically fill compartments to achieve that floating condition.

The hydrodynamic analysis may be performed using the actual floating position and independent of the panel model to determine worst loading conditions to be used in structural strength analysis. These analyses are normally performed in the frequency domain, but it is also possible to do it in time domain (Linear as well as non-linear).

The loads (pressure and accelerations) can be automatically transferred to a structural analysis. The response and loads may be represented graphically in animations.

For a vessel with forward speed, a module called WASIM is used. For a vessel without forward speed, the relevant program executed by HydroD will be WADAM.

In this case, forward speed will be neglected. Thus WADAM, which stands for "Wave Analysis by Diffraction And Morison theory", will be used. This program uses potential Airy wave theory (see section 6.2) and sink-source technique (see section 0) to describe the fluid motion and pressure. Second order-, sum- and difference frequency forces can be included if desired. From this the resulting forces on a floating body of arbitrary shape are calculated.

For large-volume bodies (or body parts), radiation-diffraction theory is employed since it gives a good prediction of mass forces, which are dominating. For slender bodies the Morison equation in linearised form is used due to the large importance of viscous terms. These two methods can be combined in a dual model where Wadam selects the most appropriate method depending on the body dimension (diameter) compared to the wavelength. For the vessels analysed in this case and in the thesis however, only radiation-diffraction theory will be used.

WADAM is based on linear methods for marine hydrodynamics and uses 3-D radiation-diffraction theory developed at the Massachusetts Institute of Technology. The required input for WADAM is a panel model, mass/buyoancy data and environmental data. If a structural analysis is to be performed or ballast tanks are to be included, a structural model is also required. This input data can be produced in the pre-processors Prefem and Prewad, or it can be modelled in HydroD. In this work, the panel model and the structural model for each barge are produced in Genie.

6.1.3 Postresp

Postresp is a graphical postprocessor for statistical processing and presentation of response in frequency and time domain.

Given the transfer functions of a vessel, the program can do statistical processing of general response from short term statistics of one sea state to long-term response statistics. The transfer functions are normally produced by a hydrodynamic program as i.e. WADAM.

The features in Postresp vary from displaying transfer functions and response spectra, through short term statistics, e.g.:

- standard deviation and mean zero-upcrossing period
- significant/expected values
- probability of exceedance and extremes of long term statistics
- fatigue
- extremes
- workability

The following features are available in the frequency domain

- Any transfer function – wave loads and global response taken from a hydrodynamic analysis, and stresses/forces taken from a structural analysis – may be processed statistically

- User defined transfer functions may be entered and processed
- Forward speed/doppler shift is handled
- Response variables (transfer functions) may be combined

The initial purpose with Postresp in this work was to perform the full postprocessing of the barge motions. However, due to limitations in calculation and the inclusion of viscous roll damping, Postresp was only used to create the point acceleration transfer functions and print them to a file.

6.1.4 Matlab

Short for Matrix Laboratory, Matlab is a technical computing environment for high-performance numeric computation and visualization. It is based on C++ programming code, but it is easier to use. It integrates numerical analysis, matrix computation, signal processing, and graphics in an easy-to-use environment where problems and solutions are expressed just as they are written mathematically, without traditional programming. Typical uses include general-purpose numeric computation, algorithm prototyping, and special-purpose problem solving with matrix formulations that arise in disciplines such as linear algebra, structural analysis, statistics, and digital signal processing.

In the present work, a Matlab code has been produced to create the wave spectra, read the RAO files printed by Postresp, calculate short-term response and short-term statistics and combine the extreme values to find the design accelerations (see Figure 8-1).

6.2 Potential wave theory

Wave potential theory is the basis for calculating wave loads on structures and structure motion in fluid. Realistic fluid behaviour is very hard to calculate exactly, thus by idealising the fluid we can perform calculations which produce good results.

Using potential theory we can describe the entire fluid with a velocity potential, ϕ. From the velocity potential we can find:

- Velocity of fluid
- Acceleration of fluid
- Pressure in the fluid through Bernoulli's equation
- Surface elevation, ζ

To be able to use potential theory we need to assume the following

- Incompressible fluid (ρ = constant)
- Inviscid fluid
- Irrotational flow

These are in some cases rough approximations i.e. with respect to finding forces on slender structures, roll damping, slamming pressure etc., where viscous terms, vortex shedding or compressibility have a significant effect. However, some of these effects can be taken into account by adding viscous terms which can be found through the velocity potential.

The assumption of incompressible and irrotational fluid yields that the velocity potential must satisfy the Laplace equation

$$\nabla \cdot \vec{V} = \frac{\partial^2 \phi}{\partial x^2} + \frac{\partial^2 \phi}{\partial y^2} + \frac{\partial^2 \phi}{\partial z^2} = 0 \qquad (7.5)$$

For a floating oscillating body this is one of several conditions the velocity potential must satisfy. These conditions are shown in Figure 6-1.

The reason for this is that the velocity potential is defined so that it describes the fluid velocity:

$$\bar{V} = \nabla \phi = \vec{i}\,\frac{\partial \phi}{\partial x} + \vec{j}\,\frac{\partial \phi}{\partial y} + \vec{k}\,\frac{\partial \phi}{\partial z} = [u,\, v,\, w] \qquad (7.1)$$

Where i, j and k are unit vectors in x-, y- and z-directions respectively. The acceleration can then be found by time derivation

$$\bar{a} = \frac{\partial}{\partial t}(\nabla \phi) \qquad (7.2)$$

The Bernoulli equation finds the pressure as follows

$$p = -\rho\left(\frac{\partial \phi}{\partial t} + \frac{1}{2}\left|\vec{V}\right|^2 + gz\right) + p_a \qquad (7.3)$$

Where ρ is water density, g is the gravity constant and p_a is the atmospheric pressure. The atmospheric pressure is neglected as we are interested in relative pressure. $\rho\frac{\partial \phi}{\partial t}$ describes the dynamic pressure (normally due to wave motion), ρgz is the hydrostatic pressure and $\rho\frac{1}{2}\left|\vec{V}\right|^2$ is the velocity pressure.

Using the linearised Bernoulli, we remove the higher order terms, meaning we keep only terms proportional to the wave amplitude of first order. Thus we can find the pressure as

$$p = -\rho\frac{\partial \phi}{\partial t} - \rho g z \qquad (7.4)$$

6.2.1 Boundary conditions

As mentioned, knowing the pressure distribution in the fluid we can find the forces on floating and fixed ocean structures. However, to achieve a velocity potential that describes the

fluid correctly we need to implement some physical boundary conditions. These will be explained in this chapter.

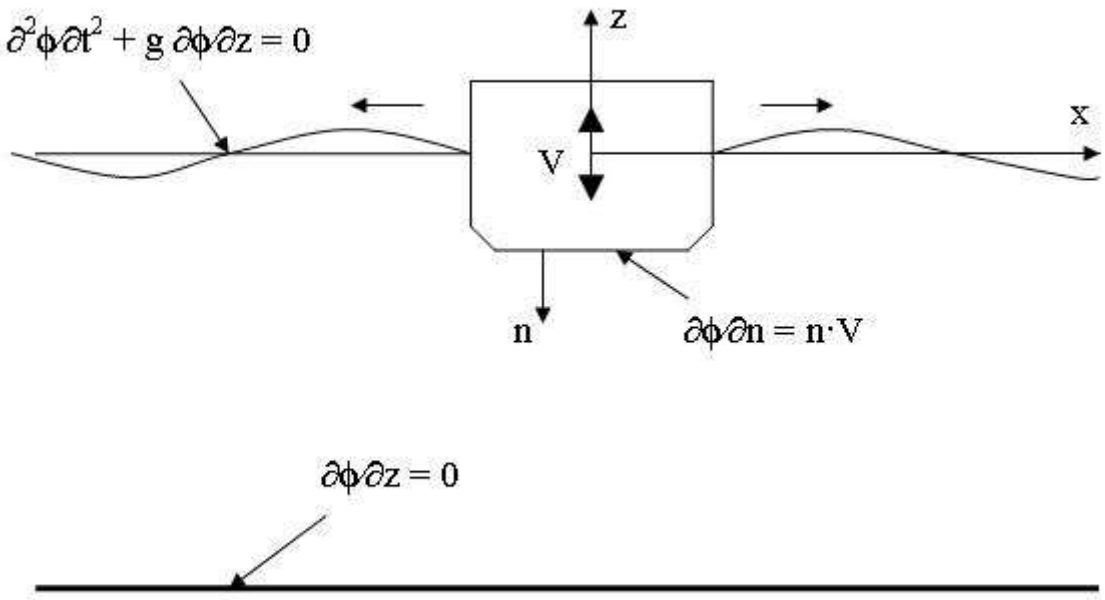

Figure 6-1: Boundary conditions for floating body with potential theory

6.2.1.1 Free-surface conditions

On the free surface there are two boundary conditions, the dynamic boundary condition and the kinematic boundary condition. The dynamic boundary condition is found from Bernoulli's linearised equation using that the pressure on the free-surface must be equal to the atmospheric pressure, or that relative pressure is equal to zero. Using the linear assumption of small wave amplitudes we can write

$$-\rho\frac{\partial\phi}{\partial t}-\rho g\zeta=0$$

$$\rightarrow g\zeta+\frac{\partial\phi}{\partial t}=0,\quad on\quad z=0 \qquad (7.6)$$

A fluid particle on the free-surface will remain on the free-surface. From this condition we can derive the kinematic boundary condition using the substantial derivative of a function *F*

$$\frac{DF}{Dt}=\frac{\partial F}{\partial t}+\vec{V}\cdot\nabla F \qquad (7.7)$$

We can describe the surface elevation as

$$z=\zeta(x,y,t)$$

And define the function

$$F(x,y,z,t) = z - \zeta(x,y,t) = 0 \qquad (7.8)$$

By removing higher order terms and approximating the free surface to z = 0 we can write

$$\frac{\partial \zeta}{\partial t} = \frac{\partial \phi}{\partial z} \quad on \;\; z = 0 \qquad (7.9)$$

By combining the kinematic boundary condition with the dynamic boundary condition we can write

$$\frac{\partial^2 \phi}{\partial t^2} + g\frac{\partial \phi}{\partial z} = 0 \quad on \;\; z = 0 \qquad (6.10)$$

If the velocity potential is oscillating harmonically with a frequency ω, we can write

$$-\omega^2 \phi + g\frac{\partial \phi}{\partial z} = 0 \quad on \;\; z = 0 \qquad (6.11)$$

6.2.1.2 Body boundary condition

Another condition is that we can have no fluid motion through the body surface. This yields the kinematic body boundary condition

$$\frac{\partial \phi}{\partial n} = \vec{n} \cdot \vec{V}_s \quad on \;\; S_B \qquad (6.12)$$

Where $\vec{n}$ is the normal vector of the body surface pointing into the fluid and $\vec{V}_s$ is the local velocity of the body surface. If the body is assumed to have no motion then the condition becomes

$$\frac{\partial \phi}{\partial n} = 0 \quad on \;\; S_B \qquad (6.13)$$

6.2.1.3 Sea bottom boundary condition

As there can be no fluid motion through the seabed, which is assumed horizontal at a depth h, the sea bottom condition becomes

$$\left.\frac{\partial \phi}{\partial z}\right|_{z=-h} = 0 \qquad (6.14)$$

6.2.2 Linear wave potential theory

Linear wave theory assumes low waves and denotes that only terms proportional to the wave amplitude ζ_a are included. This means i.e. that the Bernoulli equation and boundary conditions can be simplified as explained previously. The basic assumptions are

- Wave amplitudes are small
- Floating body oscillations are small

Because the wave amplitude is small it is not unreasonable to neglect terms proportional to the wave amplitude of higher order. As the body oscillations are small, we can calculate the forces on the body in the mean position instead of in the actual position. The free-surface conditions are set to apply on $z = 0$ instead of $z = \zeta$.

6.2.2.1 Regular first order wave loads

Regular waves are waves with only one amplitude and frequency. Using the first order (linear) wave potential with linearised Bernoulli and boundary conditions we can divide the problem into two subproblems as shown in Figure 6-2.

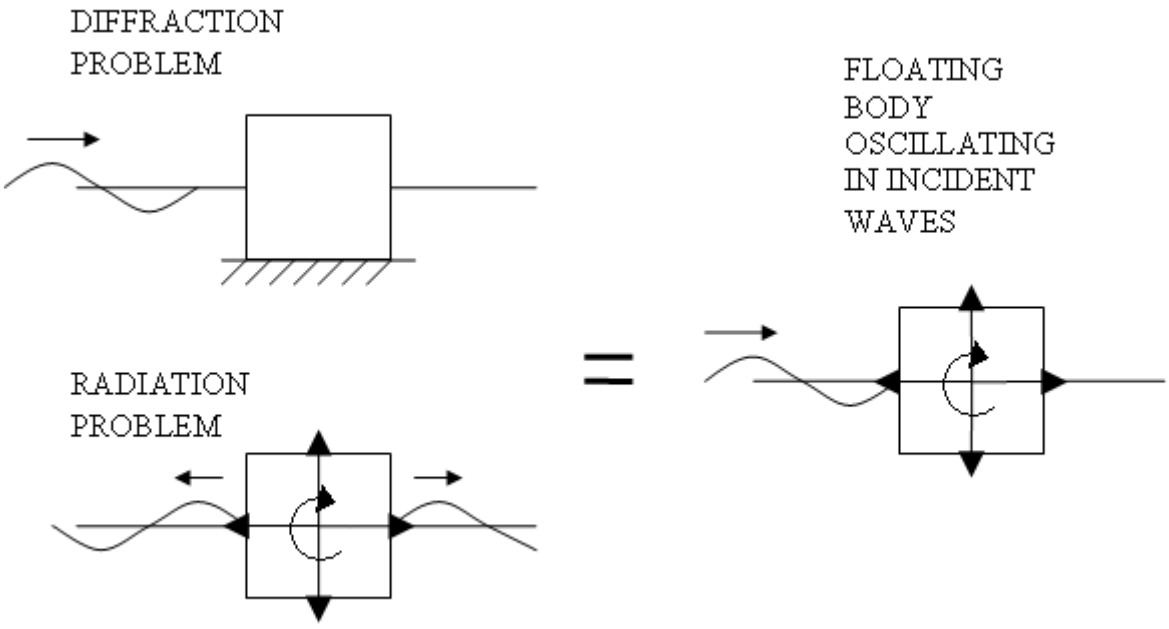

Figure 6-2: Superposition of floating body subproblems

In the diffraction problem the body is assumed to be in incident regular waves and constrained from oscillating. From this problem we can find the wave excitation loads. The excitation forces and moments are found from two contributions

- Froude-Kriloff load
- Diffraction load

The Froude-Kriloff load is derived from the pressure of the wave field with no body present. The diffraction load is the change in load due to the structure's effect on the fluid. The structures presence will change the fluid pressure field.

In the radiation problem there are no incident waves and the body is forced to oscillate with the wave excitation frequency. In the mode of oscillation, added mass, damping and restoring terms are found. These terms will be explained further in chapter 0. As a consequence of the superposition of subproblems we can write the total fluid potential as

$$\phi = \phi_I + \phi_D + \phi_R \qquad (6.15)$$

Where ϕ_I is the incident wave potential, ϕ_D is the diffraction potential and ϕ_R is the radiation potential.

In reality, higher order terms of the wave amplitude up to 5th order have been proven to have an effect in several cases, but the magnitude decreases rapidly with increasing order. Potentials of higher order than 2nd are rarely used. For a motion response analysis of a floating vessel, linear theory is normally considered sufficient, while 2nd order theory is necessary to include mean and slowly varying drift forces from the waves. However, in some cases, especially for high sea states, 2nd order theory or Stoke's wave theory is used in calculating dynamic response of vessels, but this will not be treated here. The higher order wave will appear more realistic with a higher crest and a shallower trough.

6.2.3 Irregular waves

6.2.3.1 Long crested waves

In reality, waves are not regular and consisting of one amplitude and frequency, but can be considered a superposition of many waves of different frequency and amplitude as seen in Figure 6-3 from "Kompendium I Marin Teknikk 3, Hydrodynamikk". The resulting surface elevation can be expressed as follows for an irregular wave propagating in the positive x-direction

$$\zeta = \sum_{j=1}^{N} A_j \sin(\omega_j t - k_j x + \varepsilon_j) \qquad (6.16)$$

per square meter and wave amplitude Where A_j, ω_j, k_j and ε_j are respectively the wave amplitude, circular frequency, wave number and random phase angle of wave component number j. The wave is assumed long-crested, meaning all the waves are in the same direction.

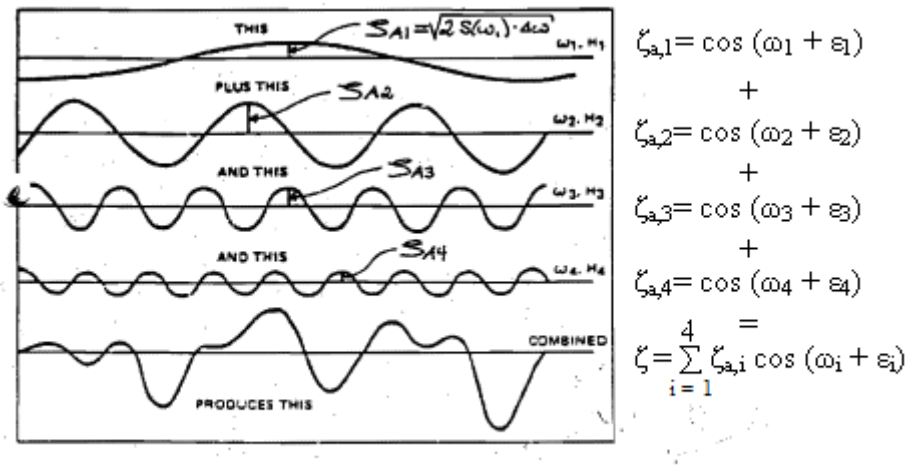

Figure 6-3: Superposition of regular waves

An irregular wave can be represented by a wave spectrum showing the energy density as a function of wave frequency. Using the relation between wave energy

$$\frac{E}{\rho g} = \sum_{j=1}^{N} \frac{1}{2} A_j^2 \qquad (6.17)$$

The wave spectrum (wave energy distribution) can be described as follows

$$\frac{1}{2} A_j^2 = S\left(\omega_j\right) \Delta\omega \qquad (6.18)$$

Where $S\left(\omega_j\right)$ is the wave spectrum value at the circular frequency j. This means the total area under the wave spectrum curve is the total wave energy per square meter.

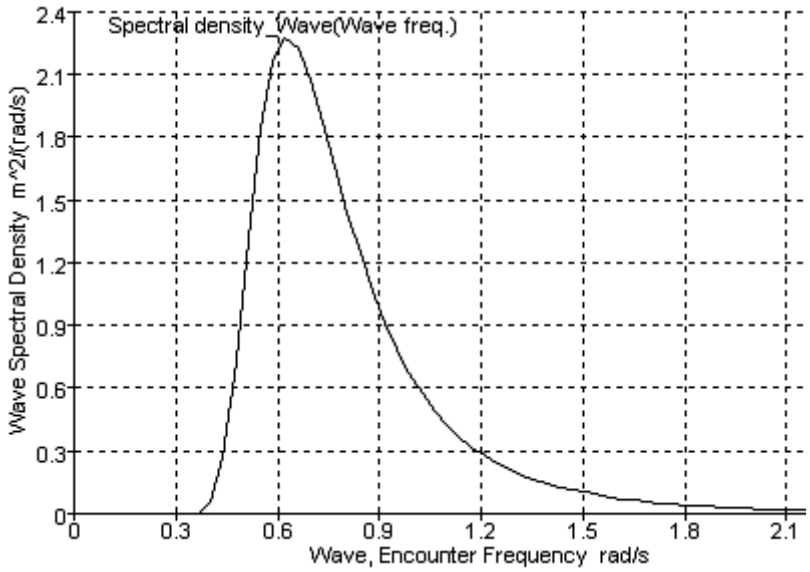

Figure 6-4: Wave spectrum

There are several types of wave spectra designed for different geographic areas, i.e. Pierson-Moskovitz or JONSWAP. The type, or shape, of the sea-spectrum is selected so that the energy distribution over the wave frequencies coincides with statistical wave data from the area where the ship/structure is to be operating. Then additional parameters such as significant wave height and zero crossing periods are set.

6.2.3.2 Short-crested waves

In reality, waves are not only long-crested but three-dimensional not only with different frequencies and amplitudes but also different directions. The short-crestedness can be taken into account by adding another dimension to the wave spectrum

$$S\left(\omega,\theta\right) = S\left(\omega\right) f\left(\theta\right) \qquad (6.19)$$

Where θ is the wave propagation angle of the wave components. Using equations (6.16) and (6.19), the surface elevation of short crested sea can be described as

$$\zeta = \sum_{j=1}^{N}\sum_{k=1}^{K}\sqrt{2S\left(\omega_j,\theta_k\right)\Delta\omega_j\Delta\theta_k}\,\sin(\omega_j t - k_j x\cos\theta_k - k_j \sin\theta_k + \varepsilon_{jk}) \qquad (6.20)$$

6.3 Source technique

The methods used by Wadam for solving linear wave-induced motions and loads on structures with zero Froude number (no forward speed) are

- Diffraction theory - large-volume structures (ships, semi-submersible platforms)
- Morison theory – slender structures (risers, jackets etc.)

As the subject of the thesis is a floating barge, only Diffraction theory will be treated here.

To describe the fluid correctly with a velocity potential we need to implement the boundary conditions described in chapter 6.2. There exist several numerical methods to solve this problem. Wadam uses a panel method to describe large-volume structures. This means using a mixed distribution of potential sources, sinks and normal dipoles distributed over the mean wetted body surface to fulfil the condition of no fluid penetration of the body surface. This makes the method suitable for arbitrary body shapes. The method is based on potential theory, meaning oscillations are assumed small relative to the cross-sectional dimensions of the body.

In short, through implementing the body boundary condition with a finite number of elements with constant source density, the method finds

- The added mass, damping and restoring forces from the radiation problem
  $\frac{\partial \phi_R}{\partial n} = \vec{n}\cdot\vec{V}_s \quad on \;\; S_B$ (eq. (6.12))
- The excitation forces from the diffraction problem
  $$\frac{\partial \phi_D}{\partial n} = -\frac{\partial \phi_I}{\partial n} \quad on \;\; S_B \qquad (6.21)$$

Where ϕ_I is the incident wave potential and ϕ_D is the diffraction potential (see eq.(6.15))

A source is a point from which fluid is imagined to flow out uniformly in all directions. The total flux, or the strength of the source, is denoted Q. A sink is simply a negative source, meaning Q is negative, thus the fluid flows uniformly towards the point of the sink. The velocity potential of a three-dimensional point source in still water and infinite fluid can be written

$$\phi = -\frac{Q}{4\pi r} \qquad (6.22)$$

Where r is the radial distance of a point P from the source point. This gives a radial flow from the point, and if ds is a surface element of a spherical surface with its centre at the source, the velocity flux through the spherical surface can be written as

$$\iint \frac{\partial \phi}{\partial r} dS = \frac{1}{4\pi} \frac{Q}{r^2} 4\pi r^2 = Q \qquad (6.23)$$

6.3.1 Fundamental 2D-theory

At first we will look at a simplified two-dimensional case of a body in infinite fluid forced to oscillate in the heave direction (radiation problem).

A two-dimensional point source can be written

$$\phi = \frac{Q}{2\pi} \log r \qquad (6.24)$$

The source velocity become infinite at r = 0, but if we use a continuous distribution of sources over a surface the velocity will be finite in the entire fluid.

To find the velocity potential we distribute sources over the body surface. This means we write the source velocity potential as

$$\phi(y,z) = \int_S q(s) \log \sqrt{((y-\eta(s))^2 + (z-\zeta(s))^2)} ds \qquad (6.25)$$

Where (η(s) , ζ(s)) are coordinates on the body surface, s is an integration variable along the body surface and (y,z) are coordinates in the fluid domain. S is the body surface and q(s) is a source density determined by the integration variable s. The source density q(s) is found from satisfying the body boundary condition. The total velocity potential must satisfy all boundary conditions, but in this case, with infinite fluid, the only condition is the body boundary condition. We solve the boundary problem numerically through the following steps

1. **Approximate the surface into N straight elements**

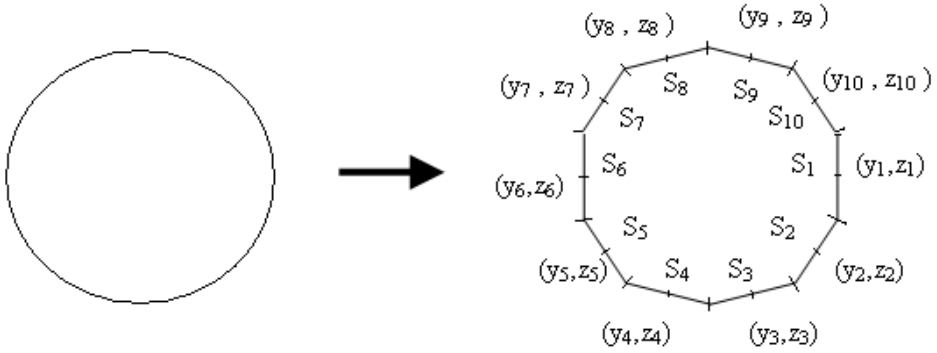

Figure 6-5: Element subdivision (coordinates (y,z) are in element mid-position)

2. **Assume constant source density over each element**
   We can now solve the integral in equation (6.25) numerically by summarizing the contributions from all the elements

$$\phi = q_1 \int_S \log\sqrt{((y-\eta(s))^2 + (z-\zeta(s))^2)}\,ds + ... + q_{10} \int_S \log\sqrt{((y-\eta(s))^2 + (z-\zeta(s))^2)}\,ds \qquad (6.26)$$

3. **Separate out time-dependence and satisfy the body boundary condition on the mid position (y_i,z_i) of each element**
   As the body is oscillating harmonically, we can define the normalised source density

$$q(s) = -\bar{q}(s)\eta_{3,a}\omega\cos\omega t \qquad (6.27)$$

   This means we separate out the time-dependence and the unknown heave motion.

   Further, through the body geometry, we can set up the body boundary condition (see eq. (6.12)), which becomes a linear equation system

$$A_{ij}\bar{q}_j = B_i \qquad (6.28)$$

   Where *i* and *j* run from 1 to the number of elements, 10. The matrix A is a 10x10 matrix containing the surface integrals over each element surface (logarithmic expression in eq. (6.25)) for coordinate (y_i,z_i) differentiated by the normal vector *n*. The $\bar{q}$-vector contains the normalized source densities and the B-vector contains the

body geometric condition so that the normal velocity from the source in (y_i,z_i) is opposite equal to the normal velocity found from oscillation, giving no penetration.

4. **Define the normalised velocity potential and solve the equation system in point 3 for $\bar{q}$, thus finding the normalised radiation velocity potential**

$$\phi = \bar{\phi}\dot{\eta}_3 = -\bar{\phi}\eta_{3,a}\omega\cos\omega t \qquad (6.29)$$

5. **Having achieved the normalised velocity potential we can find the dynamic pressure through Bernoulli**

$$p = -\rho\frac{\partial\phi}{\partial t} = -\rho\bar{\phi}\eta_{3,a}\omega^2\sin\omega t \qquad (6.30)$$

With the pressure distribution for the radiation problem we can find the added mass and damping terms. In this case, where we have infinite potential fluid, there is no damping. How to find these terms will be explained closer in chapter 6.4.3.

The integrals described in equation (6.25) and (6.26) can be solved analytically. This can be shown by analysing the influence from a source distribution along a unit element length.

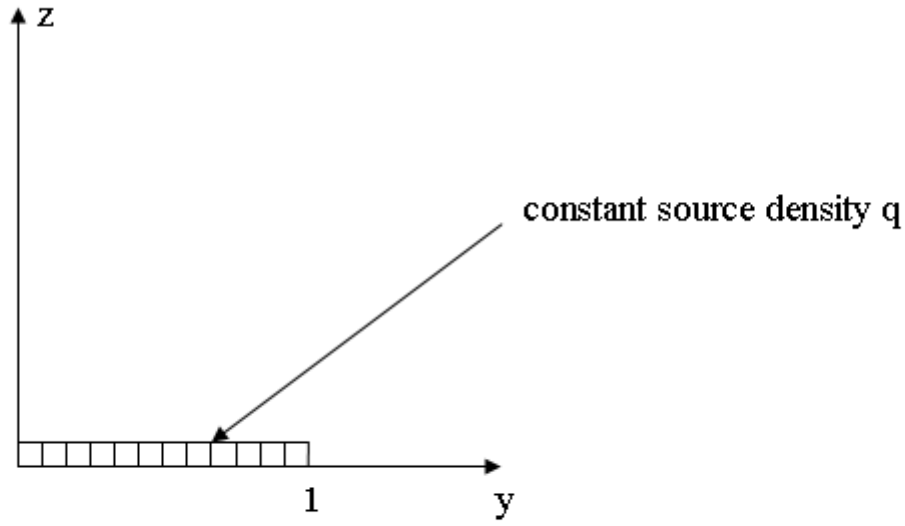

Table 6-1: Source distribution over unit length

The normalised velocity potential can be written

$$\phi(y,z) = \int_0^1 \log\sqrt{((y-\eta)^2 + z^2)}ds \qquad (6.31)$$

Where ds is a length element. The corresponding velocities can be written

$$\frac{\partial \phi}{\partial y} = \int_0^1 \frac{y-\eta}{(y-\eta)^2} d\eta = \frac{1}{2} \log \frac{y^2+z^2}{(y-1)^2+z^2} \tag{6.32}$$

$$\frac{\partial \phi}{\partial z} = \int_0^1 \frac{z}{(y-\eta)^2+z^2} d\eta = -\frac{z}{|z|}\left[arctg \frac{y-1}{|z|} - arctg \frac{y}{|z|} \right] \tag{6.33}$$

When we plot the vertical velocity $\frac{\partial \phi}{\partial z}$ as a function of z along the line y = 1/2 we get the graph shown in Figure 6-6 (from Faltinsen (1990)). Also plotted is an approximation with a single source in y = ½.

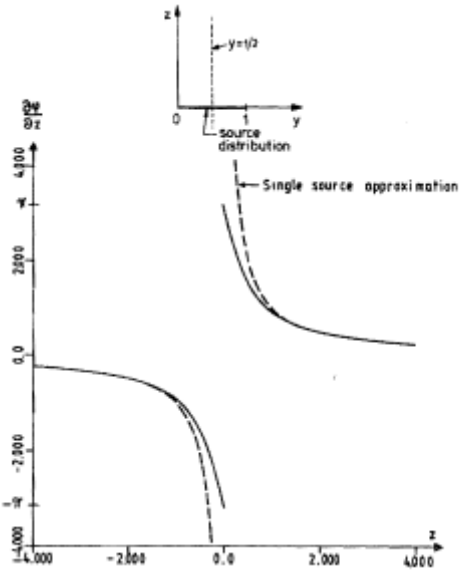

Figure 6-6: Vertical velocity at midpoint of unit source length

We see that the distributed source velocity $\frac{\partial \phi}{\partial z} \to \pi$ as we approach the element, while for the single source approximation $\frac{\partial \phi}{\partial z} \to \infty$ when we approach the velocity goes to infinite close to the element. From the equations for velocity we see that the velocity approach infinite at the endpoints of the segment. This is not a problem if we have a continuous distribution of elements but it can present a problem however for sharp corners etc., thus one should be careful when examining velocities close to the body.

Symmetry and antisymmetry properties of the source density can be used with great advantage in sink-source technique. For the example of the oscillating body in infinite fluid the source density is symmetric about the z-axis as the flow is symmetric about the z-axis. This is due to that the body is symmetric about the z-axis and the body is oscillating in heave. It can be shown that the source densities have to cancel each other at the z-axis. By using this we halve the number of equations. Further we can use the antisymmetry about the y-axis to halve the equations once more.

6.3.2 Three-dimensional source technique with wave effects

When analysing linear wave-induced motions and loads on large-volume structures, three-dimensional source technique is used. In this case we do not have an infinite fluid, thus we have more boundary conditions the velocity potential needs to satisfy.

As an example, we will look at the radiation potential (see chapter 6.2.2) in heave for a ship with zero forward speed. The velocity potential is found from the following conditions

$\frac{\partial^2\phi}{\partial x^2}+\frac{\partial^2\phi}{\partial y^2}+\frac{\partial^2\phi}{\partial z^2}=0$ in the fluid (as eq. (6.1)) (I)

$-\omega^2\phi+g\frac{\partial\phi}{\partial z}=0$ on z = 0 outside body mean pos. (mean free-surface) (as eq. (6.11)) (II)

$\frac{\partial\phi}{\partial n}=n_3\frac{d\eta_3}{\partial t}$ body boundary condition on mean position of ship surface (eq. (6.12)) (III)

$\left.\frac{\partial\phi}{\partial z}\right|_{z=-h}=0$ on the sea bottom (for finite depth) (as eq. (6.14)) (IV)

$|\nabla\phi|\to 0$ when $z\to-\infty$ for infinite water depth (V)

The first conditions listed above are the three-dimensional Laplace-equation (I), the linear free-surface condition for harmonic oscillation (II) and the body boundary condition. For deep water the infinite water depth sea bottom condition (V) is used. The boundary conditions are explained in more detail in chapter 6.2.1.

For a three-dimensional radiation problem we have to include the radiation condition as well to ensure that the waves propagate away from the ship. An example of an outgoing wave potential is

$$\phi\sim\frac{Ae^{kz}}{\sqrt{r}}\sin(kr-\omega t+\varepsilon) \qquad (6.34)$$

Where $r=\sqrt{y^2+z^2}$ is a large distance from the body. Wee see that the wave amplitude decay with a factor of $\frac{1}{\sqrt{r}}$.

As we have three dimensions we represent the hull numerically with quadrilateral panels instead of two-dimensional straight elements. The source strength is constant over the panel (see point 1 and 2 chapter 6.3.1).

However, the source potential is not the same in this case as for infinite fluid (point 3 chapter 6.3.1). It is more complicated to find. We need to correct the potential so that it satisfies conditions (II), (V) and the radiation condition. The strength of the source density is found

from the body boundary condition to ensure no flow trough the body surface. Havelock (1942, 1955) showed that the velocity potential for infinite water depth can be written as the real part of

$$G(x,y,z;\xi,\eta,\zeta)e^{-i\omega t} = [\ \frac{1}{R}+\frac{1}{R'}-\frac{4\nu}{\pi}\int_0^\infty [\nu\cos k(z+\zeta)-k\sin k(z+\zeta)]\frac{K_0(kr)}{k^2+\nu^2}dk \qquad (6.35)$$
$$-2\pi\nu e^{\nu(z+\zeta)}Y_0(\nu r)+i2\pi\nu e^{\nu(z+\zeta)}J_0(\nu r)\ ]e^{-i\omega t}$$

Where *i* is the complex unit, (ξ, η , ζ) are coordinates on the body surface and *s* is an integration variable along the body surface. Further we have

$$R=\sqrt{(x-\xi)^2+(y-\eta)^2+(z-\zeta)^2} \qquad (6.36)$$

$$R'=\sqrt{(x-\xi)^2+(y-\eta)^2+(z+\zeta)^2} \qquad (6.37)$$

$$r=\sqrt{(x-\xi)^2+(y-\eta)^2} \qquad (6.38)$$

$$\nu=\frac{\omega^2}{g} \qquad (6.39)$$

J_0 - Bessel function of the first kind of zero order, roughly described as an oscillating function that decays with the ratio $\frac{1}{\sqrt{\nu r}}$ in this case, where νr is the input variable.

Y_0 - Bessel function of the second kind of zero order, an oscillating function that is singular for νr = 0.

K_0 - modified Bessel function of zero order, an exponentially decaying function of kr in this case

In “Abramowitz & Stegun, 1964” the Bessel functions are explained further. The same work explains how the Green function (eq. (6.35)) satisfies the radiation condition by using asymptotic expansions for the Bessel function for large r-values.

We can write

$$\mathrm{Re}\left\{\left(-Y_0(\nu r)+iJ_0(\nu r)\right)e^{-i\omega t}\right\}\approx \mathrm{Re}\{[-\sqrt{\frac{2}{\pi\nu r}}\sin\left(\nu r-\frac{\pi}{4}\right)+i\sqrt{\frac{2}{\pi\nu r}}\cos\left(\nu r-\frac{\pi}{4}\right)]e^{-i\omega t}\}$$
$$=-\sqrt{\frac{2}{\pi\nu r}}\sin\left(\nu r-\omega t-\frac{\pi}{4}\right) \qquad (6.40)$$

We know that the two first terms in (6.35) decay exponentially with *kr* since they are proportional to K_0, which is real, while the two last terms, seen from (6.40) decay with $\frac{1}{\sqrt{\nu r}}$. Thus we can neglect the first two terms for large r.

Thus we have an oscillating outgoing wave decaying with $\frac{1}{\sqrt{\nu r}}$, meaning we satisfy the radiation condition for large r.

It can also be shown that the free-surface condition is satisfied by image sources/sinks. It is possible to show that equation (6.35) when the frequency goes to zero becomes

$$G(x,y,z;\xi,\eta,\zeta)e^{-i\omega t} = \left[\frac{1}{R} + \frac{1}{R'}\right]e^{-i\omega t} \quad \text{for } \omega \to 0 \qquad (6.41)$$

This equation expresses the source potential as a combination of a source in infinite fluid and an image source above the free-surface.

For infinite frequency of oscillation the source function (6.35) becomes

$$G(x,y,z;\xi,\eta,\zeta)e^{-i\omega t} = \left[\frac{1}{R} - \frac{1}{R'}\right]e^{-i\omega t} \quad \text{for } \omega \to \infty \qquad (6.42)$$

This equation expresses the source potential as a source potential and an image sink above the free surface, thus the equation satisfies the surface condition $\phi = 0$ on $z = 0$ when $\omega \to \infty$.

The solution for the velocity potential for the heave radiation problem can be written as a distribution of sources over the mean wetted hull S_B

$$\phi(x,y,z,t) = \mathrm{Re}\left\{\iint_{S_B} dS Q(s) G\left(x,y,z;\xi(s),\eta(s),\zeta(s)\right)e^{-i\omega t}\right\} \qquad (6.43)$$

Where the Green function (source function) is given by equation (6.35) for infinite water depth. The source function Q(s) is complex and is found by satisfying the body boundary condition. We continue the procedure as in point 4 in chapter 6.3.1 and define the normalised source potential to separate out the time dependence and the heave motion

$$Q(s)e^{-i\omega t} = \bar{Q}(s)\omega\eta_{3,a}e^{-i\omega t} \qquad (6.44)$$

The integral equation for $\bar{Q}(s)$ is solved numerically by dividing the hull into panels and we get a linear equation similar to that of the body in infinite fluid which can be solved. Thus we can find the resulting radiation velocity potential which in turn can give us added mass and damping.

For the diffraction problem, the body boundary condition is satisfied by setting

$$\frac{\partial\phi}{\partial n} = -\frac{\partial\phi_I}{\partial n} \quad on \ S_B \quad \text{(as eq. (6.21))}$$

6.3.3 Considerations

The procedure of solution for the three-dimensional free-surface heave oscillation problem described in chapter 6.3.2 can be generalised to any degree of freedom. The method is in principle equal to that of the two-dimensional infinite fluid example. However, there are a few considerations to be made regarding use of three-dimensional source technique

- More boundary conditions to satisfy
- Complex source densities
- Far more complicated source expression (Green's function)
- The normal velocity induced on an element by a source distribution over the same element is different in 2D and 3D
- Occurrence of irregular frequencies (numerical problem)
- Poor representation of velocities close to the body due to singularities
- Poor representation of sharp corners as there is no fluid separation

Other ways of solving the source potential can be found in Wehausen & Laitone or Newman (1985). This includes solutions for finite water depth, which Wadam uses. This will however not be treated in this review.

6.3.4 Grid density

The panel grid on the hull surface has an impact on the accuracy of the calculations and may have a large effect on the predicted response. In general, the panel density should be larger in areas where we have large changes in the flow, i.e. around sharp corners and edges.

For a dense grid, the computational time can be very large. The ideal grid is therefore one that produces good enough results without using an unreasonable amount of time. Looking at different grid densities, one can examine the convergence of the results. If one increases the density from a coarse grid, one can expect a noticeable improvement in the results. However, as we refine the mesh, we should eventually see a convergence towards the correct result. One way of determining the right mesh can therefore be to vary the grid density and plot the respective results.

6.4 Equations of motion in the frequency domain

To find the dynamic motion characteristics of a floating body we have to solve the dynamic equilibrium equation for regular waves at different wave frequencies (and wavelengths). The dynamic equations of motion are established from Newton's 2nd law and d'Alemberts principle.

For a floating body in waves the general dynamic equilibrium equation for all six modes of motion can be written

$$\sum_{k=1}^{6}[(M_{jk}+A_{jk})\ddot{\eta}_k + B_{jk}\dot{\eta}_k + C_{jk}\eta_k] = F_j e^{-i\omega t}, \qquad j=1,...,6 \tag{6.45}$$

Where

η_k - motion in mode k

$\dot{\eta}_k$ - velocity in mode k

$\ddot{\eta}_k$ - acceleration in mode k

M_{jk} - generalized mass(inertia) matrix component in mode *j* due to motion in mode *k*

A_{jk} - added mass(inertia) matrix component in mode *j* due to motion in mode *k*

B_{jk} - damping matrix component in mode *j* due to motion in mode *k*

C_{jk} - restoring matrix component in mode *j* due to motion in mode *k*

F_j - complex amplitude of exciting force in mode *j* with the force/moment components given by the real part of $F_j e^{-i\omega t}$

ω - wave excitation frequency

As we have six degrees of freedom we get 6x6 matrices for the mass, added mass, damping and restoring forces and a 6x1 vector for the excitation force. Normally the matrices are not diagonal, meaning we have coupling, or interaction effects, between the different modes of motion.

We want to solve the equation system for the response for different frequencies so that we can achieve the transfer functions (RAOs) of the vessel for all the relevant modes of motion. E.g. the heave transfer function expresses the body's response amplitude divided by wave amplitude in the frequency domain, thus for a wave with a given frequency and amplitude we can find the body's response.

Thus we have to find the mass-, added mass-, damping- and restoring matrices as well as the excitation forces.

6.4.1 Excitation forces

This chapter will review the theory used to find the excitation forces on a floating large-volume body. Slender-structure theory will not be treated. The excitation forces come from the waves which create a harmonic oscillating force on the body.

There exist different methods of calculating excitation forces for a floating body. The two most frequently used are

- Diffraction theory – forces are computed directly from pressure distribution
- Haskind relation – forces are computed from radiation potential

Most hydrodynamic programs use diffraction theory to calculate the wave excitation force, because it finds the distributed load (pressure) that can be used for load transfer to a structural analysis. However, the global excitation forces can also be calculated from the Haskind relation that uses the radiation potential.

6.4.1.1 Diffraction theory

As explained in chapter 6.2.2.1, we can find the excitation forces on a large-volume body by the diffraction problem, where the body is in incident waves and restrained from oscillating. To find the fluid pressure we need to know the undisturbed wave potential and the body

diffraction potential from when the body is constrained in the mean position in incident waves. In Wadam, this potential is found by source-technique as explained in section 6.3.

The resulting dynamic pressure on the body in the mean position from incident waves and diffraction can be written

$$p = -\rho \frac{\partial \phi}{\partial t} = -\rho \left(\frac{\partial \phi_I}{\partial t} + \frac{\partial \phi_D}{\partial t} \right) \qquad (6.46)$$

Knowing the Froude-Kriloff pressure and the diffraction pressure, we can find the excitation forces and moments by integrating over the body surface.

6.4.1.2 Haskind relation

For a body with zero forward speed, which is a requirement in Wadam, we can use the Haskind relation to calculate the excitation forces. This calculation method uses Green's second identity to derive excitation forces from the radiation problem instead of the diffraction problem. However, we do not find the pressure distribution with this method, only global forces.

With complex velocity potentials, we can write the diffraction force in direction k as

$$F_k^D = i\omega \int_{S_B} \phi_7 \frac{\partial \phi_k}{\partial n} dA \quad \text{for} \quad k \in \{1,2,3\} \qquad (6.47)$$

Where ϕ_7 is the complex diffraction potential defined by $\phi_7 = e^{i\omega t}\dot{\varphi}(\bar{r})$ and ϕ_k is the complex radiation potential in direction k. S_B is the surface of the body.

Using Green's second identity over a closed surface and the Laplace condition we can write the integral as

$$\iint_{S_B} \left[\phi_7 \frac{\partial \phi_k}{\partial n} - \phi_k \frac{\partial \phi_7}{\partial n} \right] dA = \iiint_V \left[\phi_7 \nabla^2 \phi_k - \phi_k \nabla^2 \phi_7 \right] dV = 0 \qquad (6.48)$$

We can then write

$$F_k^D = i\omega \iint_{S_B} \phi_7 \frac{\partial \phi_k}{\partial n} dA = i\omega \iint_{S_B} \phi_k \frac{\partial \phi_7}{\partial n} dA \qquad (6.49)$$

Using the body boundary condition

$$\frac{\partial \phi_7}{\partial n} = -\frac{\partial \phi_0}{\partial n} \qquad (6.50)$$

Where ϕ_I is the incident wave potential, we can write the diffraction force independent of the diffraction potential

$$F_k^D = -i\omega \iint_{S_B} \phi_k \frac{\partial \phi_0}{\partial n} dA \quad \text{on } S_B \tag{6.51}$$

The Froude-Kriloff force can be written as

$$F^{FK} = \int_{S_B} p(-\vec{n})dA = -\int_{S_B} \frac{\partial \phi_0}{\partial t}(-\vec{n})dA \tag{6.52}$$

If we insert $\phi_0 = \frac{g\zeta_a}{\omega} f(z)e^{i(\omega t - kx)}$ and use that $\overline{e}_k \cdot \vec{n} = \frac{\partial \phi_k}{\partial n}$ we can write the Froude-Kriloff force as

$$F_k^{FK} = i\omega\rho \int_{S_B} \phi_0 \frac{\partial \phi_k}{\partial n} dA \tag{6.53}$$

Combining with the diffraction force we can write the total excitation force as

$$F_k^{ex} = F_k^{FK} + F_k^D = i\omega\rho \int_{S_B} \left[\phi_0 \frac{\partial \phi_k}{\partial n} - \phi_k \frac{\partial \phi_0}{\partial n} \right] dA \tag{6.54}$$

As mentioned, the Haskind relation does not find the distribution of the pressure, thus it is often used to check for numerical error. However, if we are only interested in global responses, it is a valid method.

6.4.2 Mass matrix

The mass matrix consists of the generalized mass and inertia terms which multiplied by acceleration creates the inertia force or moment.

For a body that is symmetric about the X-Z plane and has its centre of gravity in $(0,0,z_G)$ we can write the mass matrix as

$$M_{jk} = \begin{bmatrix} M & 0 & 0 & 0 & Mz_G & 0 \\ 0 & M & 0 & -Mz_G & 0 & 0 \\ 0 & 0 & M & 0 & 0 & 0 \\ 0 & -Mz_G & 0 & I_4 & 0 & -I_{46} \\ Mz_G & 0 & 0 & 0 & I_5 & 0 \\ 0 & 0 & 0 & -I_{46} & 0 & I_6 \end{bmatrix}$$

The mass is found from the body density or mass distribution

$$M = \iiint_V \rho_b dV \approx \sum_{i=1}^{N} m_i \tag{6.55}$$

Where ρ_b and V are respectively the density and the volume of the body and m_i is a mass component. In a computer program such as Wadam, the mass, COG and the mass distribution (inertia data) need to be defined before any calculations can be made. From the mass data and the hull shape the program can calculate the floating position and thus the inertia forces from the following relation

$$I = \iiint_V \rho_b r^2 dV \approx \sum_{i=1}^{N} m_i r_i^2 \qquad (6.56)$$

Where r is the distance from the axis of rotation. r_i is the distance from the axis of rotation to the local COG of a point mass m_i. E.g. the pitch inertia (about the y-axis) is

$$I_{55} = \iiint_V \rho_b \left(x^2 + z^2\right) dV \approx \sum_{i=1}^{N} m_i (x_i^2 + z_i^2) \qquad (6.57)$$

Where x_i and z_i are the coordinates in the X-Z plane of the local COG of m_i. In Wadam, alternatively, the radii of gyration can be input directly for a specific load condition. In this case we use the following relation to find the inertia

$$r = \sqrt{\frac{I}{M}} \qquad (6.58)$$

Where *r*, *I* and *M* are as explained above. In any case, the mass distribution over the body must be known. If we know the total mass, but not the distribution, we can perform a rough approximation by setting the body density as constant.

6.4.3 Damping and Added mass

Added mass is defined as an addition to the body's mass or inertia due to that the body will accelerate the fluid it is oscillating in. The whole fluid is accelerated but the acceleration decreases rapidly at a further distance from the body, thus the added mass can be represented with a finite addition of the mass. The added mass is not necessarily of unit [kg]. E.g. the added mass in pitch will be an added inertia about the y-axis of unit [m^4]. In strip theory the pitch added mass would be found from the two-dimensional added mass in heave, but by use of Wadam, it is found from the radiation potential.

The damping is the dissipation of energy for the vibration. For a free, damped oscillation, the response will decay exponentially (subcritical damping). The damping coefficient can be found from the critical damping. The critical damping is when we have zero in the root of the 2^{nd} order equation, meaning we have maximum one zero crossing. The damping ratio is defined as the ratio of critical damping

$$\xi = \frac{B}{B_{critical}} = \frac{B}{2(M + A)\omega_n} \qquad (6.59)$$

Often, the damping ratio is known or it can be approximated for a type of dynamic system. Then the damping coefficient is found from the relation between critical damping and

damping ratio. For Wadam however, the damping is found from the radiation velocity potential, except for viscous roll damping, which is found from strip theory.

6.4.3.1 Potential damping

As mentioned, the damping components B_{jk} and the added mass components A_{jk} are found by solving the radiation problem. We can write the induced hydrodynamic force in degree of freedom *k* on the body by the forced harmonic motion mode η_j as

$$F_k = -A_{kj}\frac{d^2\eta_j}{dt^2} - B_{kj}\frac{d\eta_j}{dt} \qquad (6.60)$$

Knowing the radiation potential we can find the hydrodynamic force on the body. The radiation potential can be found through source technique as seen in chapter 6.3. We can use the two-dimensional body from chapter 6.3.1 as an example. The dynamic pressure has been found to be

$$p = -\rho\frac{\partial\phi}{\partial t} = -\rho\bar{\phi}\eta_{3,a}\omega^2\sin\omega t \qquad (6.61)$$

Where $\bar{\phi}$ is the normalised velocity potential independent of time and motion, $\eta_{3,a}$ is the amplitude of the forced heave motion and ω is the frequency of oscillation. From the numerical division into elements with constant source strength, the hydrodynamic force in heave becomes

$$F_3 = -\int_S pn_3 ds \approx -\left\{\sum_{j=1}^{10}\left[\int_{S_j}\bar{\phi}n_{3i}ds\right]\right\}\omega^2\eta_{3,a}\sin\omega t \qquad (6.62)$$

Where *S* is the surface of the body and *j* denotes the element number. Thus, by using equation (6.60) and knowing that there is no damping in infinite potential fluid we can set the added mass to

$$A_{33}^{(2D)} = -\rho\sum_{j=1}^{10}\left[\int_{S_j}\bar{\phi}n_{3i}dS\right] \qquad (6.63)$$

In general, for a floating body on the free-surface, the damping and added mass can be found by using fluid energy relations, the equation of motion and using the control surfaces shown in Figure 6-7. The figure shows a forced heave motion as an example. The damping can be linked to the amplitude of the radiated wave.

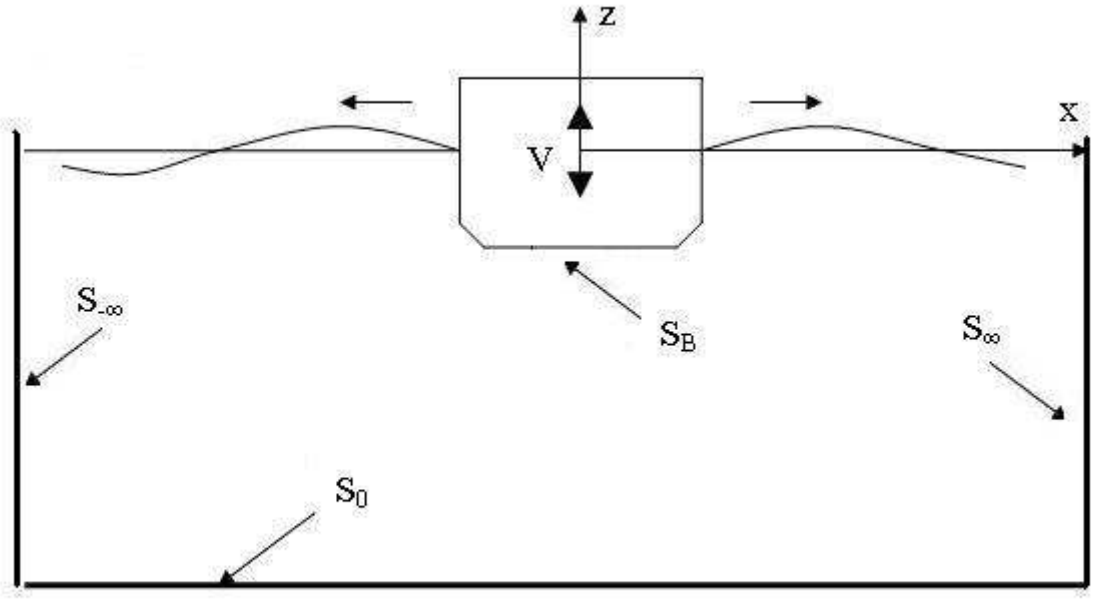

Figure 6-7: Control surfaces for radiation problem

For the case to be studied, a rectangular barge, we have no forward speed and no current. The barge is also symmetric about the X-Z and the Y-Z planes. In this case we should have symmetry about the diagonal for the damping and added mass matrices as well as no coupling between sway, roll and yaw and surge, heave and pitch, meaning

$B_{jk} = B_{kj}$, $A_{jk} = A_{kj}$ (6.64)

6.4.3.2 Viscous roll damping

In roll, the viscous effects can increase the damping significantly, thus giving a significant decrease in the roll response, especially around the roll eigenfrequency. The radiation potential does not include viscous effects, thus the viscous roll damping must be included in another way. This is normally done by adding a viscous roll damping term in addition to the potential damping term, represented as follows:

$$F_{VD}^{non-linear} = B_{44}\dot{\eta}_4\left|\dot{\eta}_4\right| \quad (6.65)$$

However, as seen in equation (6.65), the viscous damping term is non-linear. In order to use the viscous-damping in the linear equation of motion, we need to linearise the term. Thus, we introduce the linear viscous damping coefficient as follows

$$F_{VD}^{linear} = B_{44}^{*}\dot{\eta}_4 \quad (6.66)$$

Where the linearised damping coefficient takes the following form

$$B_{44}^{*} = K\eta_{4,\max} \quad (6.67)$$

K is a constant depending on encounter frequency, hull form and bilge keel dimensions. It is found so that the linearization gives minimal error. $\eta_{4,\max}$ is the most probable largest roll amplitude in a seastate, typically of three hours duration (see section 6.6.4). The linearised roll damping is dependent on the maximum roll amplitude, which is found from the transfer function following the solution of the equation of motion. As the viscous damping is part of the equation of motion, we need to iterate to find the correct damping. This in turn means that we get a different transfer function for each seastate due to the variation in the viscous damping. The variation will be large or small depending on the magnitude of the viscous damping.

WADAM calculates the viscous roll damping coefficient from the following contributions:

- Skin-friction – found through strip theory, Kato (1966)
- Eddy-making from bilge keel – Kato(1966)
- Eddy-making from the naked hull – Empirical data and strip theory, Tanaka (1961)

In this work, no bilge keel will be included, thus the relevant components are skin-friction and eddy-making from the hull. Due to the rectangular hull form of a barge, the viscous roll damping will be dominated by the hull eddy-making component, but for a conventional ship hull the skin-friction component will dominate. Both the skin-friction component and the eddy-making component are found using strip theory. Further, the skin-friction term is calculated according to Kato (1966), while the eddy-making component is found trough empirical data, Tanaka (1961).

In short, strip theory divides the hull into 2D-strips over the vessel length and neglects water flow in the longitudinal direction. In this manner, the calculations are simplified significantly and we only need to find wave motion and excitation force on each strip. Hydrodynamic coefficients such as damping and added mass can be found using experimental 2D-data. In this case, strip theory will only be used to find the viscous roll damping components. They are found using experimental data for 2D-sections from Kato(1966) and Tanaka(1961). There are some limitations to the use of strip theory, thus the following assumptions apply in calculation of the viscous roll damping term:

- Slender body, L/B>>1 (L/B>2 normally produce good results)
- Low Froude number, Fn
- Linear relation between wave amplitude and vessel response

All the conditions listed are satisfied in the following analyses, as the barges have an L/B-ratio between 3 and 4, and zero forward speed. A linear relation between wave amplitude and response is already assumed as we are using linear wave potential theory.

6.4.4 Restoring forces

The dynamic restoring forces or moments are induced by a change in buoyancy or buoyancy distribution and thus proportional to the vessel motion. We will take a look at restoring forces in heave and pitch as examples of how to find the restoring coefficient.

E.g. for a rectangular barge in heave moving into the fluid the static fluid pressure will give an increase in the buoyancy from the neutral level, giving a net restoring force opposite of the

motion. The same decrease in buoyancy occurs when the barge is moving out of the fluid. It can be written

$$F_3^R = -C_{33}\eta_3 \qquad (6.68)$$

Where

$$C_{33} = \rho g A_{WL} \qquad (6.69)$$

Where A_{WL} is the vessel waterline area. For a normal body the area of the waterline will vary with changing submergence as the hull gets narrower towards the keel. This means that the restoring coefficient will be a function of motion. This is often neglected for small motions.

E.g. for a positive pitch motion the buoyancy centre moves forward due the increased buoyancy at the bow and the decreased buoyancy at the stern, creating a righting arm GZ_L. The righting arm can be expressed through the longitudinal metacentric height

$$GZ_L = \overline{GM_L}\sin\eta_5 \qquad (6.70)$$

Where η_5 is the pitch angle. For small angles we have that $\sin\eta_5 \approx \eta_5$, thus we can express the righting moment as

$$F_5^R = -\rho g \nabla GZ_L \approx -\rho g \nabla \overline{GM_L}\eta_5 = -C_{55}\eta_5 \qquad (6.71)$$

Where ρ is the water density, g is the gravity constant and ∇ is the volume displacement of the ship. Thus the restoring coefficient becomes

$$C_{55} = \rho g \nabla \overline{GM_L} \qquad (6.72)$$

We can have coupling of restoring in different modes of motion.

6.4.4.1 Linearised roll restoring

In roll, the restoring coefficient is found in same manner as for the pitch motion (shown in the section above), except the distance between the centre of gravity and the transverse metacentre is used instead of the longitudinal metacentre. However, the roll motion poses a new problem as the roll angles can become quite large. This means that the roll angles exceed the linear part of the GZ-curve, which is the basis for the roll restoring moment.

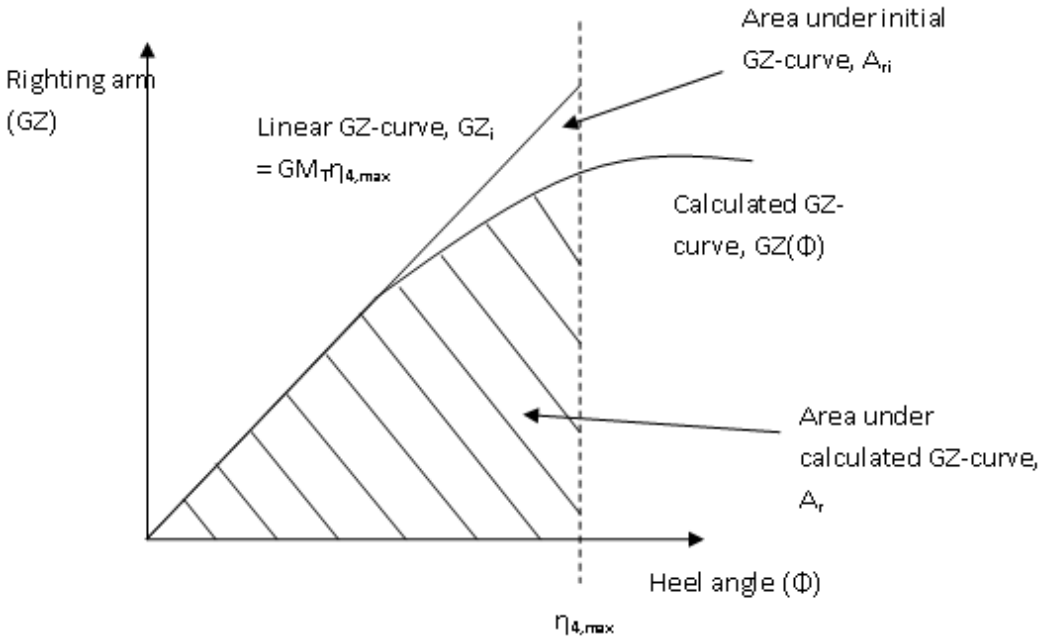

Figure 6-8: Linearised roll restoring moment from the GZ-curve

Using the area under the estimated GZ-curve (A_r) and the area under the initial GZ-curve (A_{ri}), as defined in Figure 6-8, the roll restoring coefficient can be linearised by introducing a factor, *f*. First, assuming small angles, we expand the restoring work in a Taylor series:

$$W_{ri} = \frac{1}{2}\rho g \nabla GZ_i \Phi = \rho g \nabla A_{ri} \qquad (6.73)$$

Thus we can find the relation between the work of the real restoring and the initial restoring as the factor *f*:

$$f = \frac{W_r}{W_{ri}} = \frac{A_r}{A_{ri}} = \frac{2A_r}{GZ_i \eta_{4,\max}} = \frac{2A_r}{\overline{GM}_T \eta_{4,\max}^2} \qquad (6.74)$$

Thus we can write the restoring moment in roll at large angles as

$$C_{44} = f \cdot \rho g \nabla \overline{GM}_T \qquad (6.75)$$

6.4.5 Transfer functions

Having achieved the equation terms, there are different ways of solving the problem for a forced vibration. The frequency response method, with complex numbers, is frequently used.

The principle of finding the transfer function can be explained as follows. We have a dynamic equilibrium function

$$(M + A)\ddot{\eta} + B\dot{\eta} + C\eta = Fe^{-i\omega t} \qquad (6.76)$$

We can write the response

$$\eta = \bar{\eta}e^{-i\omega t} = FR(\omega)Fe^{-i\omega t} \qquad (6.77)$$

Where $\bar{\eta}$ is the complex amplitude of motion (the real part is implied) and FR(ω) is the complex frequency-response function. Thus we can divide the equation of motion by $e^{-i\omega t}$ and we get an equation that can be divided into real and imaginary parts.

$$-\omega^2(M + A)\bar{\eta} + i\omega B\bar{\eta} + C\bar{\eta} = F \qquad (6.78)$$

We can write the frequency-response function as the motion amplitude per unit excitation force

$$FR(\omega) = \frac{\bar{\eta}}{F} = \frac{1}{-\omega^2(M + A) + i\omega B + C} \qquad (6.79)$$

In linear theory we assume a linear relation between wave excitation force and wave amplitude. Using this we can find the transfer function defined as

$$\left|H(\omega)\right| = \left|\frac{\bar{\eta}}{\zeta_a}\right| \qquad (6.80)$$

For the full six degree of freedom system the equations are more complicated. For a body symmetric about the X-Z axis, we can utilize that there is no coupling of surge, heave and pitch with sway, roll and yaw. Thus we get two sets of three coupled equations for the imaginary and real parts. We write

$$\eta_k = \bar{\eta}_k e^{-i\omega t} = FR(\omega)F_j e^{-i\omega t} \qquad (6.81)$$

$$\sum_{k=1}^{6}[-\omega^2(M_{jk} + A_{jk})\bar{\eta}_k + i\omega B_{jk}\bar{\eta}_k + C_{jk}\bar{\eta}_k] = F_j, \quad j = 1,...,6 \qquad (6.82)$$

We can then find the frequency-response function from

$$FR_j(\omega) = \left[\sum_{k=1}^{6}[-\omega^2(M_{jk} + A_{jk})\bar{\eta}_k + i\omega B_{jk}\bar{\eta}_k + C_{jk}\bar{\eta}_k]\right]^{-1}, \quad j = 1,..,6 \qquad (6.83)$$

By taking the absolute-value of the complex frequency-response function, we find the mechanical transfer function. The hydrodynamic transfer function is found by finding the motion per unit wave amplitude instead of per unit force.

6.5 Design accelerations

In order to find the maximum accelerations on the seafastening and the uplift acceleration, we need to change the accelerations from an earth fixed coordinate system (x,y,z) to a body fixed coordinate system (X,Y,Z). This will give us accelerations for X and Y in the deck plane, as well as Z-acceleration normal to the deck plane, thus we can estimate the forces on the seafastening equipment. Both systems have origo in the centre of rotation.

We start by combining the global accelerations (transfer functions) into point accelerations for a random point P = (x_p,y_p,z_p).

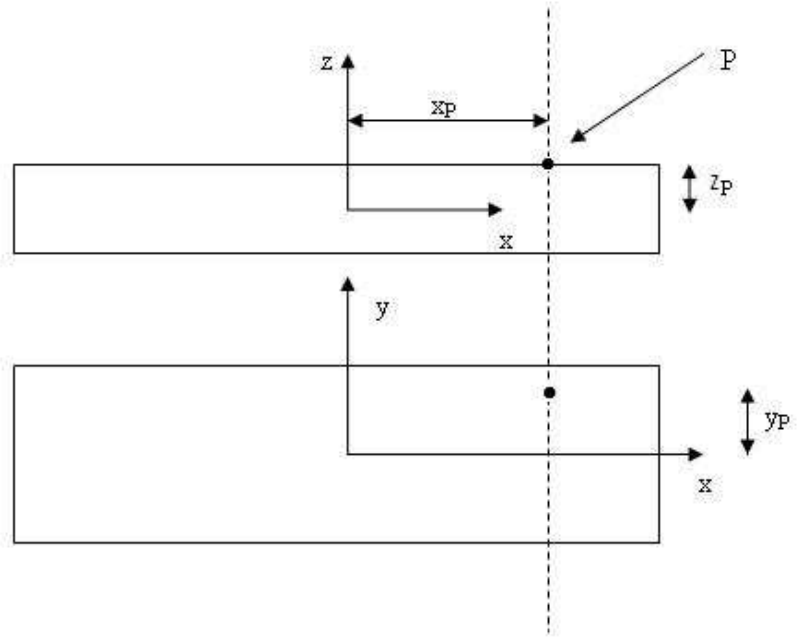

Figure 6-9: Calculation of acceleration in a point P

Looking at Figure 6-9, assuming small motions, one can see that the motion in an arbitrary point P on the barge in the earth fixed coordinate system can be found from the following expressions:

$$\begin{aligned} s_1 &= \eta_1 + z_p\eta_5 - y_p\eta_6 \\ s_2 &= \eta_2 - z_p\eta_4 + x_p\eta_6 \\ s_3 &= \eta_3 + y_p\eta_4 - x_p\eta_5 \end{aligned} \qquad (6.84)$$

Global motions and accelerations are given in the vessel centre of rotation. Thus, using the complex transfer functions for the harmonic motion, we can find the transfer functions for acceleration of P in the global coordinate system as follows:

$$\begin{aligned} a_x &= \ddot{\eta}_1 + z\ddot{\eta}_5 - y\ddot{\eta}_6 = -\omega^2[|H_1(\omega)| + z|H_5(\omega)| - y|H_6(\omega)|] \\ a_y &= \ddot{\eta}_2 - z\ddot{\eta}_4 + x\ddot{\eta}_6 = -\omega^2[|H_2(\omega)| - z|H_4(\omega)| + x|H_6(\omega)|] \\ a_z &= \eta_3 + y\eta_4 - x\eta_5 = -\omega^2[|H_3(\omega)| + y|H_4(\omega)| - x|H_5(\omega)|] \end{aligned} \qquad (6.85)$$

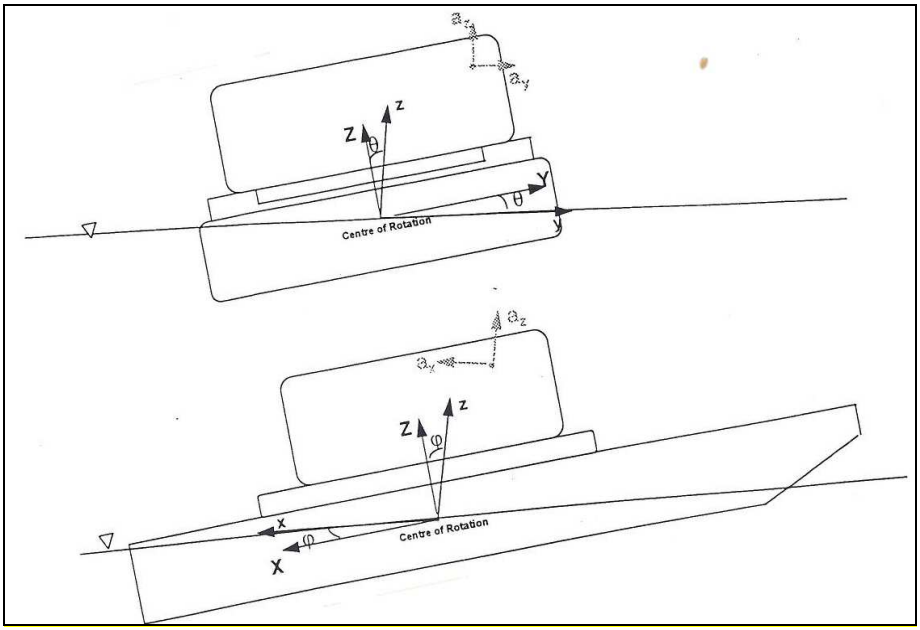

Figure 6-10: Body fixed (X,Y,Z) and earth fixed (x,y,z) coordinate system

To convert the accelerations to the body fixed coordinate system, we include pitch and roll angles due to waves and decompose the translational accelerations. Due to the angles we have to include the gravity component *g*. Static angle due to wind is not considered and is therefore neglected. We can now write the accelerations in the body-fixed coordinate system as

$$\begin{aligned} A_X &= a_x \cos\eta_5 - g\sin\eta_5 - a_3 \sin\eta_5 \\ A_Y &= a_y \cos\eta_4 + g\sin\eta_4 - a_3 \sin\eta_4 \\ A_Z &= a_z \cos\eta_5 \cos\eta_4 + g\cos\eta_5 \cos\eta_4 + a_1 \sin\eta_5 + a_2 \sin\eta_4 \end{aligned} \qquad (6.86)$$

Assuming small pitch and roll angles we can write $\cos\eta \approx 1$ and $\sin\eta \approx \eta$. This means we can simplify equation (6.86) to the following:

$$\begin{aligned} A_X &\approx a_x - g\eta_5 - a_3\eta_5 \\ A_Y &\approx a_y + g\eta_4 - a_3\eta_4 \\ A_Z &\approx a_z + g + a_1\eta_5 + a_2\eta_4 \end{aligned} \qquad (6.87)$$

Having obtained these expressions, meaning RAOs for the accelerations in the body-fixed coordinate system, we only need to use the theory of short-term statistics (as in section 6.6.4) to find the design accelerations, the extreme values of A_X, A_Y and A_Z. However, Postresp cannot only calculate the two first terms of the accelerations in equation (6.87) as the remaining terms are non-linear with respect to wave amplitude.

In the Z-direction, these two non-linear terms in equation (6.87) can be neglected due to their small magnitude. However, to find the extreme values in the X- and Y-direction, we need to combine the extreme value from Postresp (the two first terms of A_X and A_Y in equation (6.87)) with the extreme values for heave acceleration, pitch and roll. This means the design accelerations are calculated as follows:

$$A_{X,\max} = \pm\left(A_{X,\max}^{postresp} + a_{3,\max}\eta_{5,\max}\right)$$
$$A_{Y,\max} = \pm\left(A_{Y,\max}^{postresp} + a_{3,\max}\eta_{4,\max}\right) \quad (6.88)$$

Where the terms calculated by Postresp are:

$$A_X^{postresp} = a_x - g\eta_5$$
$$A_Y^{postresp} = a_y + g\eta_4 \quad (6.89)$$

As the purpose of checking acceleration in the Z-direction is to check for uplift force, the gravity component is not included for this component. Thus the Z-component of the acceleration is calculated directly from the RAO created in Postresp.

6.6 Statistical analysis

After the transfer functions are calculated for all the relevant degrees of freedom, the response of the vessel can be calculated in a longer term, i.e. for a sea-state of 3 hours duration to find extreme responses. For the case-study and the thesis, this will be done in the program Postresp. In this chapter we will look at the theory used to calculate the statistical responses.

6.6.1 Basic assumptions

- Linear relation between wave amplitude and vessel response
- Waves are assumed long-crested. This means that no wave spreading function is included in this analysis. Long-crestedness is considered to give slightly conservative results
- The wave-spectrum is considered narrow-banded. This allows the use of Rayleigh distribution of the wave heights instead of Rice distribution

6.6.2 Wave spectrum

For this case, regarding a barge to be used for transport operations in the North Sea, a JONSWAP spectrum will be used. It is assumed narrow-banded, meaning that the energy is assumed concentrated around a narrow band of frequencies. JONSWAP stands for Joint North Sea Wave Project and is derived from a Pierson-Moskowitz spectrum. The Pierson-Moskowitz spectrum is based on North-Atlantic statistic data and is governed by wind velocity for low frequency waves and gravity for high velocity waves. The Pierson-Moskowitz spectrum can be written:

$$S^{PM}(\omega)=\frac{A}{\omega^5}e^{(-\frac{B}{\omega^4})} \qquad (6.90)$$

Where

$$A=0.0081g^2, \quad B=0.74(\frac{g}{U})^4$$

ω - wave frequency (rad/s)
U - wind velocity (m/s)
g - gravity constant (m/s^2)

By introducing the following parameters we create a JONSWAP spectrum:

α - parameter describing the spectrum in the high frequency area (0.0081 for PM)

$\omega_P = 0.87\frac{g}{U}$ - peak frequency

$$\sigma=\begin{cases}\sigma_a & for\ \omega \le \omega_P \\ \sigma_b & for\ \omega \succ \omega_P\end{cases}$$

If we use a PM spectrum and a JONSWAP spectrum to describe the same sea state, then the total energy, the area under the spectrum curve, will be the same. The difference is that the JONSWAP uses a peak parameter, γ, which is described by:

$$\gamma = \frac{S_{JONSWAP,\max}}{S_{PM,\max}} \cdot C \qquad (6.91)$$

Thus the γ describes the peakedness of the JONSWAP spectrum. The JONSWAP spectrum is designed for areas close to the shore and sea states that are not as fully developed as the PM spectra. The spectra for these sea states have proven more concentrated around the peak frequency, which is represented in JONSWAP with the parameter γ .

The spectrum can then be written

$$S(\omega) = \alpha \frac{g^2}{\omega^5} e^{-\frac{5}{4}(\frac{\omega_P}{\omega})^4} \cdot \gamma^{e^{-\frac{1}{2}(\frac{\omega-\omega_p}{\sigma\omega_p})}} \qquad (6.92)$$

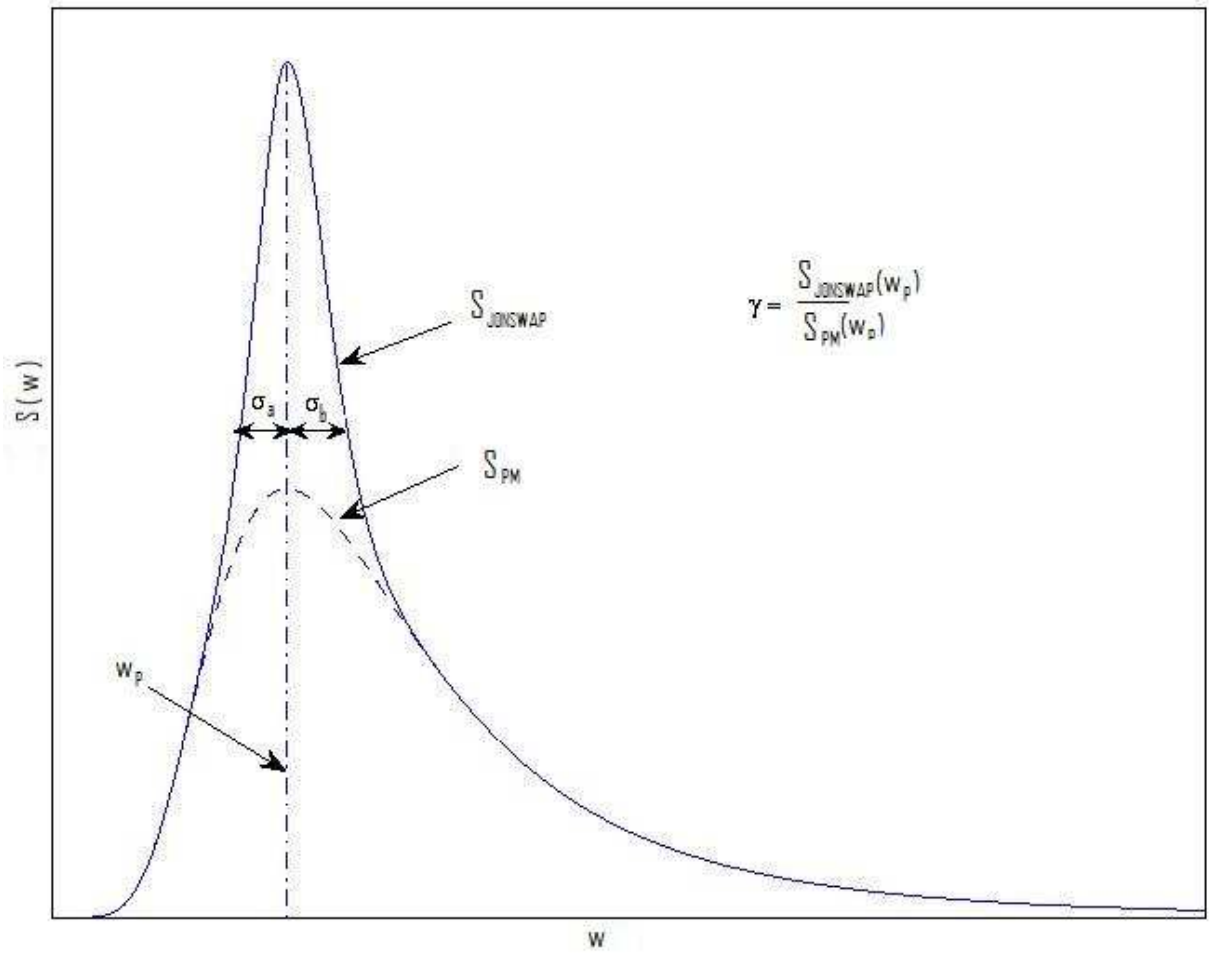

Figure 6-11: JONSWAP and Pierson-Moskowitz spectra

Among others, Hasselmann established the following mean values for the JONSWAP parameters:

$\overline{\gamma}=3.3$

$\sigma_a = 0.07 \; and \; \sigma_b = 0.09$

$$\alpha = 0.076\left(\frac{gx}{U^2}\right)^{-0.22}$$

$$\omega_P = 7.0\pi\left(\frac{g}{U}\right)\left(\frac{gx}{U^2}\right)^{-0.33}$$

Where U is the wind velocity (m/s) and x is the fetch (m), the effective distance the wind excites the sea.

However, it is more convenient to establish the parameters H_s and T_z to describe the spectrum. These are respectively significant wave height (the average of the 1/3 highest waves) and the average zero crossing period. Thus, using Hasselmann's values for σ_a and σ_b, we express α, γ and ω_p as functions of H_s and T_z with the approximations seen in Figure 6-12.

$$\alpha = \left(5/16\right)\cdot\left(H_s^{\,2}\,\omega_p^{\,4}/g^2\right)\cdot\left(1 - 0.287\ln(\gamma)\right)$$

$$\omega_p = 2\pi/T_p$$

$$T_p = T_z\sqrt{\frac{11+\gamma}{5+\gamma}}$$

$$\gamma = 5 \qquad for \qquad \frac{T_z}{\sqrt{H_s}} < 2.7$$

$$\gamma = e^{\left(5.75 - \frac{1.55\,T_z}{\sqrt{H_s}}\right)} \qquad for \qquad 2.7 \le \frac{T_z}{\sqrt{H_s}} \le 3.7$$

$$\gamma = 1 \qquad for \qquad \frac{T_z}{\sqrt{H_s}} > 3.7$$

Figure 6-12: Wave spectrum conditions

H_s and T_z can be expressed by the wave spectral moments as following

$$H_s = 4\sqrt{m_0} \qquad (6.93)$$

$$T_z = T_{m02} = \frac{2\pi}{\omega_{m02}} = 2\pi\sqrt{\frac{m_0}{m_2}} \qquad (6.94)$$

Where

$$m_n = \int_0^\infty \omega^n S(\omega)\,d\omega \qquad (6.95)$$

Thus we have a JONSWAP wave spectrum that can describe a sea state wave energy distribution for a given H_s and T_z combination.

6.6.3 Short-term response and response spectrum

A sea state is the time interval where we have a constant wave spectrum, i.e. constant H_s and T_z. Given the wave spectrum for a sea state and the transfer functions (RAOs) for a floating vessel we can find the vessels response spectra for that sea state in all modes of motion. This is based on the assumption that there is a linear relation between the wave amplitude and the vessel response. This can be derived as follows with a heave motion as an example

$$H_{heave}(\omega_j) = \frac{|\eta_{3,j}|}{\zeta_{a,j}} \qquad (6.96)$$

$$S_{\eta_3}(\omega_j)\Delta\omega = \frac{1}{2}|\eta_{3,j}|^2 \qquad (6.97)$$

$$S(\omega_j)\Delta\omega = \frac{1}{2}\zeta_{a,j}^2 \qquad (6.98)$$

Where $\eta_{3,j}$ and $\zeta_{a,j}$ are the response- and wave amplitude for frequency ω_j. $S_{\eta_3}(\omega)$ and $S(\omega_j)$ are respectively heave response- and wave spectrum for frequency ω_j. By dividing equation (6.97) by equation (6.98) and inserting equation (6.96) we get the expression for the response spectrum

$$S_{\eta_3}(\omega_j) = H_{heave}(\omega_j)^2 S(\omega_j) \qquad (6.99)$$

Thus from the response spectrum $S_x(\omega)$ of a response x, we can find the significant response height (double amplitude), equivalent of finding the significant wave height for a wave spectrum, and the zero-crossing period for the response

$$X_s = 4\sqrt{m_0^x} \qquad (6.100)$$

$$T_{z,x} = T_{m02,x} = \frac{2\pi}{\omega_{m02,x}} = 2\pi\sqrt{\frac{m_0^x}{m_2^x}} \qquad (6.101)$$

Where the response spectral moments are given as:

$$m_n^x = \int_0^\infty \omega^n S_x(\omega) d\omega \qquad (6.102)$$

The variance of the response is given by the 0^{th} spectral moment

$$\sigma_x^2 = m_0^x = \int_0^\infty S_x(\omega) d\omega \qquad (6.103)$$

The short term response or significant response, X_s, is normally plotted against T_z for a constant H_s. Significant response is the double amplitude of the average of the 1/3 highest responses in a sea state. Further, as shown in the next section, the variance of the response can be used to calculate extreme response in a seastate.

6.6.4 Short-term statistics, design accelerations

Given a criteria for maximum allowed response, one can find the limiting sea state, the sea state that gives maximum allowed response. As we are calculating a transport phase, the relevant statistical analysis will be a short term response statistics analysis.

Assuming that the wave amplitudes, and thus the response amplitudes, can be described by a standard normal (Gaussian) distribution around zero, the response height can be described by a Rayleigh or Rice distribution. This distribution gives us i.e. the probability of exceeding a given response value. The cumulative probability function gives the probability that a response is equal to or smaller than a given response value x. The Rice cumulative distribution function is given by:

$$F_s(x) = \Phi\left(\frac{x}{\varepsilon\sigma_x}\right) - \sqrt{1-\varepsilon^2}\,\Phi\left(\frac{\sqrt{1-\varepsilon^2}}{\varepsilon}\frac{x}{\sigma_x}\right) e^{-\frac{1}{2}\left(\frac{x}{\sigma_x}\right)^2} \qquad (6.104)$$

Where $\Phi()$ is the normal cumulative probability integral, σ_x and ε is the spectral parameter given by

$$\varepsilon = \sqrt{1 - \frac{m_2^2}{m_0 m_4}} \qquad (6.105)$$

Where m_0, m_2 and m_4 are spectral moments for the response spectrum. In our case we have a narrow-banded process. This means that $\varepsilon \approx 0$, or that $m_2^2 \approx m_0 m_4 \approx \omega^4 S(\omega)^2$. Thus the cumulative distribution function becomes

$$\rightarrow F_s(x) = \Phi(\infty) - \Phi(\infty) e^{-\frac{1}{2}\left(\frac{x}{\sigma_x}\right)^2} = 1 - e^{-\frac{1}{2}\left(\frac{x}{\sigma_x}\right)^2} \qquad (6.106)$$

Thus the probability of exceeding a given response value x is

$$P(X \geq x) = 1 - F_s(x) = e^{-\frac{1}{2}\left(\frac{x}{\sigma_x}\right)^2} \qquad (6.107)$$

In a sea state of duration $T_{seastate}$, the number of response cycles can be calculated from the response zero-crossing period which is the same the wave zero-crossing period

$$N = \frac{T_{seastate}}{T_z} \qquad (6.108)$$

We can calculate the most probable largest response by setting the probability of exceeding response X_{max} equal to 1/N (only one wave exceeds X_{max}).

$$1 - F_s(X_{\max}) = \frac{1}{N} \qquad (6.109)$$

$$\rightarrow \; e^{-\frac{1}{2}\left(\frac{X_{\max}}{\sigma_x}\right)^2} = \frac{1}{N} \qquad (6.110)$$

$$\rightarrow \; X_{\max} = \sqrt{2}\sigma_x\sqrt{\ln N} \qquad (6.111)$$

With respect to design accelerations (see section 6.5), we need to find the most probable largest response (X_{max}) for all the components of the design accelerations as demonstrated above.

Alternatively, by setting a maximum probability of exceeding a given limiting vertical acceleration, one can find the limiting sea state for the transport. In this case the response standard deviation (or variance) will be the unknown variable. We can write

$$e^{-\frac{1}{2}\left(\frac{X_{\max}}{\sigma_x}\right)^2} = P_{\max} \qquad (6.112)$$

$$\rightarrow \; \sigma_{x,\max} = -\frac{X_{\max}}{\sqrt{2\ln P_{\max}}} \qquad (6.113)$$

Where P_{max} is the maximum probability of exceeding the given limiting response X_{max}.

7 Analysis setup

There will be a total of six different cases examined in this work, consisting of selected combinations of barges and module weights. There are three different barges and four different module weights. The cases to be analysed are listed in Table 7-1.

Annotation	Barge	Module weight
B3L1	300 ft (UR109)	1000 t
B3L3	300 ft (UR109)	3000 t
B4L1	400 ft (H404)	3000 t
B4L5	400 ft (H404)	5000 t
B6L5	600 ft (S600)	5000 t
B6L8	600 ft (S600)	8000 t

Table 7-1: Case analyses

The modules are assumed to have an evenly distributed mass. The module dimensions and required grillage heights are shown in Table 7-2.

Module weight [tonnes]	Length [m]	Breadth [m]	Height [m]	Grillage height [m]
1000	30	12	14	1.5
3000	40	25	17	3.0
5000	45	30	20	4.0
8000	50	35	25	5.0

Table 7-2: Module weights and dimensions

The modules are assumed to have an evenly distributed mass. In all cases they are placed with their own COG $0.1L_{module}$ aft of the midship, meaning they have 60% of their length aft of the midship. As a given module weight has the same dimensions and grillage height independent of which barge it is applied to, the vertical position of the module bottom from the keel baseline depends only on the barge depth. The arrangement of the modules can be seen in Table 7-3 and Figure 7-16.

Barge	Module weight	Module COG X [m]	Y [m]	Z [m]
300 ft	1000 t	3	0	14.60
300 ft	3000 t	4	0	17.60
400 ft	1000 t	3	0	16.10
400 ft	5000 t	4.5	0	21.60
600 ft	5000 t	4.5	0	25.58
600 ft	8000 t	5	0	29.08

Table 7-3: Module positions for all cases

7.1 Barge geometry

The barge geometry is modelled through a panel model, representing the shape of the barge hull. The panel model defining the hull geometry is created in Genie and then exported to

HydroD through a .FEM file. The structural model is created and exported in the same manner, except the structural model includes the tank walls and internal tank pressures as well as the hull to define the ballast tanks.

The 300 feet barge is based on the standard North Sea barge UR109, property of Ugland Shipping. The 400 feet barge is based on the barge H-404 of Heerema Marine Contractors, while the 600 feet barge is modelled as Saipem's S600 barge. The dimensions and lightship data for the three barges can be seen in Appendix A.

7.2 Mass modelling

The complete mass model for the system is found from three contributions:

- Lightship model – given by Aker Solutions
- Module weight - calculated manually (own inertia) and in Genie (global inertia)
- Ballast - calculated in HydroD

The mass and inertia data for the lightship and the mass data for the modules are provided by Aker Solutions. The inertia moments for the modules are calculated using the evenly distributed mass assumption. The given barge lightship inertia moments are also calculated in this manner. However, to account for concentration of weight along the sides and aft/forward, the barge lightship radii of gyration are multiplied with a factor of 1.2. This means that the inertia moments calculated from the evenly mass distribution assumption are multiplied by $1.22^2 = 1.44$.

The mass model for the lightship and the module are combined in Genie. The module mass is added as a generic point mass in the module COG with its own inertia calculated manually. The combined lightship/module mass model is calculated and input in HydroD. The mass and inertia of the ballast is added in HydroD and thus the loading condition can be determined.

It would have been sufficient to calculate the combined barge/module mass model in i.e. Microsoft Excel, but due to an initial misunderstanding regarding mass model input in HydroD, the Genie model was modelled with correct COG and inertia. In Aker Solutions' calculations, no coupling inertia is calculated. For this analysis however, a small coupling moment of inertia, I_{xz}, calculated from the Genie model, was included.

7.3 Coordinate systems

The input coordinate system for the model in Genie and HydroD has origo placed midship at the keel on the centreline. The X-axis is positive in the aft direction, the Y-axis is positive in the starboard direction and the Z-axis is positive in the vertical upwards direction. All input data are given in the input coordinate system except for the points for calculation of acceleration RAOs in Postresp.

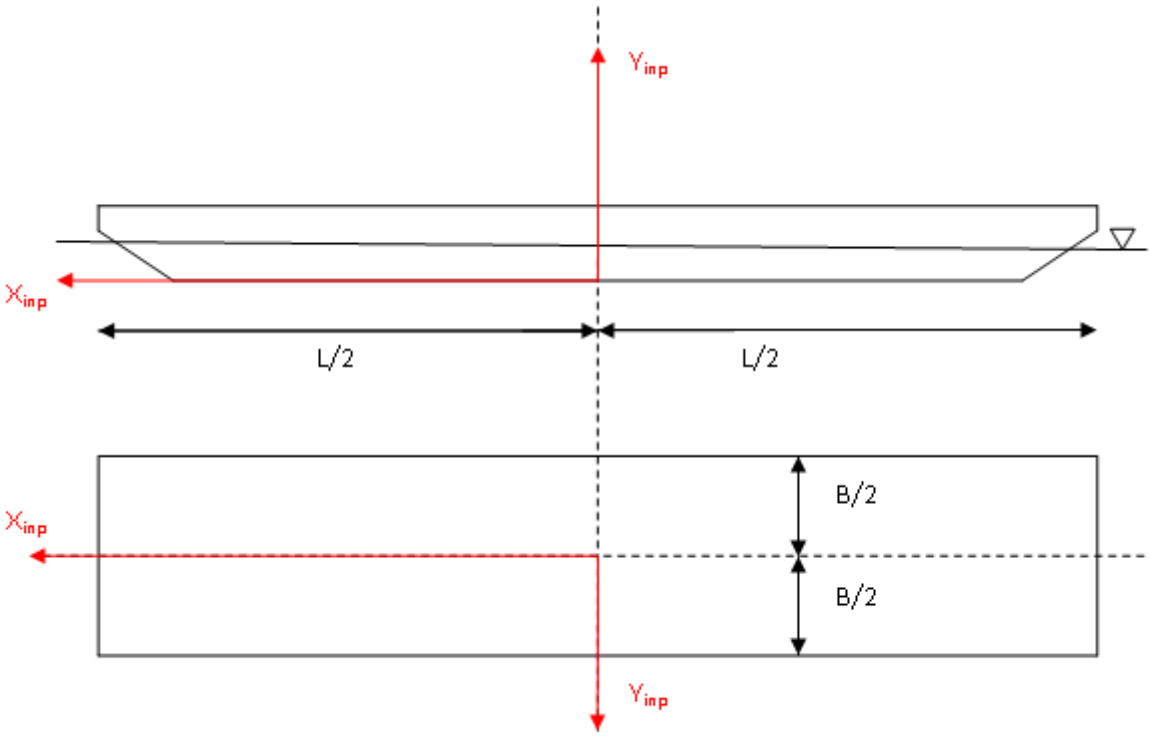

Figure 7-1: Input coordinate system

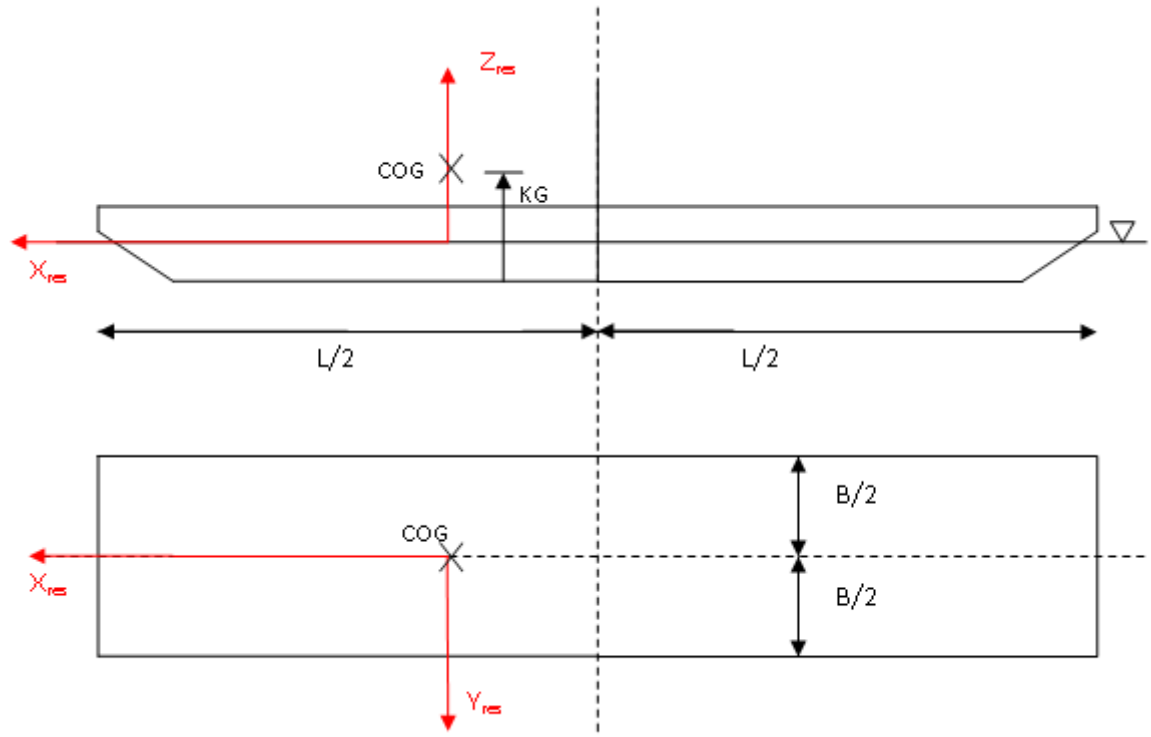

Figure 7-2: Result coordinate system

The result coordinate system, giving motion responses, has origo in the projection of the COG at the waterline, thus meaning the COG is in most of the present cases just shifted slightly aft of midship and up from the keel to the waterline (mean draught).

7.4 Loading conditions

Stability calculations are not part of the scope for this work. However, hydrostatic calculations are needed to find a reasonable waterline or loading condition to use in the hydrodynamic calculation. Factors such as draught and GM may have a large effect on accelerations and motions of the barge, thus it is important that these values are realistic. The loading conditions used in this work are based on examples provided by Aker Solutions. A small positive trim ($0.2^o - 0.4^o$) is desirable.

The hydrostatic calculations were performed in HydroD, using mass- and inertia data for the barge lightship and the module weight combined. In practice, as the mass model is given, the ballast determines the equilibrium position. The tanks were either set to be full or to have 2% filling, and from trying different combinations, a reasonable loading condition was achieved. The 2% filling of the remaining tanks is to account for residual water and adds a free surface effect.

The ballast is placed aft, forward and on the sides of the barge as that increases the system mass moment of inertia, thus making the rotational accelerations (roll, pitch, yaw) slower. This is also a safer alternative with respect to collision and potential flooding of tanks, as the tanks inflicted by a collision will already be filled and there will be no additional heeling/trimming moment.

The load is assumed to have an evenly distributed mass and is placed with 40% of the length forward of the midship and 60% of the length aft of the midship, thus the load COG is located $0.1L_{module}$ aft of the midship

Using the complete model of the lightship with tank arrangement, the .FEM file for the panel model and tank configuration is produced. This file along with the mass data calculated in Excel will represent the barge in HydroD.

7.4.1 300 feet barge

7.4.1.1 1000 tonne load

The resulting loading condition can be seen in Table 7-4 and Figure 7-4.

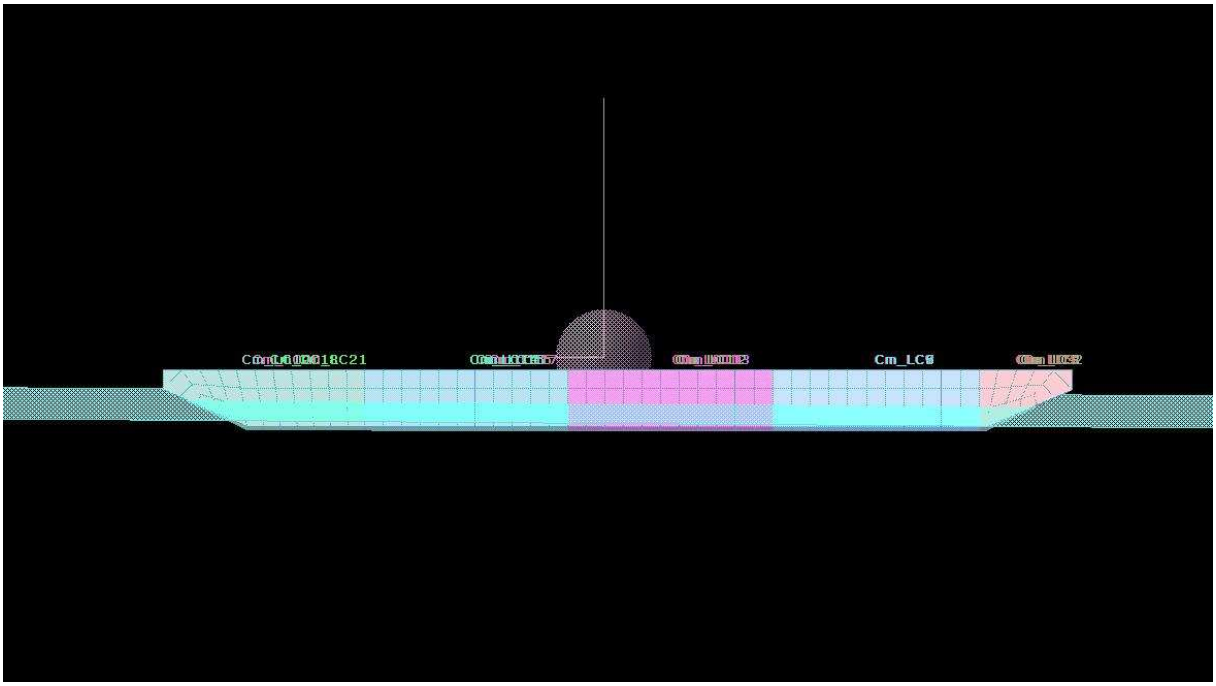

Figure 7-3: HydroD view, case B3L1

Total displacement, Δ	6263 t
Lightship weight, W_{LS}	1830 t
Ballast weight, $W_{BALLAST}$	3433 t
Module weight, W_{MOD}	1000 t
System centre of gravity, COG_{SYS}	(1.48 m, 0 m, 4.98 m)
Mean draught, D_{mean}	2.78 m = 45.6 %
Trim	0.36 ^{o}
Draught at stern, D_{stern}	3.07 m
Draught at bow, D_{bow}	2.49 m
Radius of gyration about X-axis, K_{xx}	10.63 m
Radius of gyration about Y-axis, K_{yy}	28.47 m
Radius of gyration about Z-axis, K_{zz}	29.49 m

Table 7-4: Loading condition, B3L1

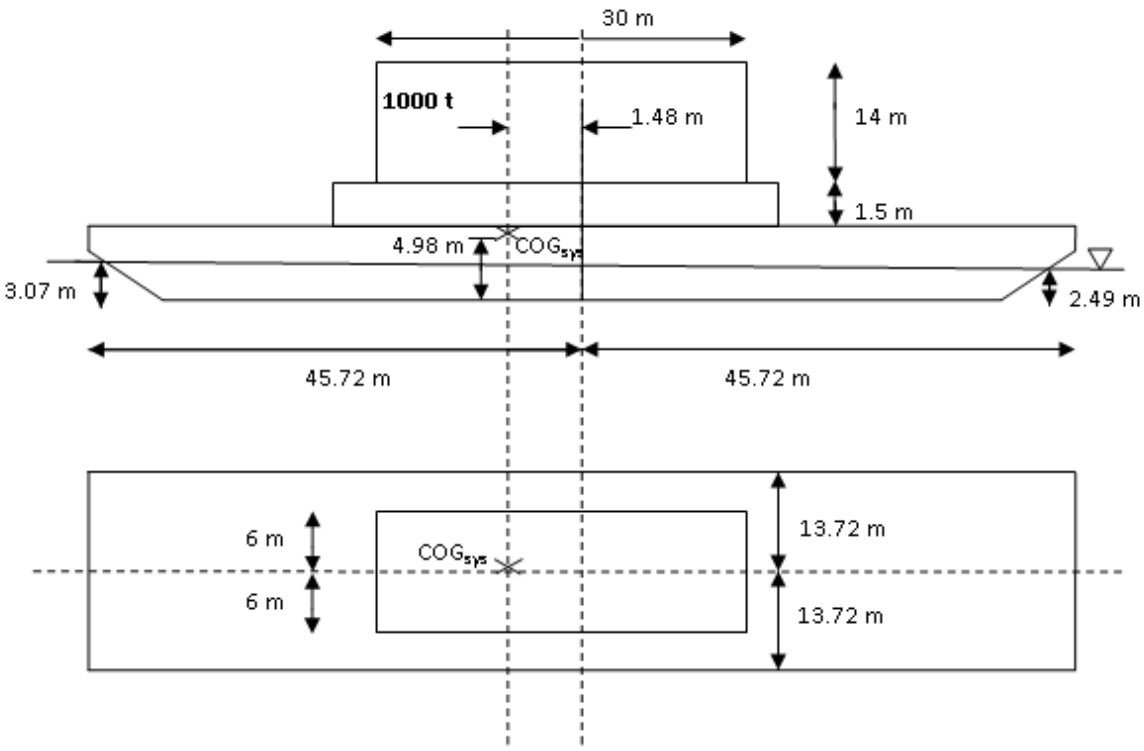

Figure 7-4: Loading condition for case B3L1

7.4.1.2 3000 tonne load

The resulting loading condition can be seen in Table 7-5 and Figure 7-6.

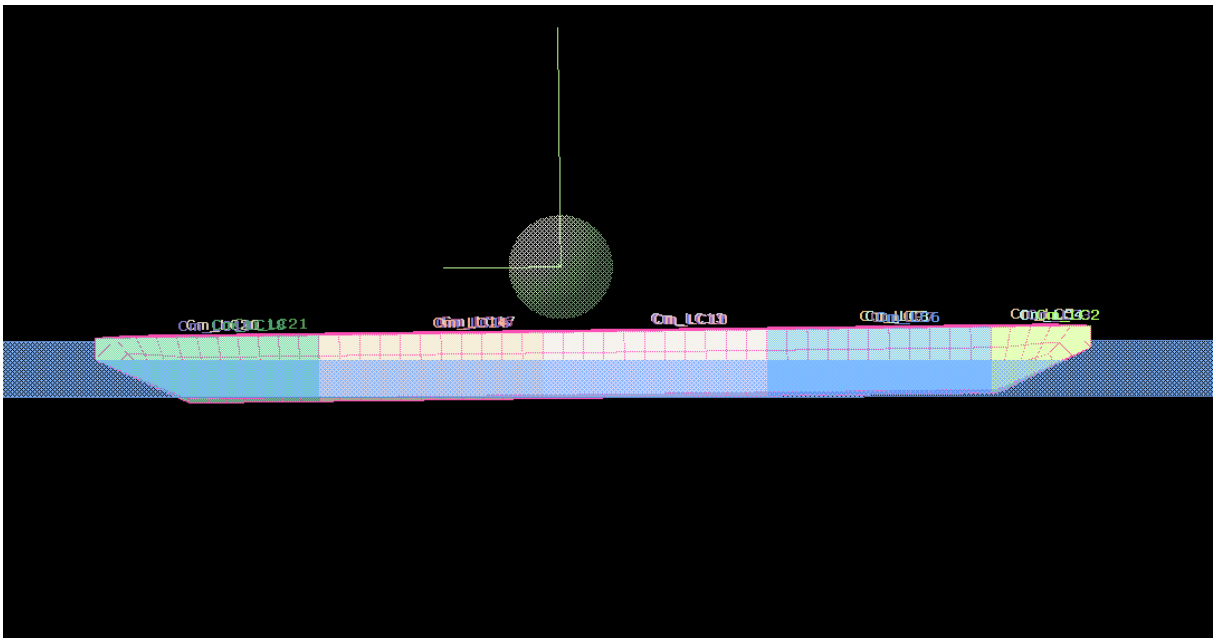

Figure 7-5: HydroD view, case B3L3

Total displacement, Δ	8263 t
Lightship weight, W_{LS}	1830 t
Ballast weight, $W_{BALLAST}$	3433 t
Module weight, W_{MOD}	3000 t
System centre of gravity, COG_{SYS}	(2.244 m, 0 m, 8.402 m)
GM	11.83 m
Mean draught, D_{mean}	3.59 m = 58.85 %
Trim	0.66 ^{o}
Draught at stern, D_{stern}	4.13 m
Draught at bow, D_{bow}	3.07 m
LCF	1.05 m

Table 7-5: Loading condition, B3L3

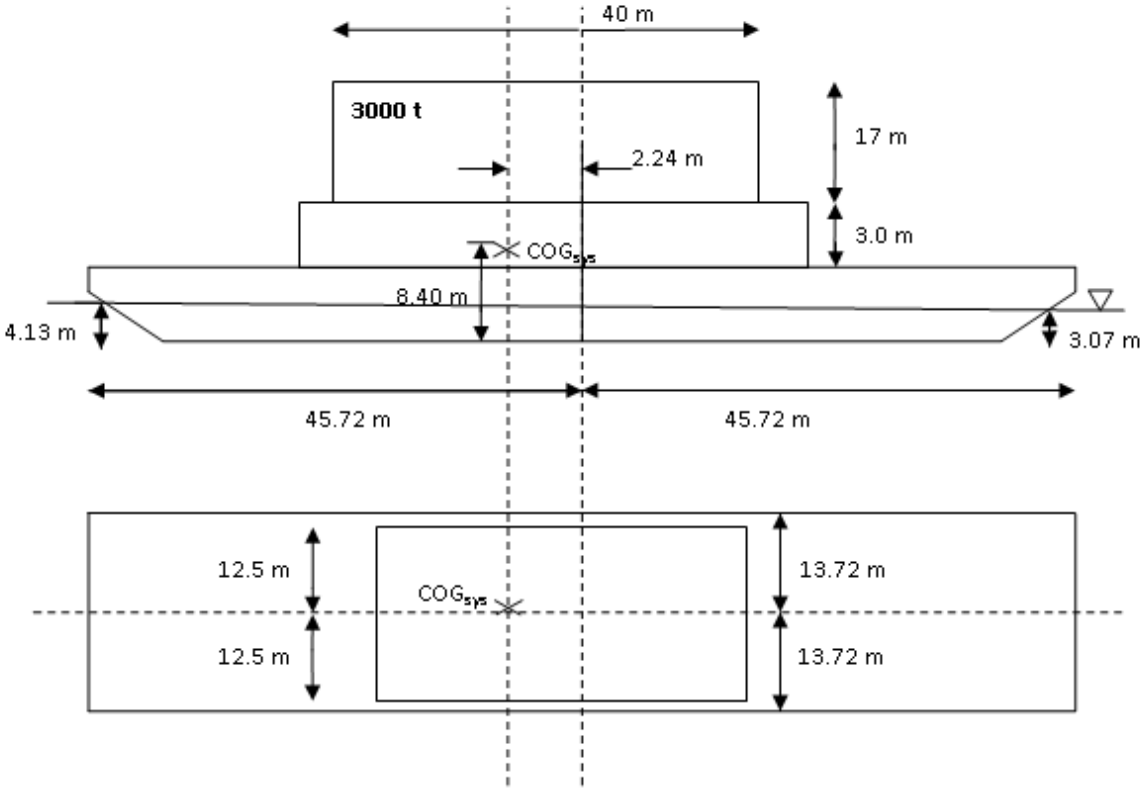

Figure 7-6: Loading condition for case B3L3

7.4.2 400 feet barge

7.4.2.1 1000 tonne load

The resulting loading condition can be seen in Table 7-6 and Figure 7-8.

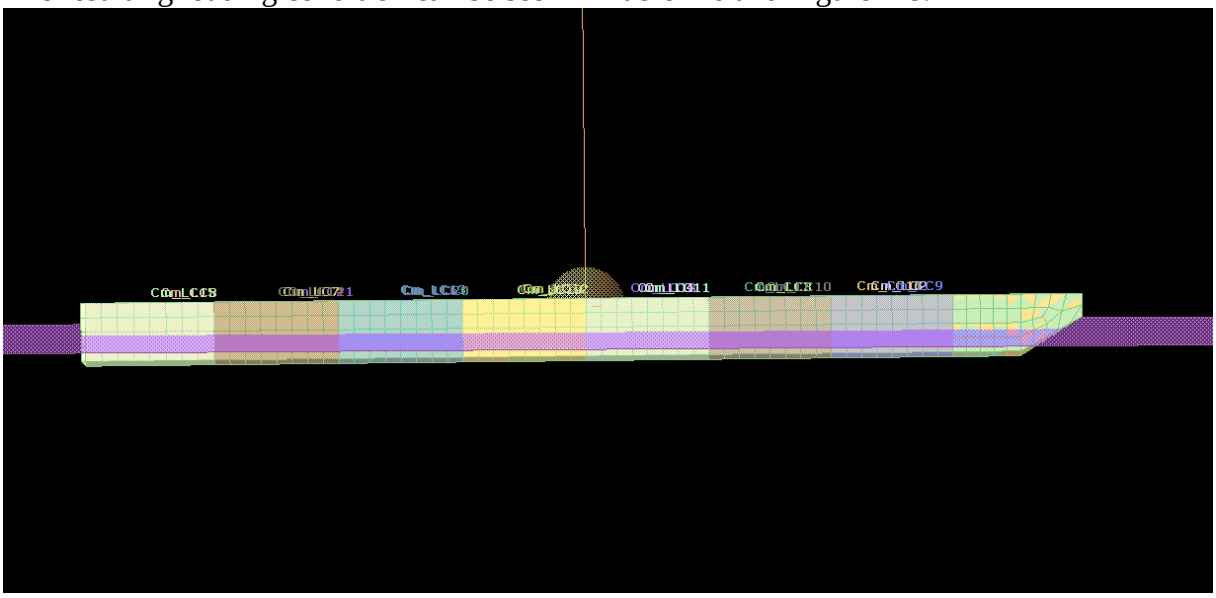

Figure 7-7: HydroD view, case B4L1

Total displacement, Δ	16128.7 t
Lightship weight, W_{LS}	3960 t
Ballast weight, $W_{BALLAST}$	11168.7 t
Module weight, W_{MOD}	1000 t
System centre of gravity, COG_{SYS}	(3.46 m, 0 m, 4.59 m)
Mean draught, D_{mean}	3.67 m = 48.3 %
Trim	0.20 ^{o}
Draught at stern, D_{stern}	3.88 m
Draught at bow, D_{bow}	3.45 m
LCF (aft of midship)	1.05 m
GM	25 m

Table 7-6: Loading condition, case B4L1

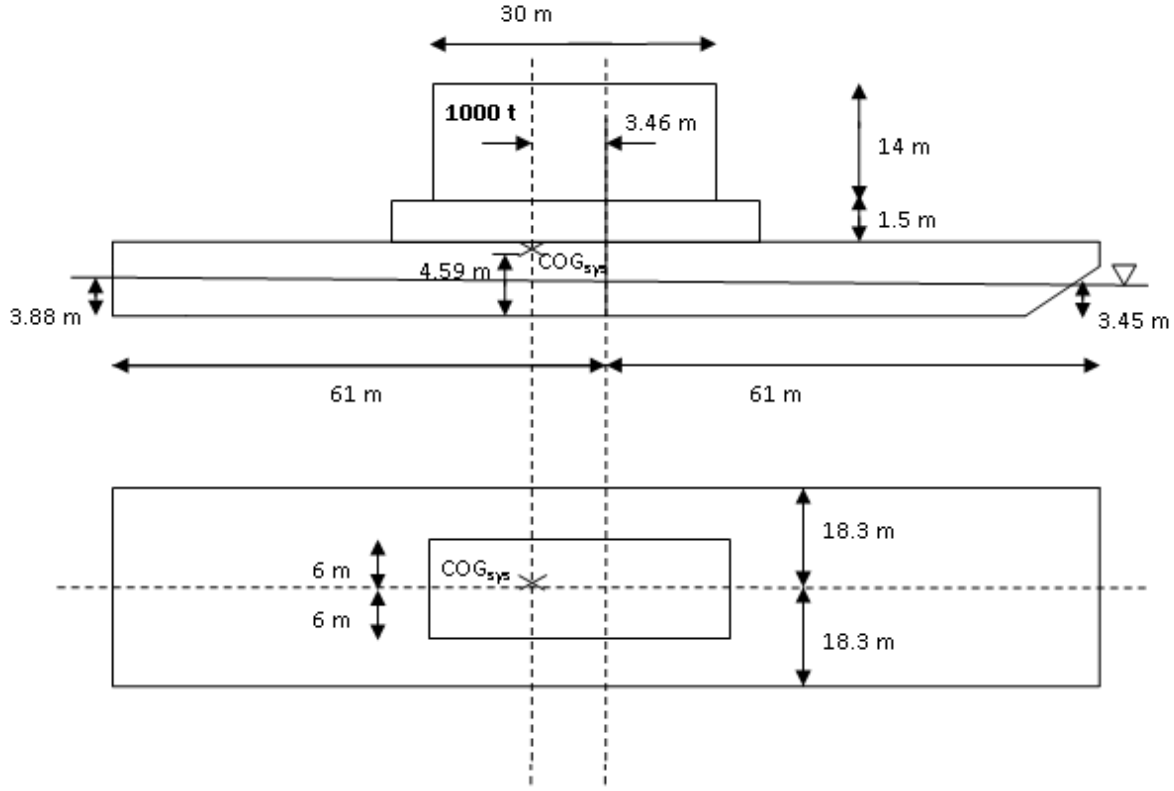

Figure 7-8: Loading condition for case B4L1

7.4.2.2 5000 tonne load

The resulting loading condition can be seen in Table 7-7 and Figure 7-10.

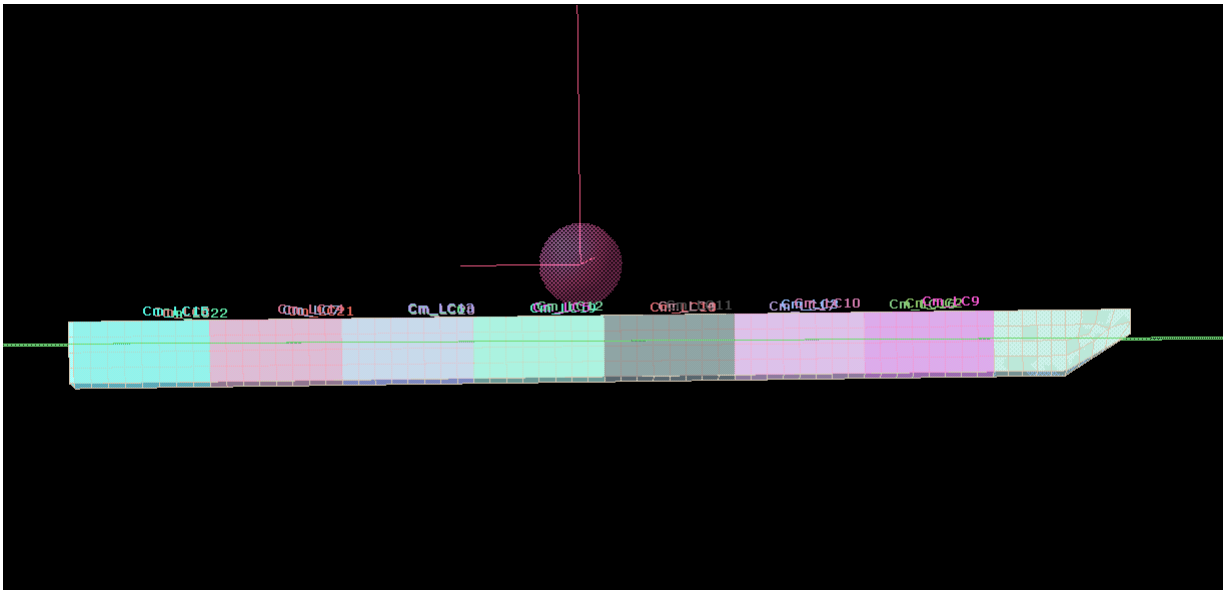

Figure 7-9: HydroD view, case B4L5

Total displacement, Δ	20129 t
Lightship weight, W_{LS}	3960 t
Ballast weight, $W_{BALLAST}$	11169 t
Module weight, W_{MOD}	5000 t
System centre of gravity, COG_{SYS}	(3.751 m, 0 m, 8.241 m)
Mean draught, D_{mean}	4.56 m = 60 %
Trim	0.38 ^{o}
Draught at stern, D_{stern}	4.97 m
Draught at bow, D_{bow}	4.16 m
LCF	0.50 m
GM	16.49 m

Table 7-7: Loading condition, case B4L5

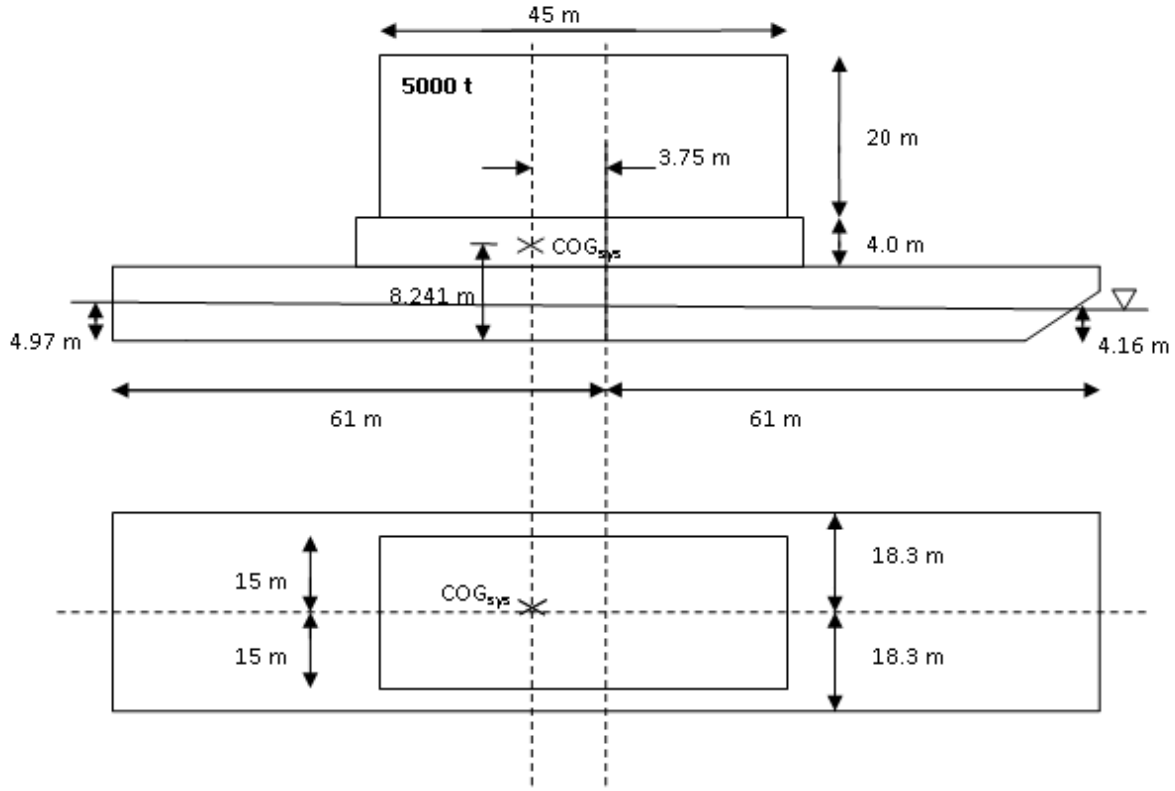

Figure 7-10: Loading condition for case B4L5

7.4.3 600 feet barge

7.4.3.1 5000 tonne load

The resulting loading condition can be seen in Table 7-8 and Figure 7-12.

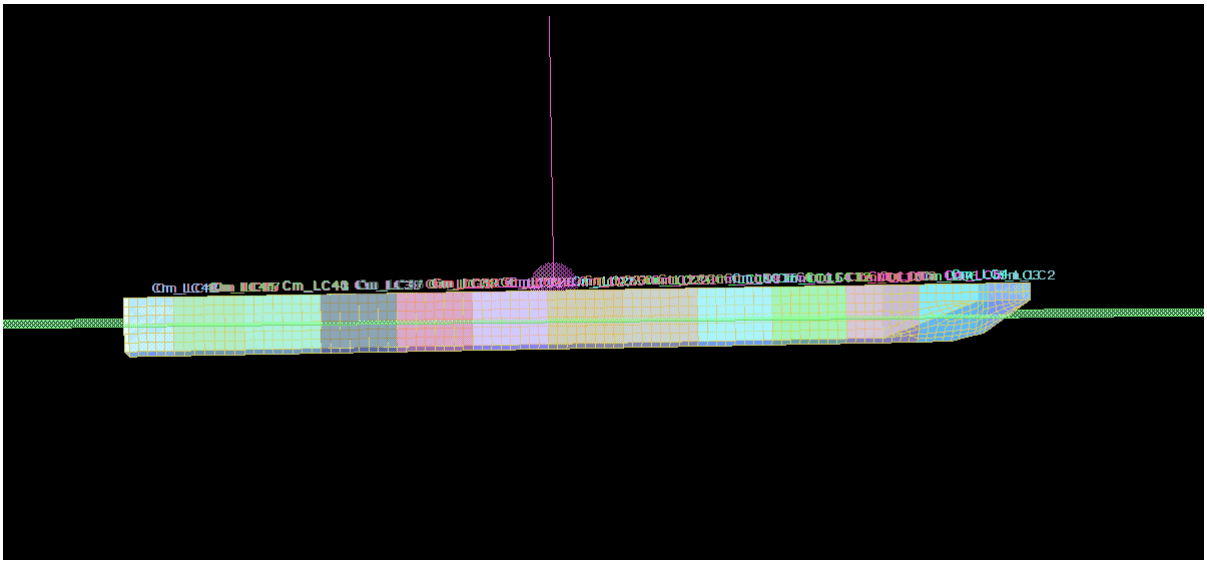

Figure 7-11: HydroD view, case B6L5

Total displacement, Δ	50436.3 t
Lightship weight, W_{LS}	10870.2 t
Ballast weight, $W_{BALLAST}$	34566.1 t
Module weight, W_{MOD}	5000 t
System centre of gravity, COG_{SYS}	(8.464 m, 0 m, 7.927 m)
Mean draught, D_{mean}	6.06 m = 52.3 %
Trim	0.41 ^{o}
Draught at stern, D_{stern}	6.69 m
Draught at bow, D_{bow}	5.38 m
LCF	3.41 m
GM	24.56 m

Table 7-8: Loading condition, case B6L5

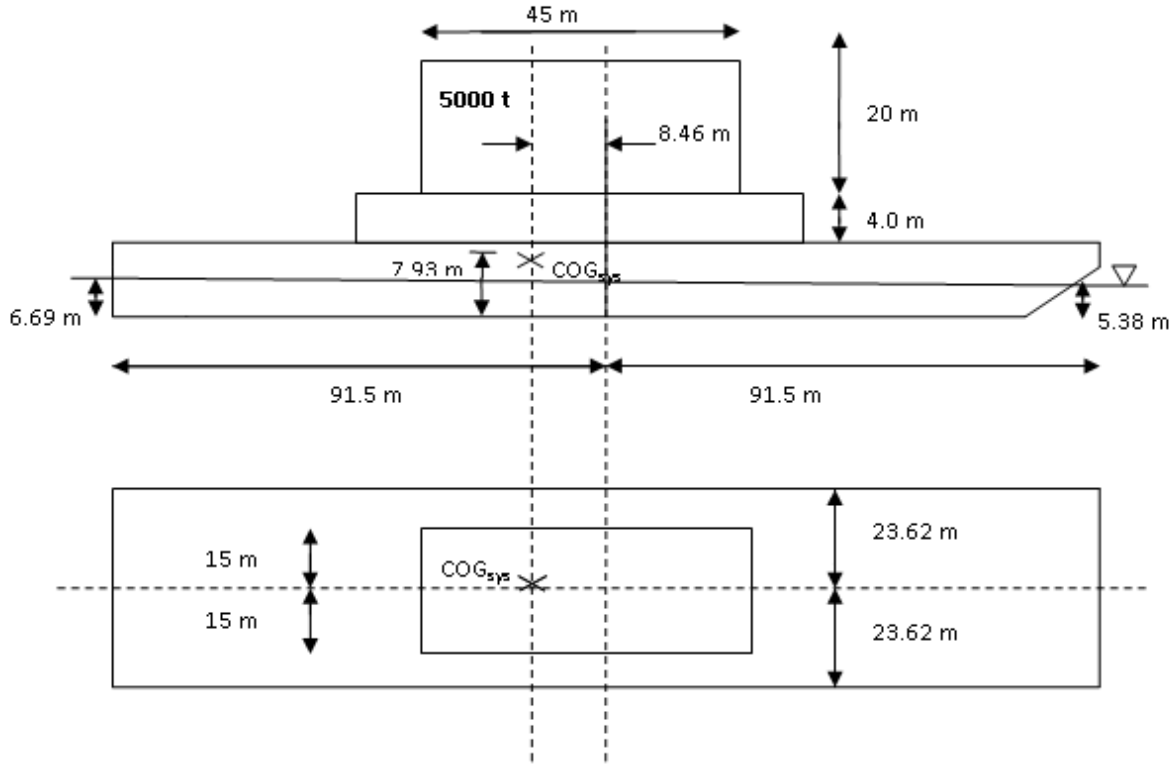

Figure 7-12: Loading condition for case B6L5

7.4.3.2 8000 tonne load

The resulting loading condition can be seen in Table 7-9 and Figure 7-14.

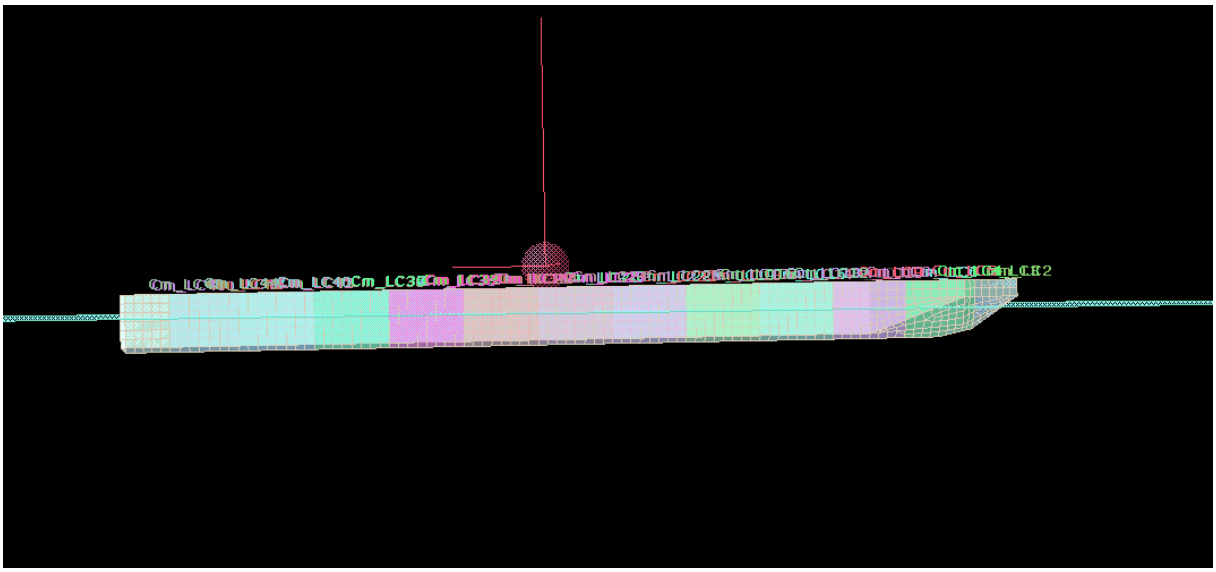

Figure 7-13: HydroD view, case B6L8

Total displacement, Δ	56405.5 t
Lightship weight, W_{LS}	10870.2 t
Ballast weight, $W_{BALLAST}$	37535.3 t
Module weight, W_{MOD}	8000 t
System centre of gravity, COG_{SYS}	(7.110 m, 0.004 m, 9.256 m)
Mean draught, D_{mean}	6.76 m = 55.3 %
Trim	0.30 ^{o}
Draught at stern, D_{stern}	7.22 m
Draught at bow, D_{bow}	6.27 m
LCF	2.84 m
GM	20.64 m

Table 7-9: Loading condition, case B6L8

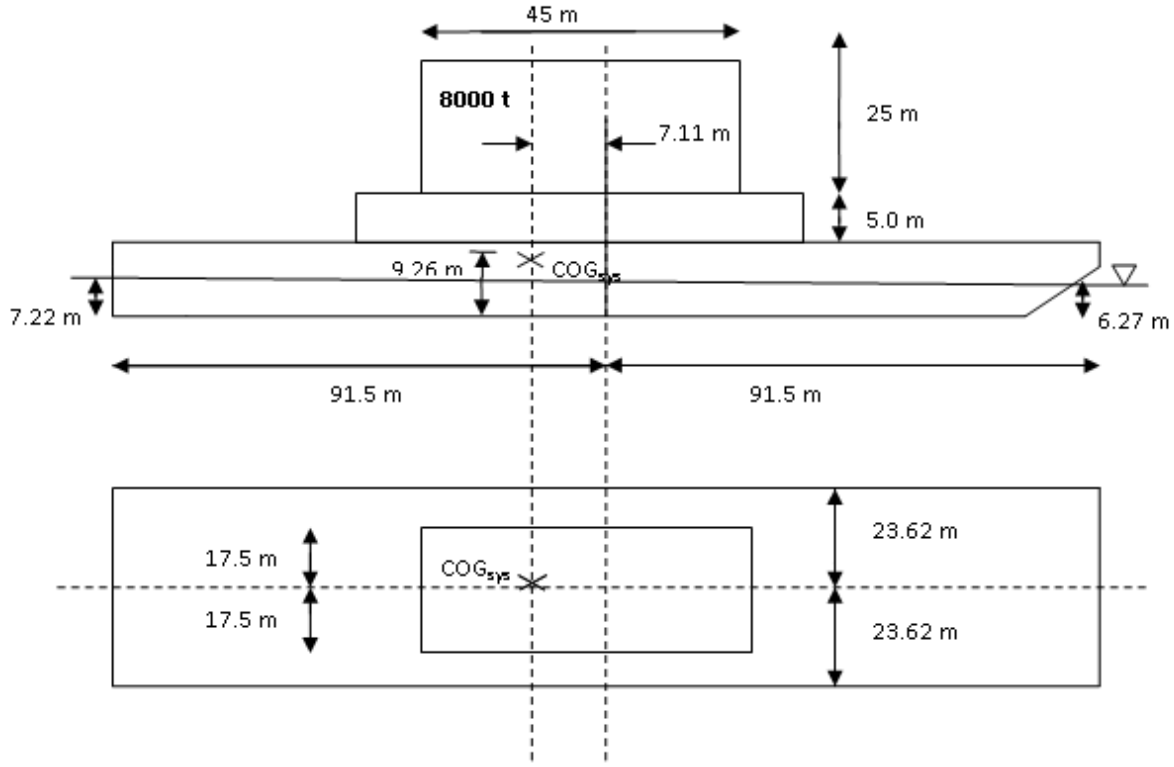

Figure 7-14: Loading condition for case B6L8

7.5 Environmental conditions (Wadam/HydroD)

7.5.1 Waveheading interval

The transfer functions of the barge are calculated with a 30^{o} spacing between the waveheadings, starting at -180^{o} and ending at 150^{o}(see Figure 7-15). This is considered sufficient to find the maximum accelerations.

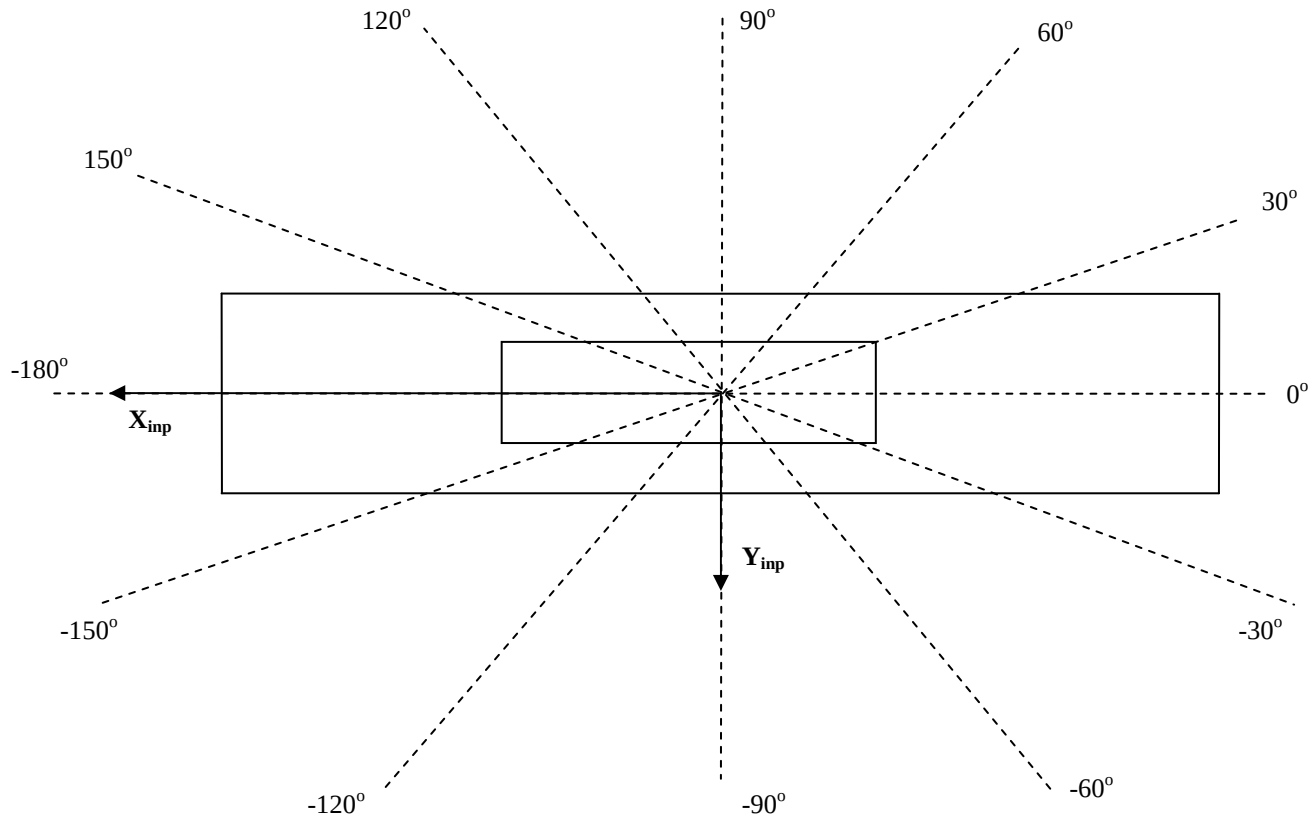

Figure 7-15: Waveheadings for calculation of motion

7.5.2 Frequency interval

The response due to single linear waves are calculated at 52 wave frequencies in the interval ω = 0.3 - 2.4 rad/s (T = 2.62 - 20.94 s). The calculation density is higher in the area ω = 0.8 – 1.0 rad/s (T = 6.28 – 7.85 s) where most of the resonance effects occur.

For the cases with high eigenperiods (ω < 0.8 rad/s) it should be noted that the density of frequencies may be slightly scarce with steps of 0.05 rad/s.

7.5.3 Water and location properties

Water density (ρ)	1025 kg/m^3
Water kinematic viscosity (υ)	1.19x10^{-6} m^2/s
Water depth (h)	300 m

Table 7-10: Water environment

7.6 Module arrangement and points for response calculation

The modules are in all cases placed with 60 % of their length aft of midship, meaning the module COG is 10 % of the module length aft of the midship as we assume the module density evenly distributed.

The accelerations are calculated in six points. These are the system COG, the module COG and the top and bottom corners of the module on the port side (see Table 7-11 and Figure 7-16).

Point notation	Description
A1	System centre of gravity (COG_{SYS})
B1	Module centre of gravity(COG_{MOD})
CAP	Lower aft module corner, port side
CFP	Lower forward module corner, port side
DAP	Upper aft module corner, port side
DFP	Upper forward module corner, port side

Table 7-11: Points for calculating accelerations

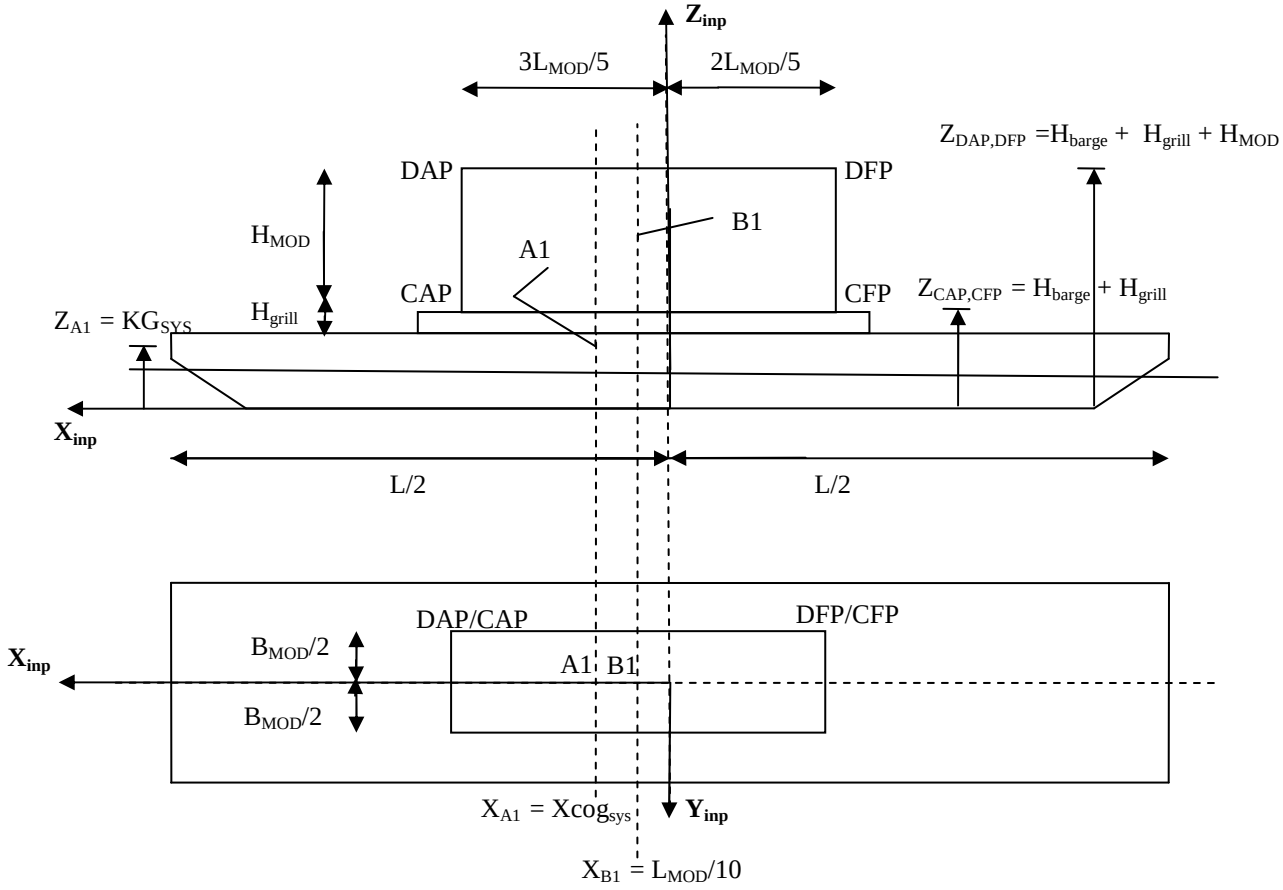

Figure 7-16: Module arrangement and points for calculation of accelerations

The vertical acceleration in the system centre of gravity (A1) is used as global heave acceleration when finding the design accelerations in the body-fixed coordinate system. Points CAP and CFP are the relevant points when it comes to seafastening, placed between the grillage and the module. As the top of the module can be situated high above the centre of rotation, it is convenient to include point DAP and DFP in the calculation of accelerations.

It should be noted that the points for calculation of acceleration are input in Postresp using the result coordinate system (see section 7.3).

7.7 Viscous roll damping – Case B3L1

The first case (B3L1) is to be tested with viscous roll damping, as this damping may have a significant effect on the accelerations and motions of the barge. Including viscous roll damping may thus give more realistic results.

7.8 Mesh density

To find a reasonable mesh density, a convergence test of acceleration values was performed for the first case (B3L1). The barge was analysed for three different meshes as listed in Table 7-12. These are all consisting of quadrilateral elements.

Annotation	Input element size	WADAM computational time [s]
Coarse mesh	5 m x 5 m	30
Medium mesh	2 m x 2 m	60
Fine mesh	0.5 m x 0.5 m	11500

Table 7-12: Meshes densities in convergence test

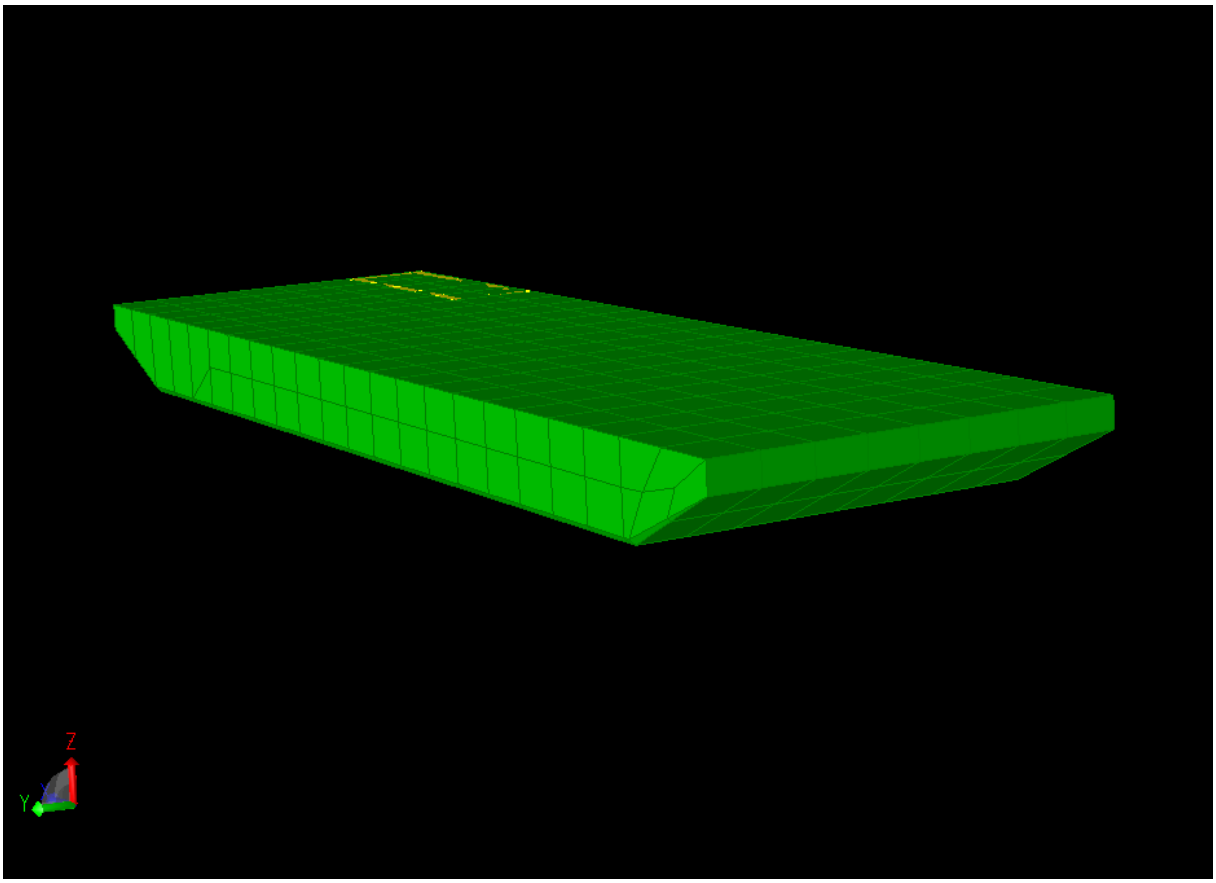

Figure 7-17: Genie model with coarse mesh

The mesh densities listed in Table 7-12 are the input mesh densities. The actual mesh in the panel model exported to HydroD is modified by Genie to fit the model. This normally means that the actual elements are smaller than the input element size. Figure 7-19, Figure 7-20 and Figure 7-21 show the convergence for accelerations in X-,Y- and Z-direction in the point

CAP. The result of the mesh sensitivity analysis for all the design accelerations are shown in Table 7-13.

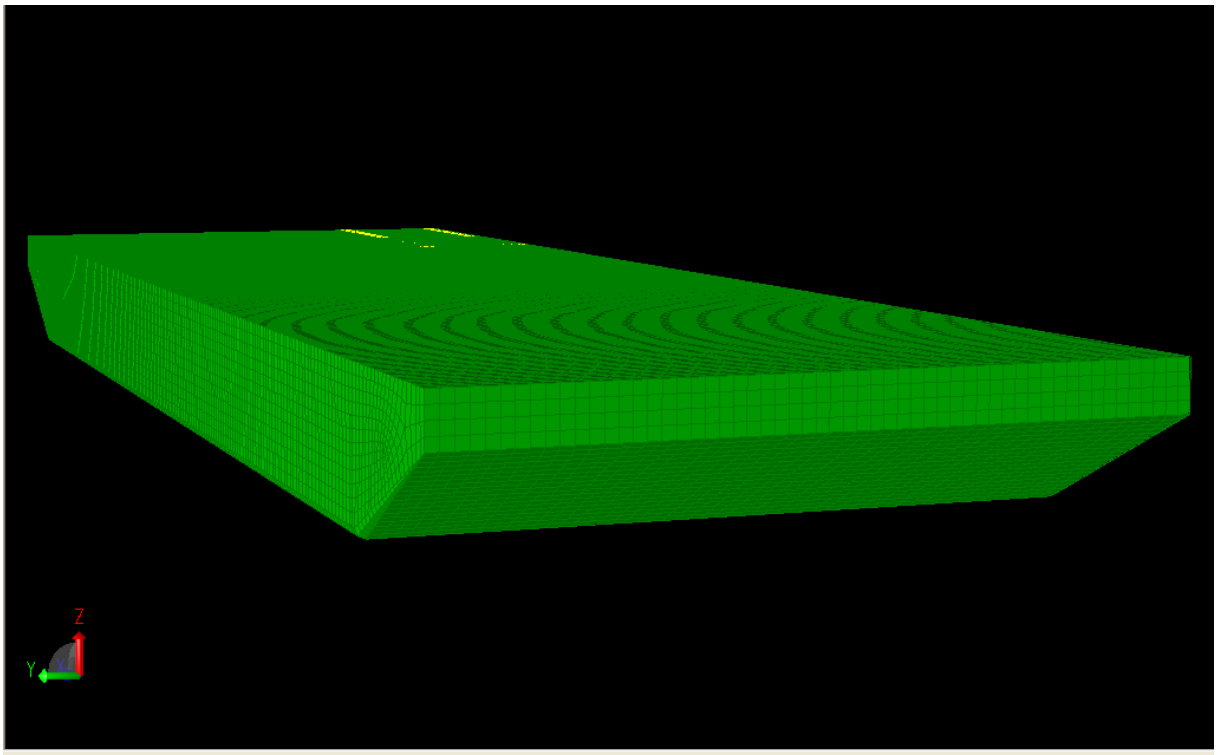

Figure 7-18: Genie model with finest mesh

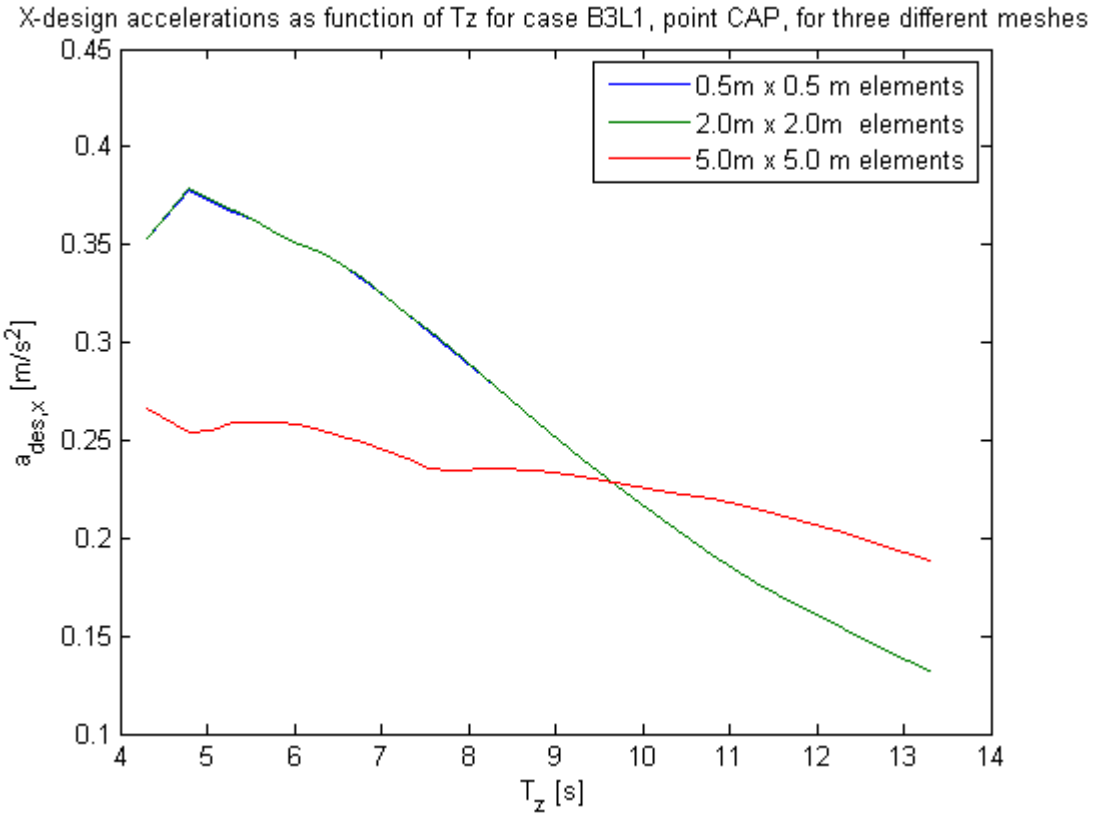

Figure 7-19: Mesh convergence for X-design accelerations in CAP, Hs = 2.0 m

As seen from Figure 7-19, the accelerations in the X-direction are poorly represented with an element size of 5m x 5m. The maximum X-acceleration in point CAP for H_s = 2.0 m for the coarse mesh is only 70 % of the same acceleration with the fine mesh. It seems that the coarse mesh switches to being more conservative for higher zero-crossing periods, but as the maximum accelerations occur for the lower T_z in the interval, a finer mesh is desirable.

Comparing the two finer meshes however, we have almost absolute convergence. There is virtually no difference in X-acceleration between 2 meters and 0.5 meters element side length. Considering the significant increase in computational time for the finest mesh, this is a great advantage.

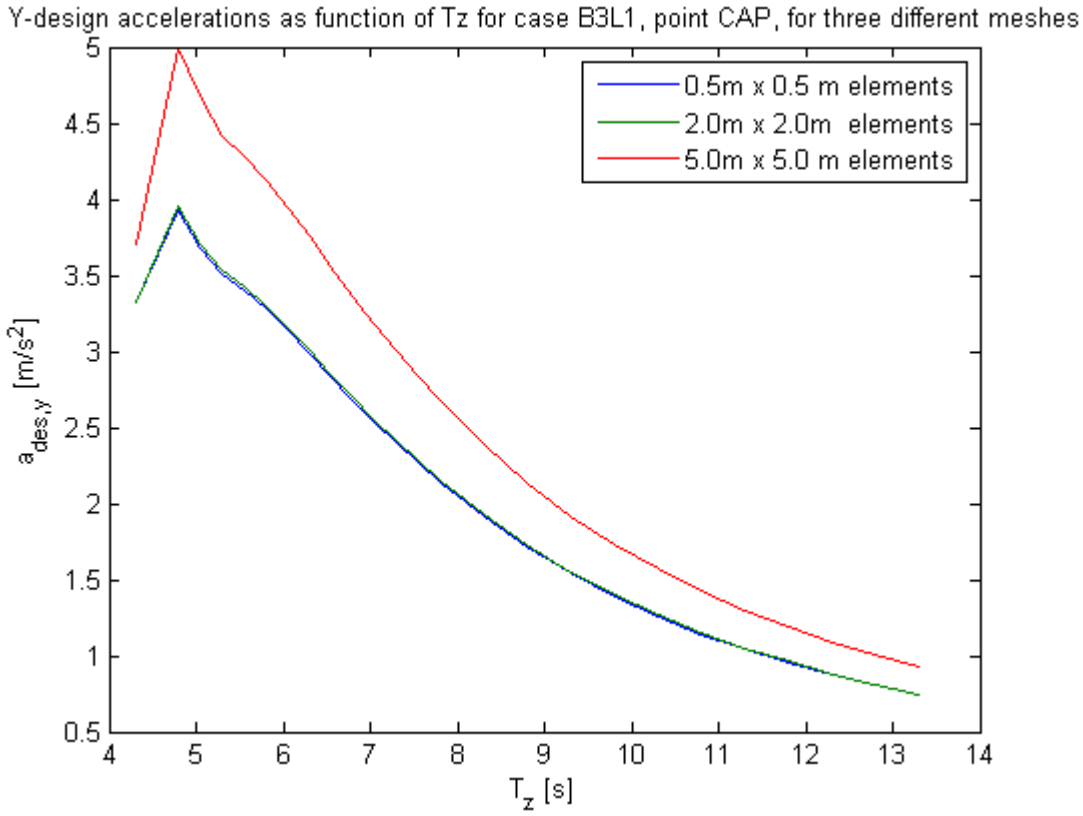

Figure 7-20: Mesh convergence for Y-design accelerations in CAP, Hs = 2.0 m

Regarding the Y-accelerations, we see that a coarser mesh is consistently more conservative than a finer mesh. The coarse mesh seem to give an overestimation of the maximum acceleration by approximately 30 %, while the medium mesh only overestimates by 0.7 % compared to the finest mesh. Thus the medium mesh seems to give a satisfactory representation of the Y-accelerations, still slightly on the conservative side.

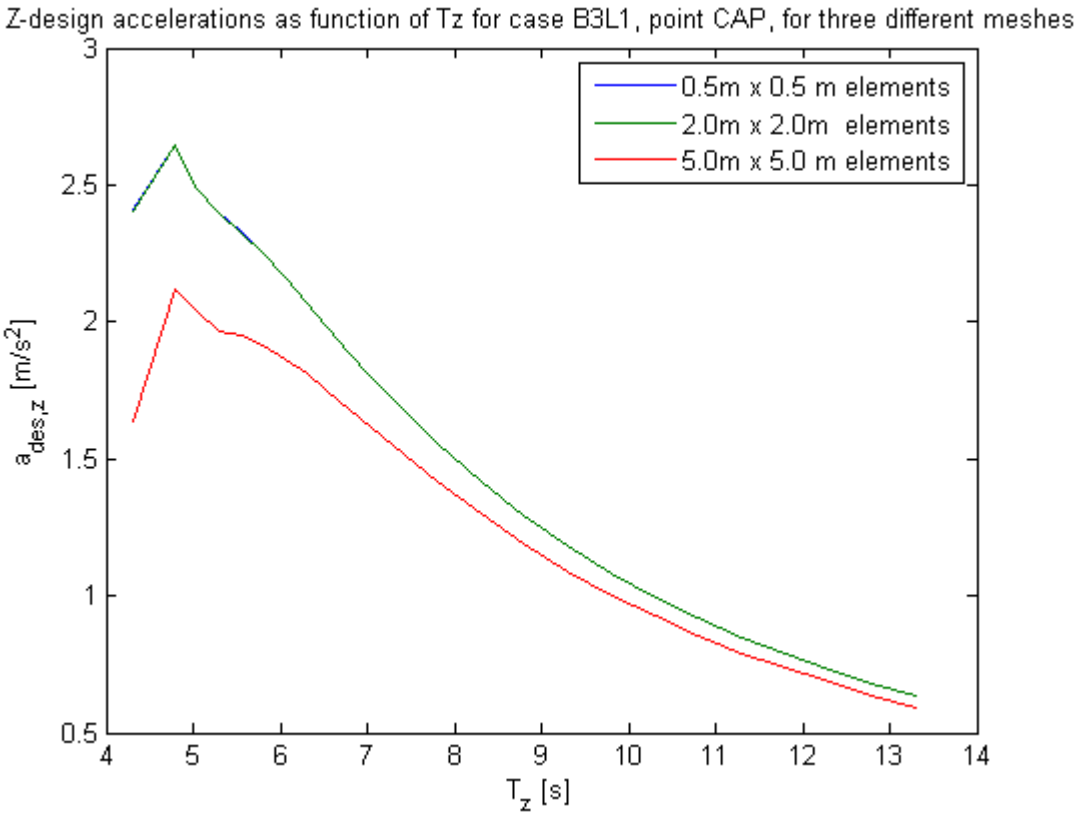

Figure 7-21: Mesh convergence for Z-design accelerations in CAP, Hs = 2.0 m

Looking at Figure 7-21, we see that the Z-acceleration maximum seems to be significantly lower for the coarse mesh, thus a sufficient fineness is required to avoid underestimating the vertical acceleration. However, we see that the medium mesh and the fine mesh have a very good convergence in this direction as well, meaning the medium mesh density should be sufficient.

Looking at all the accelerations for all the points, we see that the reasoning above seem to apply for the rest of the point accelerations. There are some small deviations where the acceleration is slightly larger for the fine mesh than for the medium mesh, but these differences are so small that they can be considered negligible.

Element size [mxm]	Acceleration component	Units	A1	B1	CAP	CFP	DAP	DFP
5x5	X	m/s^2	0.7220	0.4786	0.2660	0.2660	0.7239	0.7239
	Y	m/s^2	2.0100	6.7235	4.9993	4.9159	8.5633	8.4753
	Z	m/s^2	1.3044	1.3103	2.1203	2.1468	2.1202	2.1468
2x2	X	m/s^2	0.3777	0.5859	0.3788	0.3788	0.9173	0.9173
	Y	m/s^2	1.1978	5.8514	3.9574	3.9142	7.7932	7.7494
	Z	m/s^2	1.2215	1.2216	2.6451	2.6478	2.6451	2.6478
0.5x0.5	X	m/s^2	0.3779	0.5851	0.3780	0.3780	0.9159	0.9159
	Y	m/s^2	1.1993	5.8171	3.9284	3.8857	7.7530	7.7095
	Z	m/s^2	1.2224	1.2225	2.6446	2.6469	2.6446	2.6469

Table 7-13: Design accelerations for different meshes, case B3L1

The coarse mesh gave results that in some cases deviated a lot from the finest mesh. The medium mesh gave almost exactly the same results as the fine mesh with an immense reduction in computational time. Thus the clear choice was the mesh with 2m x 2m elements. As this case represents the smallest barge, using the same mesh density for the larger barges should only increase the accuracy of the mesh.

7.9 Statistical analysis (Postresp/MATLAB)

Having written the relevant RAOs to files for Matlab to read, we can calculate the short term response for 3 hour sea states (see chapter 6.6.3). Our goal is to find the design accelerations as a function of sea state (H_s) with a goal of determining the limiting sea state for the transportation.

H_s [m]	T_z – interval [s]	Number of spectra (T_z) per H_s
2.0	4.3 – 13.8	25
2.5	4.3 – 13.8	25
3.0	4.3 – 13.8	25
4.0	4.3 – 13.8	25

Figure 7-22: Wave spectra used in short-term statistics

The JONSWAP wave spectre (see chapter 6.6.2), based on North Sea data, will be used in these analyses. The wave spectra are narrow-banded and of wind sea type, meaning no swell is taken into consideration. The swell is considered non-critical as the eigenperiods of the barges are relatively low ($T_{n,roll}$ = 6 –10 s). Long-crested waves are used for all the seastates.

To find the maximum seastate for a transportation, or to design the seafastening for a given transport, the accelerations in the deck plane (at seafastening height) are the determining factors. In addition, uplift can cause disengaging of the seafastening if it relies on positive downward gravity force. The following criteria from Aker Solutions are to be checked against the design accelerations at the seafastening (points CAP and CFP, Figure 7-16):

- Maximum acceleration in longitudinal direction: $A_{X,\max} = 0.1g = 0.981\frac{m}{s^2}$
- Maximum acceleration in transverse direction: $A_{Y,\max} = 0.25g = 2.452\frac{m}{s^2}$
- Uplift: $A_{Z,\max} = 1.0g = 9.810\frac{m}{s^2}$

8 Analysis procedure

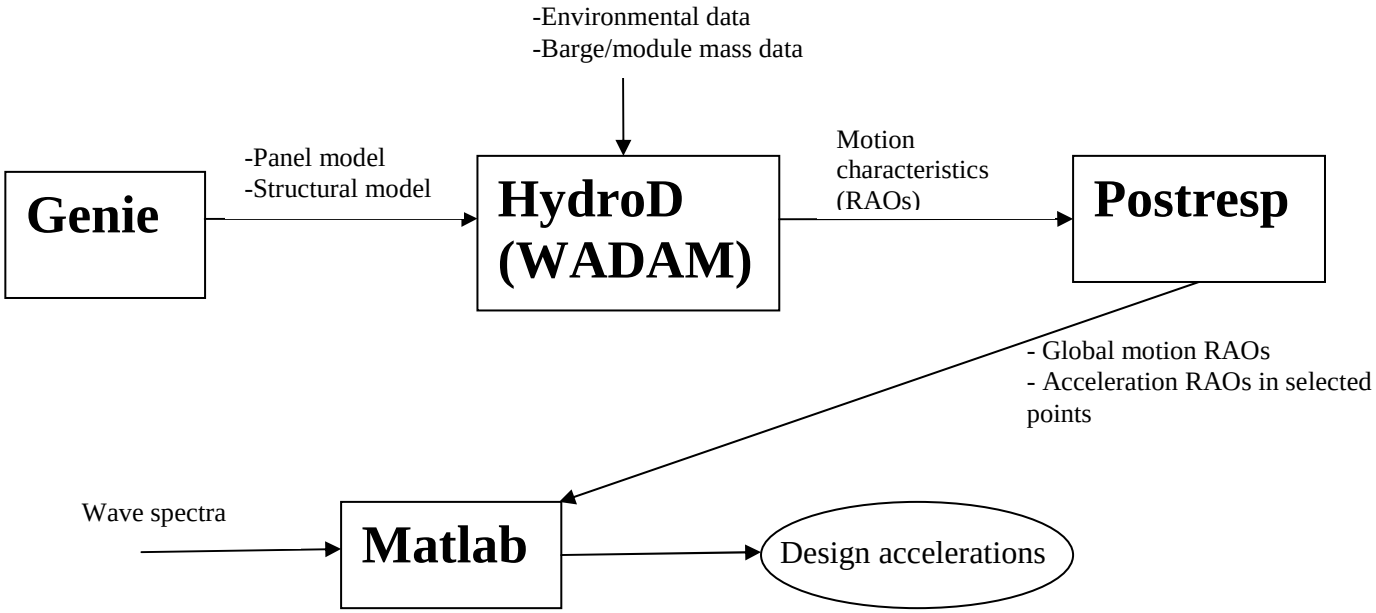

Figure 8-1: Data flow chart

First the panel model (hull geometry) and the structural model (ballast tank arrangement) are produced in Genie. Dummy hydro pressures are defined both for the outer hull and each of the ballast tanks. The mesh is then created with the desired density and the panel model and the structural model are exported to .FEM files. The panel model is superelement number one, while the structural model is superelement number two.

HydroD imports the panel model and the structural model, giving us the barge geometry and ballast tank arrangement. In addition the following parameters are defined in HydroD:

- Wave frequencies for calculation of single wave response
- Wave headings for calculation of response
- Water depth, density and viscosity
- Permeability and filling of ballast tanks
- Mass model for the combined lightship/module system
- Create wave spectra, seastates and estimated maximum roll angles for iteration of viscous roll damping (when viscous roll damping is included)

From the mass model and the ballast tank filling (and permeability) the loading condition is determined. Using the panel model created in Genie, the barge is then analysed using source technique to produce the transfer functions, meaning the response is calculated for single linear waves in the frequency interval specified. The result data from Wadam is opened in Postresp, which combines RAOs to form point acceleration RAOs. RAOs for all modes of motion and point accelerations in x-, y- and z-direction for all the wave directions are then printed to a file. The printed file is then imported to Matlab where a script analyse the barge

motions in various seastates of 3 hours duration (short term statistical analysis) and combine the extreme accelerations to form the design accelerations. Excluding viscous effects, one file is produced per case, but when viscous roll damping is included, one file is printed for each seastate in and close to the roll resonance area.

Statistical calculation of design accelerations in Matlab was compared with a statistical calculation in Postresp where the design accelerations were calculated manually. The results matched, thus the calculation method in Matlab should be in accordance with the Postresp short-term statistics theory.

9 Results

9.1 Results for non-viscous cases

The design accelerations were calculated in the six points as defined in section 7.6. In this section, the extreme accelerations in all points are represented for all significant wave heights for each of the cases.

In general, the accelerations at CAP and CFP are very similar. The same applies for DAP and DFP. The acceleration characteristics of DAP and DFP are also very similar to CAP and CFP, although the magnitude is increased due to the increased distance from the centre of rotation. Due to this, and the focus on seafastening, point CAP has been examined closer with respect to wave period and wave direction.

Further, it must be commented that the frequency density is lower for the lower frequencies ($\omega < 0.8$ s), thus the resonance frequency for the cases with a higher eigenperiod may be underestimated.

9.1.1 Case B3L1 - 300 feet barge, 1000 tonne module

H_s [m]	Acceleration component	Units	A1	B1	CAP	CFP	DAP	DFP
2.0	X	m/s^2	0.38	0.59	0.38	0.38	0.92	0.92
	Y	m/s^2	1.20	5.85	3.96	3.91	7.79	7.75
	Z	m/s^2	1.22	1.22	2.65	2.65	2.65	2.65
2.5	X	m/s^2	0.48	0.78	0.51	0.51	1.22	1.22
	Y	m/s^2	1.68	7.99	5.45	5.40	10.59	10.53
	Z	m/s^2	1.59	1.59	3.58	3.58	3.58	3.58
3.0	X	m/s^2	0.58	0.97	0.64	0.64	1.51	1.51
	Y	m/s^2	2.22	10.44	7.16	7.08	13.80	13.72
	Z	m/s^2	1.96	1.96	4.46	4.46	4.46	4.46
4.0	X	m/s^2	0.78	1.38	0.91	0.91	2.10	2.10
	Y	m/s^2	3.55	15.29	10.63	10.52	20.05	19.95
	Z	m/s^2	2.66	2.66	6.19	6.19	6.19	6.19

Table 9-1: Design accelerations, case B3L1

The analysis of the first case gave the design accelerations shown in Table 9-1. As we can see, the accelerations are quite large in the Y-direction. If we compare to the given criteria for accelerations in the Y-direction at CAP and CFP (see section 7.9), the limit is breached already at $H_s = 2.0$ m with Y-accelerations of about 0.4*g*. The accelerations in the longitudinal direction are relatively small, not breaching the criterion of 0.1*g* even at 4.0 m significant wave height. The vertical accelerations seem to be well below the limit of 1*g*, thus the risk of uplift forces is small.

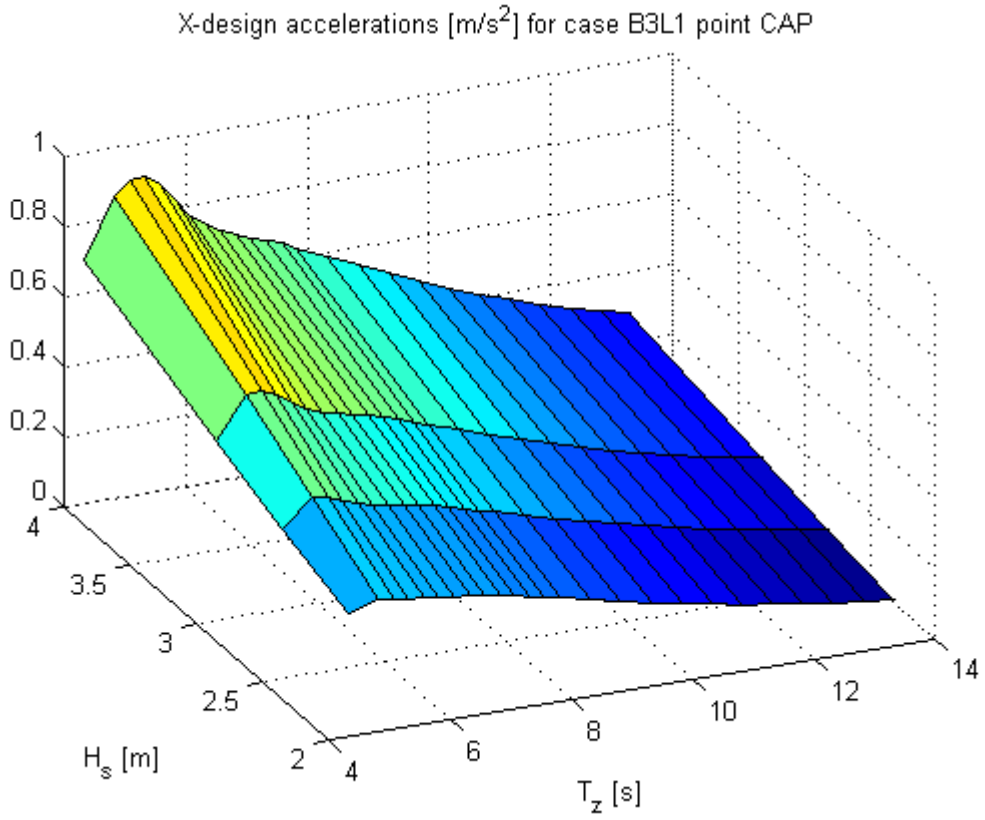

Figure 9-1: X-design acceleration in CAP, case B3L1

As seen in Figure 9-1, the maximum X-acceleration occurs for T_z = 4.5 – 5.5 s. This is equivalent to a peak period of about 6.6 seconds. The zero-crossing period for maxima shifts slightly to the right with increasing H_s. This is due to the change in peakedness(γ), meaning the difference between T_z and T_p decreases with increasing H_s (see section 6.6.2). The value of the design acceleration seems to increase almost linearly with H_s.

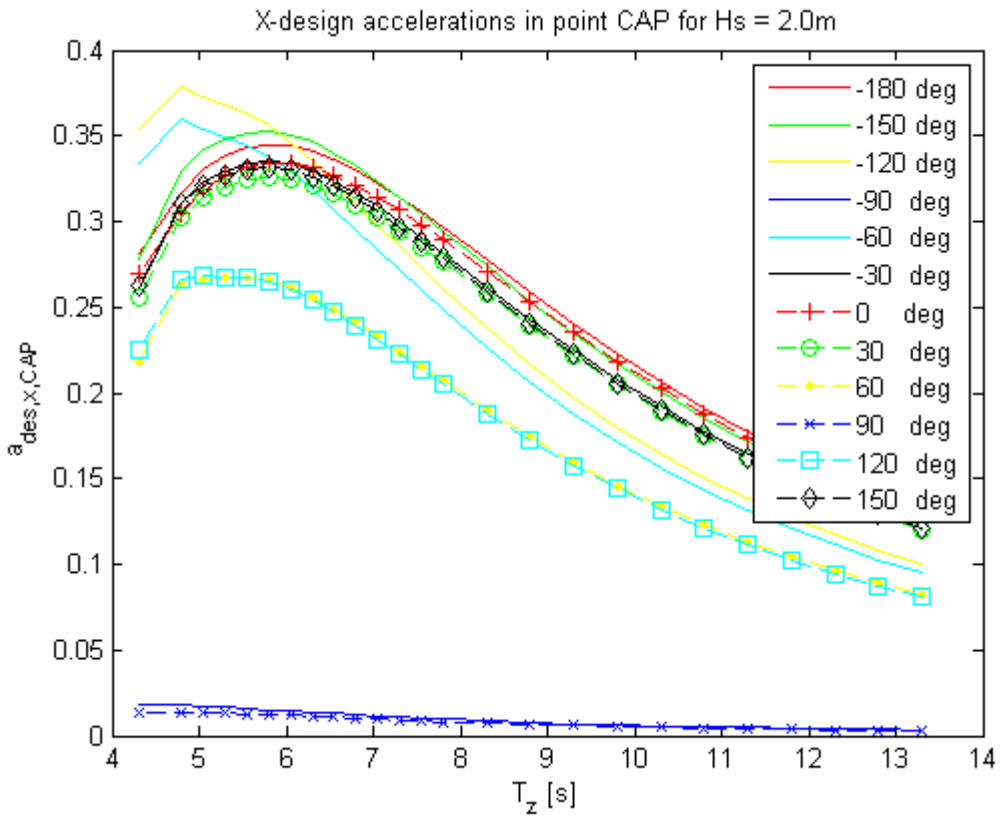

Figure 9-2: X-design acceleration for all waveheadings, case B3L1, Hs = 2.0 m

The acceleration in the X-direction is assumed to be surge, pitch and yaw dominated. The peak period that gives maximum response is neither at the surge resonance, nor at the pitch resonance, but close to the yaw resonance period (see Appendix B). This, and looking at Figure 9-2, where wave direction giving maximum acceleration in X-direction varies with period, understates that the maximum acceleration is a complex combination of surge, yaw and pitch motion. Looking at the wave directions giving the largest response, it seems that the yaw motion (-120^o) dominates for lower periods while the pitch and surge motion (0^o/-180^o, head/following sea) dominate for higher periods.

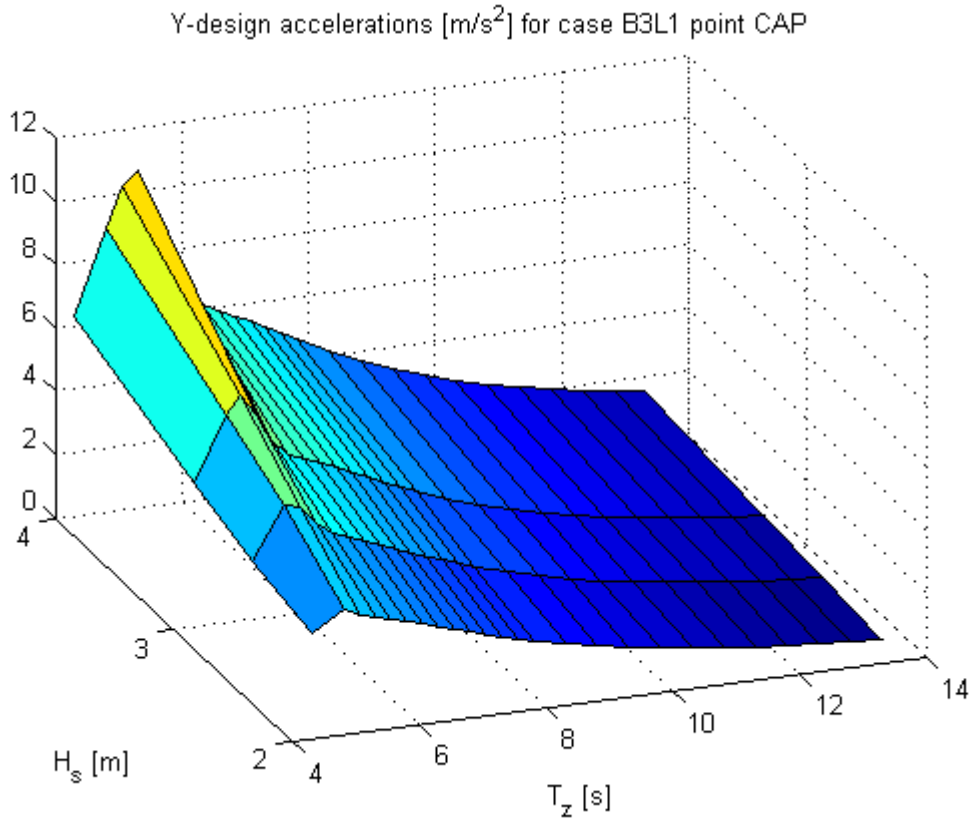

Figure 9-3: Y-design acceleration in CAP, case B3L1

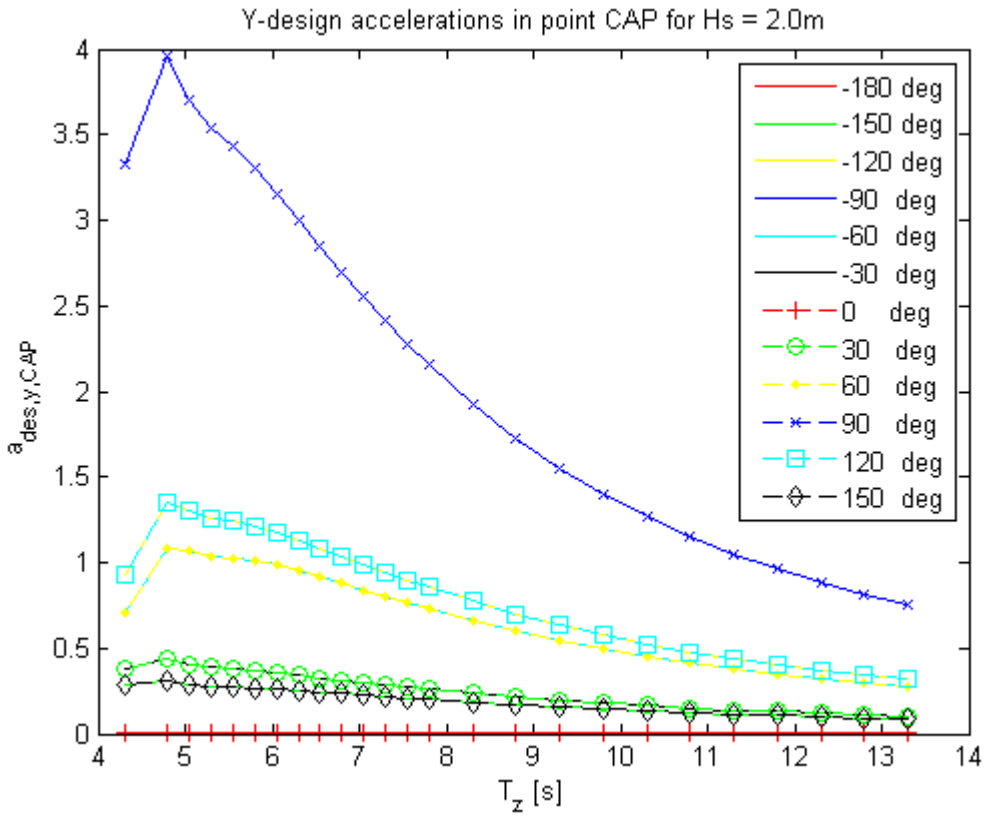

Figure 9-4: Y-design acceleration for all waveheadings in CAP, Hs = 2.0 m

As seen in Figure 9-3, the Y- acceleration maximum in CAP is highest for T_z = 4.5 – 5.5 s, same as the X-accelerations. The Y-acceleration is clearly dominated by beam sea (see Figure 9-4), and the spectrum peak period giving highest response is the roll eigenperiod. In this case the roll period is 6.68 seconds. Due to the shift in the T_z-T_p-relation for different H_s, the wave spectrum peak period hits the roll eigenfrequency at about T_z = 4.8 s for H_s = 2.0 m, and at about T_z = 5.3 s for H_s = 4.0 m, which concurs well with Figure 9-3.

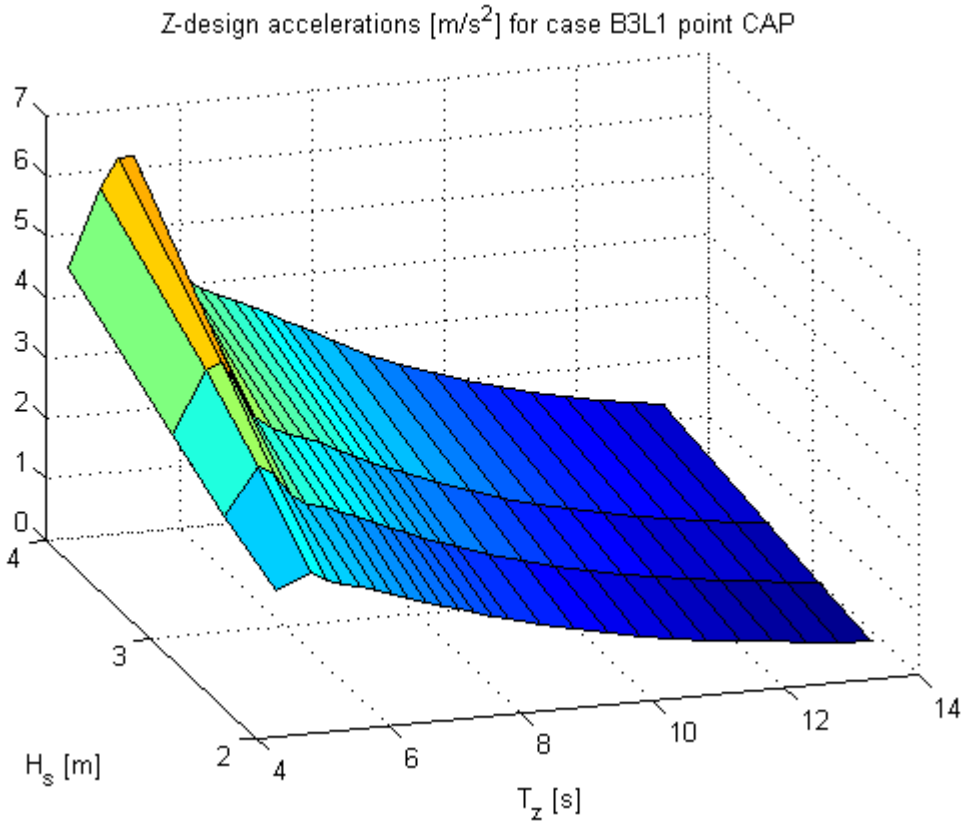

Figure 9-5: Z-design acceleration in CAP, case B3L1

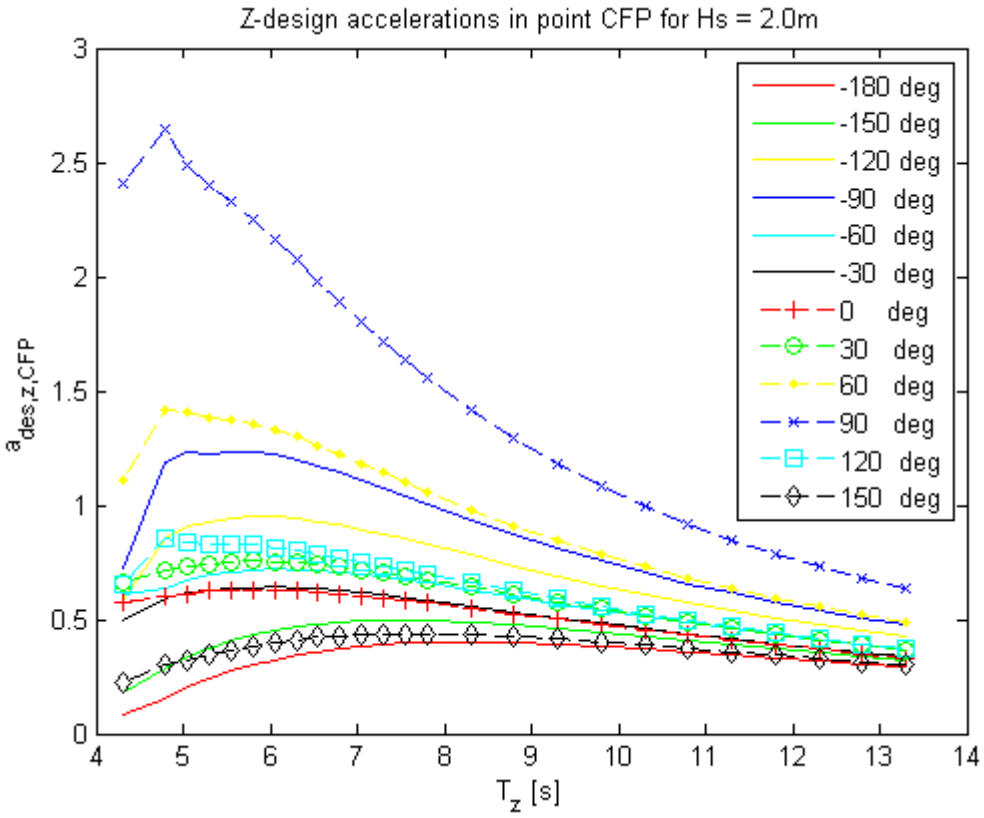

Figure 9-6: Z-acceleration for all waveheadings in CFP, Hs = 2.0 m, case B3L1

Same as the Y-acceleration, the maximum Z-acceleration occur when T_p is close to the roll eigenfrequency. Looking at Figure 9-4, it seems that the Z-acceleration is also dominated by the roll acceleration. However, it should be noted that the heave RAO has a peak in the same frequency interval as the roll motion. However, when we look at the wavedirection giving maximum response, we see that the response for $+90^o$ (waves from port side) is significantly larger than for -90^o (waves from starboard side). As the point CFP is located on the port side, this indicates that there is a significant "screening effect" when the waves are coming from the starboard side. This effect occurs for all the points, except A1 and B1 that are placed on the centerline. Due to the high response in beam seas and the significant screening effect, it can be concluded that the vertical acceleration for the points CAP, CFP, DAP and DFP largely due to the roll acceleration.

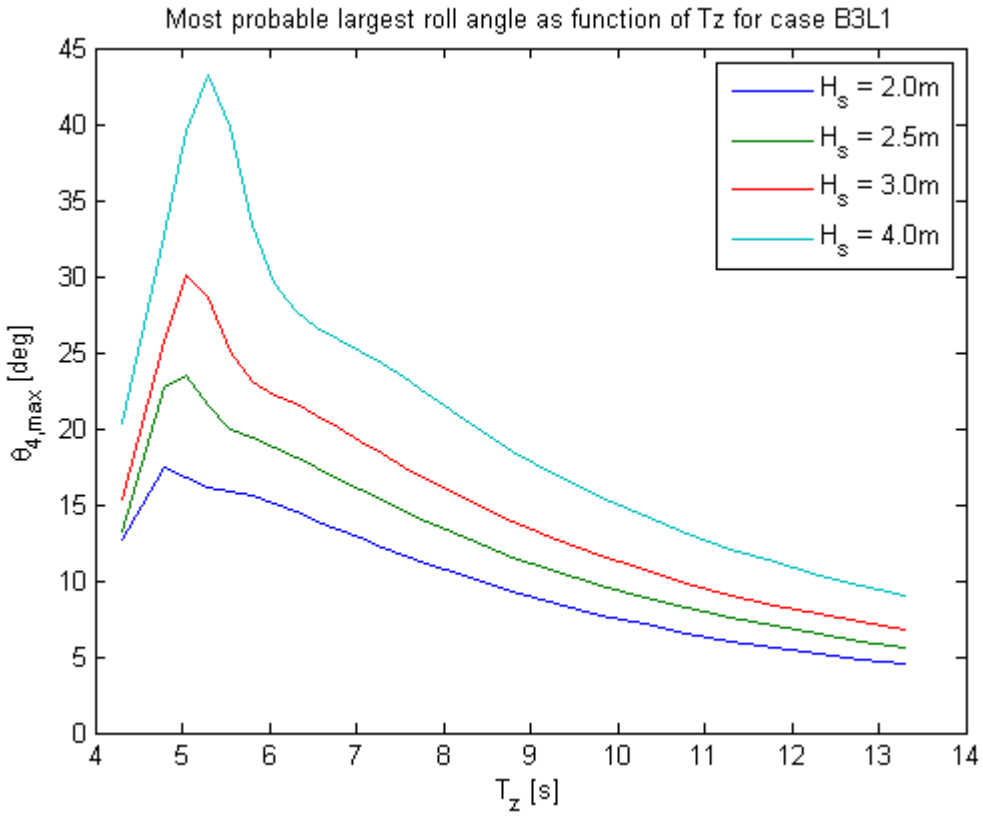

Figure 9-7: Maximum roll angles for case B3L1

In addition to accelerations, the maximum roll angle is also an important parameter for transport of heavy objects on barges. Due to the high B/D-ratio, the deck immersion angles can be relatively small compared to a conventional ship. In addition, large roll angles will introduce non-linearities that may increase the error of the linear calculations. Thus, it is convenient to also check the maximum roll angle. In Figure 9-7, the maximum roll angle is plotted for all sea states for the current case. As one can see, the roll angles become relatively large, up to almost 45 degrees for H_s = 4.0 m, which is above what any barge transportation is designed for. However, including viscous roll damping may reduce the responses in roll significantly (see section 9.2).

9.1.2 Case B3L3 – 300 feet barge, 3000 tonne module

H_s [m]	Acceleration component	Units	A1	B1	CAP	CFP	DAP	DFP
2.0	X	m/s^2	0.36	0.56	0.41	0.41	1.04	1.04
	Y	m/s^2	1.15	5.26	3.82	3.74	6.78	6.69
	Z	m/s^2	1.21	1.21	2.77	2.75	2.77	2.75
2.5	X	m/s^2	0.45	0.75	0.55	0.55	1.38	1.38
	Y	m/s^2	1.55	6.69	4.90	4.79	8.59	8.48
	Z	m/s^2	1.57	1.57	3.46	3.44	3.46	3.44
3.0	X	m/s^2	0.55	0.95	0.69	0.69	1.72	1.72
	Y	m/s^2	2.00	8.48	6.25	6.12	10.84	10.71
	Z	m/s^2	1.94	1.95	4.30	4.27	4.30	4.27
4.0	X	m/s^2	0.78	1.35	0.97	0.97	2.40	2.40
	Y	m/s^2	3.12	12.89	9.59	9.40	16.39	16.19
	Z	m/s^2	2.68	2.68	6.17	6.13	6.17	6.13

Table 9-2: Design accelerations, case B3L3

Comparing the results (Table 9-2) with the criteria given in section 7.9, as in case B3L1, the limit for Y-acceleration is breached already at H_s = 2.0 m. However, although the grillage is higher than for the 1000 tonne load, the transverse accelerations are slightly smaller. This may be due to the reduced GM, as the ballast condition is unaltered from the first case while the module weight is increased. The acceleration in the longitudinal direction (X-direction) does not exceed the limit at seafastening height (CAP and CFP) and is about the same as for case B3L1. The vertical acceleration is below 1*g* for all seastates, almost equal to case B3L1, thus no uplift occurs.

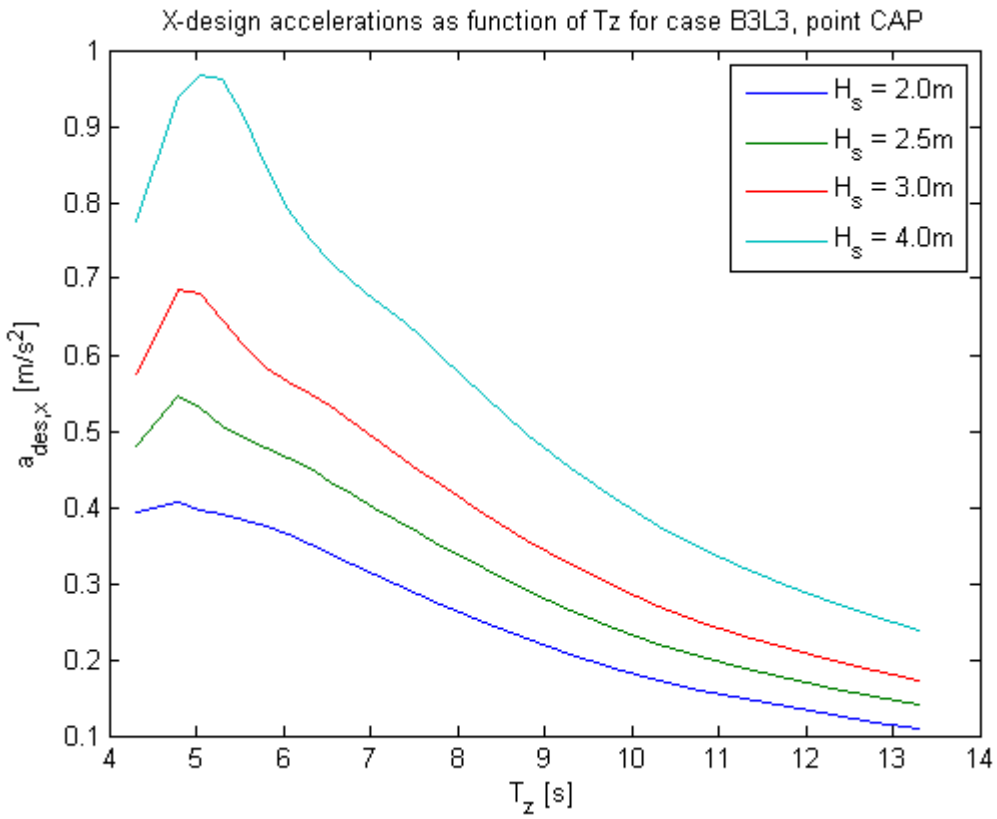

Figure 9-8: X-design accelerations in CAP, case B3L3

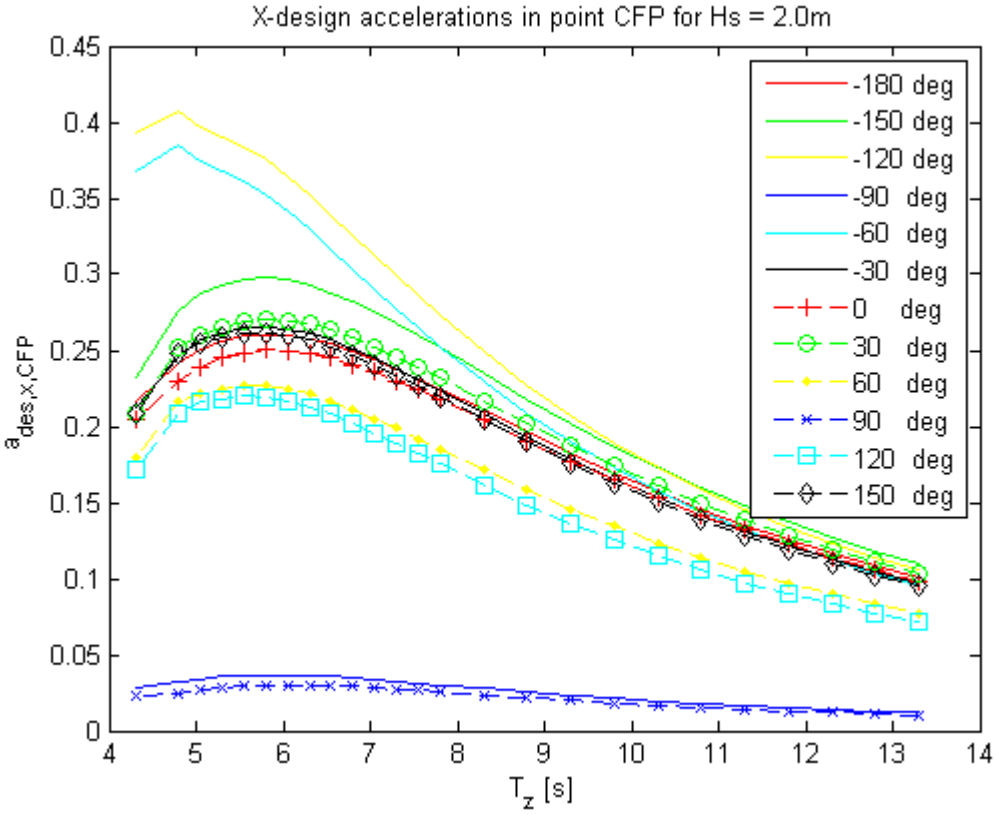

Figure 9-9: X-design accelerations for all waveheadings in CFP, Hs = 2.0 m

The frequency interval giving the highest acceleration in the X-direction is about the same as with the 1000 tonne load (B3L1). However, the yaw direction seems to be more dominating than for the lighter load as the worst wave directions are -60° and -120° for most of the T_z-interval.

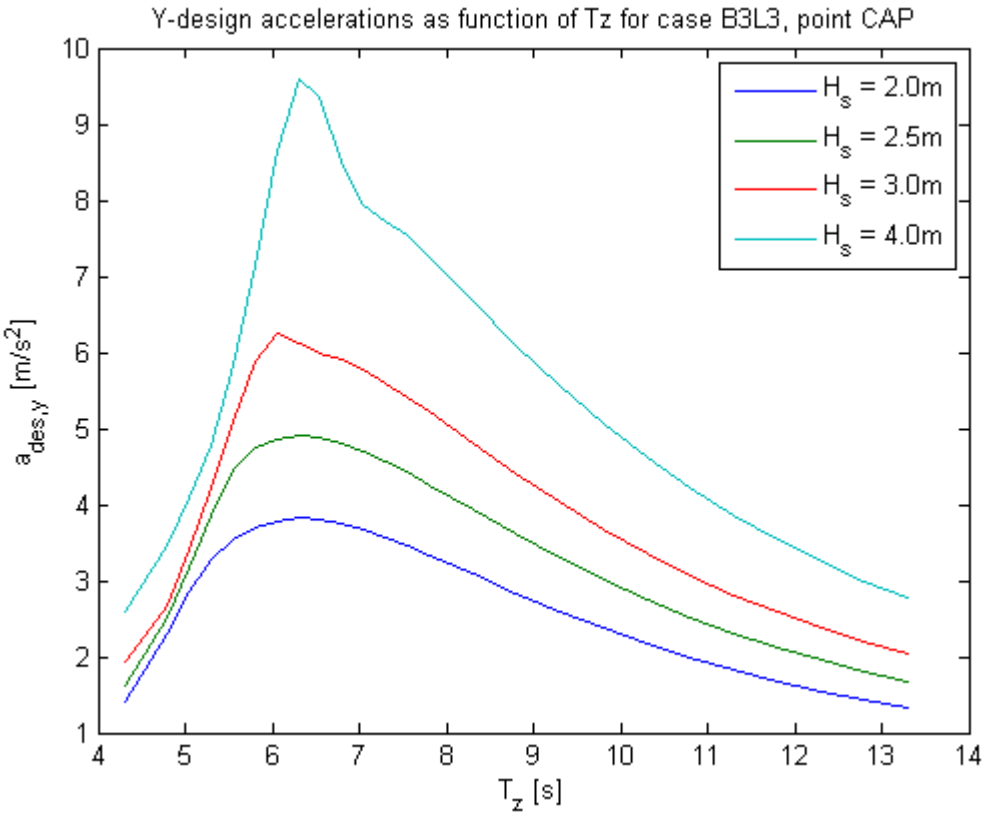

Figure 9-10: Y-design accelerations in CAP, case B3L3

The transverse accelerations occur in the interval T_z = 6.0 – 6.6 s, which is the interval where the peak period coincides with the roll eigenperiod (about 9 seconds). As for the first case, beam seas give the highest acceleration.

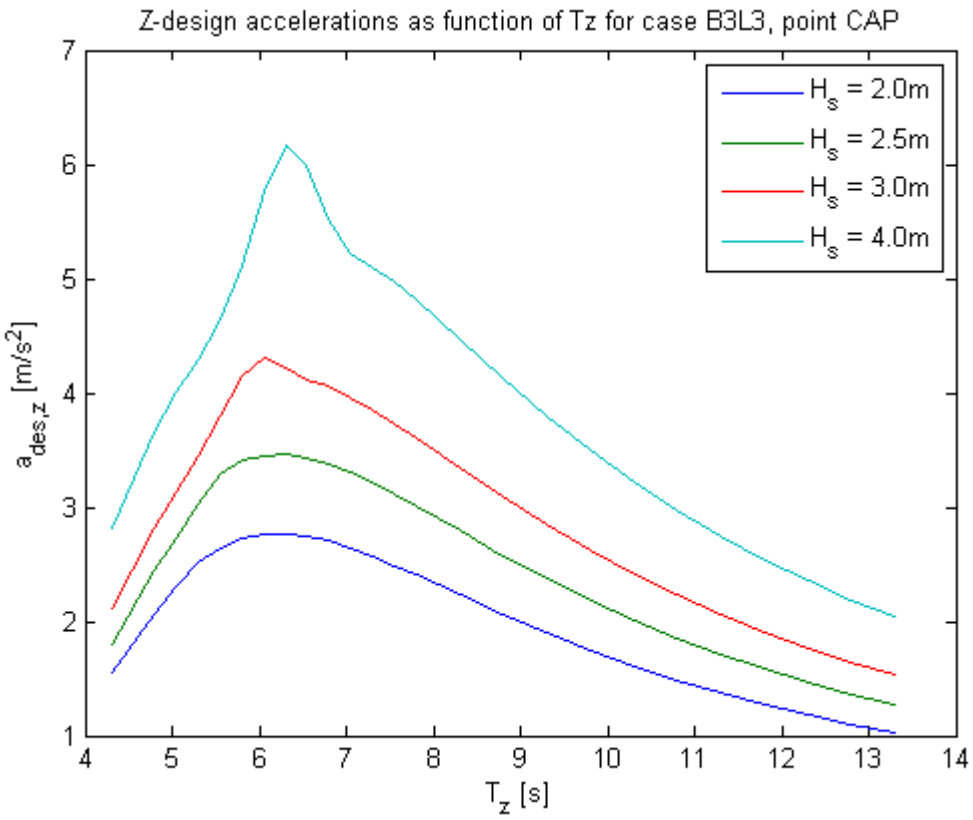

Figure 9-11: Z-design acceleration in CAP, case B3L3

The highest vertical accelerations in the points CAP, CFP, DAP and DFP occur in beam sea from the port side at the roll eigenperiod, as for case B3L1. Thus, the roll acceleration is dominating in this case as well.

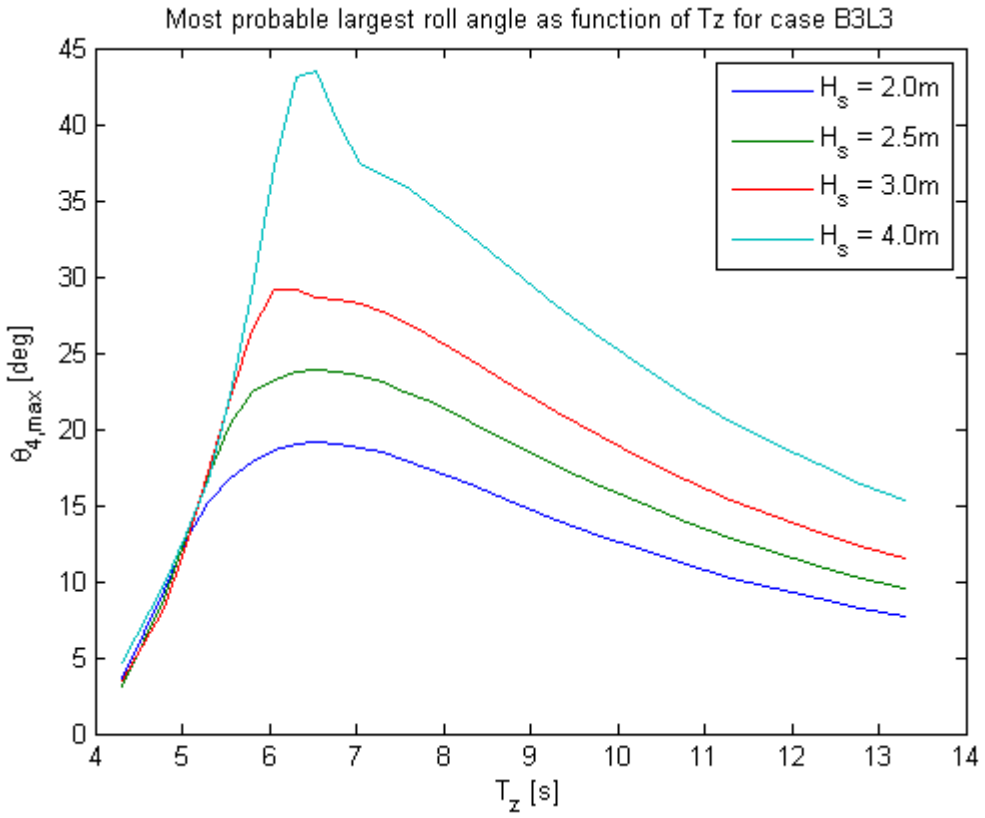

Figure 9-12: Maximum roll angle, case B3L3

The maximum roll angle does not change much from the first case (B3L1), with extreme angles still quite large. Thus, the reduced GM has seemingly not lead to increased roll amplitudes, though it has decreased the roll acceleration.

9.1.3 Case B4L1 – 400 feet barge, 1000 tonne module

H_s [m]	Acceleration component	Units	A1	B1	CAP	CFP	DAP	DFP
2.0	X	m/s^2	0.24	0.42	0.33	0.33	0.58	0.58
	Y	m/s^2	0.81	3.53	2.60	2.57	4.55	4.52
	Z	m/s^2	0.88	0.88	1.55	1.56	1.55	1.56
2.5	X	m/s^2	0.30	0.52	0.42	0.42	0.76	0.76
	Y	m/s^2	1.07	4.65	3.44	3.41	5.98	5.94
	Z	m/s^2	1.10	1.10	2.02	2.04	2.02	2.04
3.0	X	m/s^2	0.37	0.65	0.51	0.51	0.94	0.94
	Y	m/s^2	1.37	5.98	4.45	4.40	7.68	7.63
	Z	m/s^2	1.35	1.35	2.53	2.54	2.53	2.54
4.0	X	m/s^2	0.51	0.92	0.72	0.72	1.33	1.33
	Y	m/s^2	2.09	8.79	6.59	6.52	11.23	11.16
	Z	m/s^2	1.85	1.85	3.56	3.58	3.56	3.58

Table 9-3: Design accelerations, case B4L1

The accelerations for case B4L1 are, as seen in Table 9-3, smaller than for the two preceding cases. Comparing to the criteria in section 7.9, the X- and Z-acceleration limits are still not

breached for any of the seastates, while the Y-acceleration exceeds the limit already at H_s = 2.0 m.

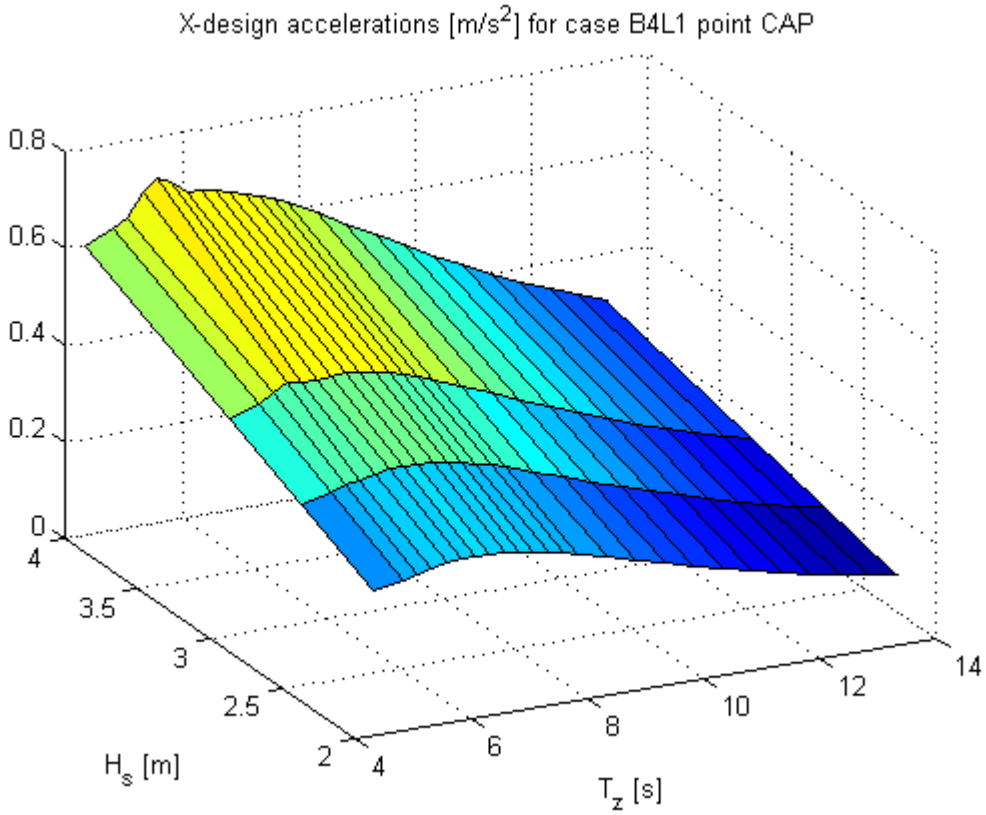

Figure 9-13: X-design acceleration in CAP, case B4L1

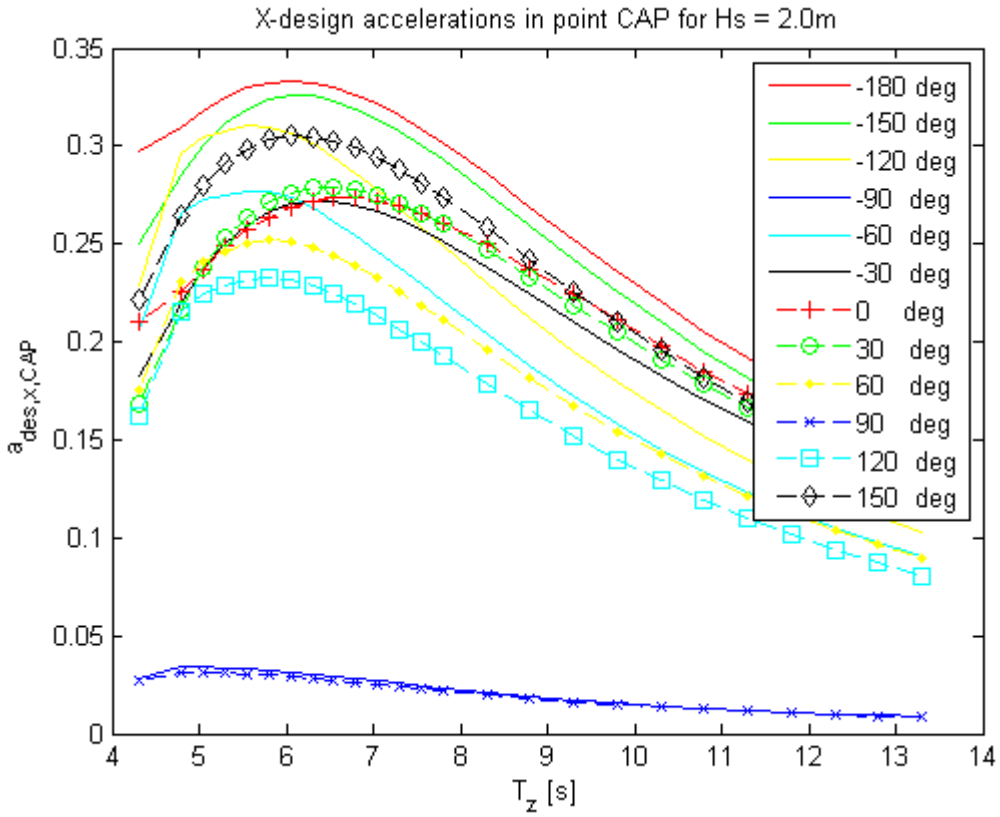

Figure 9-14: X-design acceleration for all waveheadings in CAP, case B4L1

As seen in Figure 9-14, the longitudinal acceleration is for case B4L1 dominated by following sea (-180°). This indicates that the surge and pitch motions dominate in CAP, contrary to the two preceding cases, where the yaw acceleration played a more important part. Judging by Figure 9-13, the maximum acceleration occurs at a spectral peak period of about 7 seconds.

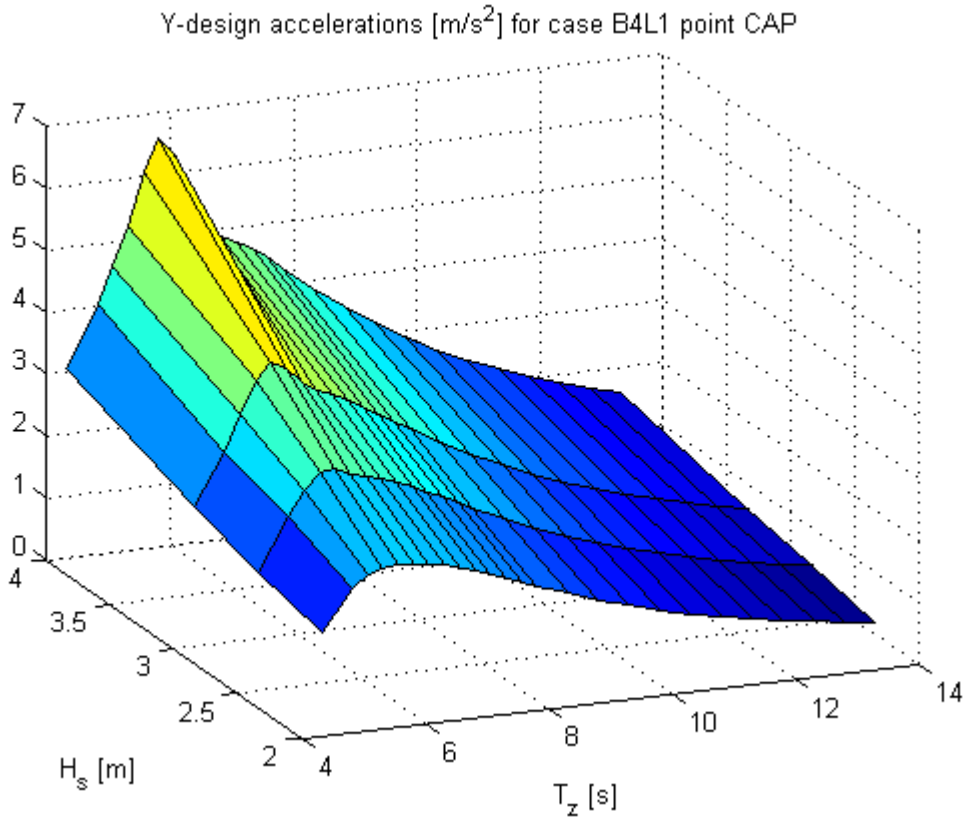

Figure 9-15: Y-design acceleration in CAP, case B4L1

As in the other cases, the transverse acceleration reaches its maximum for beam seas when the spectral peak period reaches the roll eigenperiod. In this case the roll eigenperiod is about 7.6 seconds.

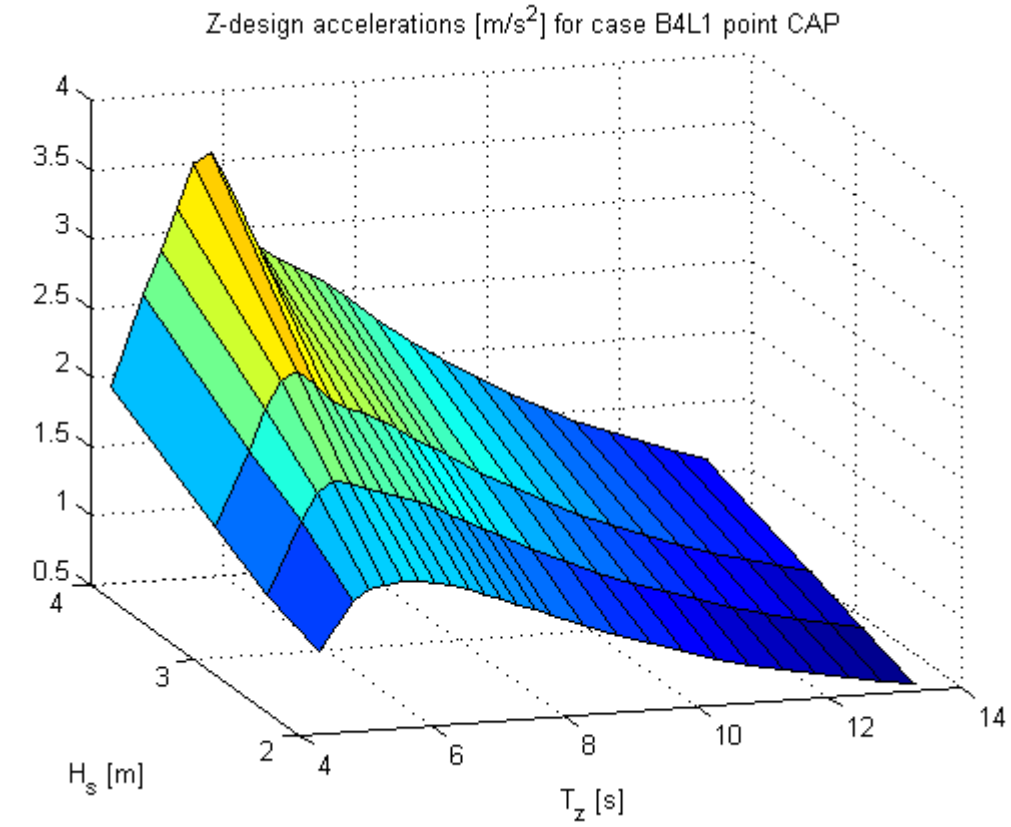

Figure 9-16: Z-design acceleration in CAP, case B4L1

The vertical acceleration is dominated by the roll eigenperiod and reaches the highest values for the same T_z as the transverse acceleration.

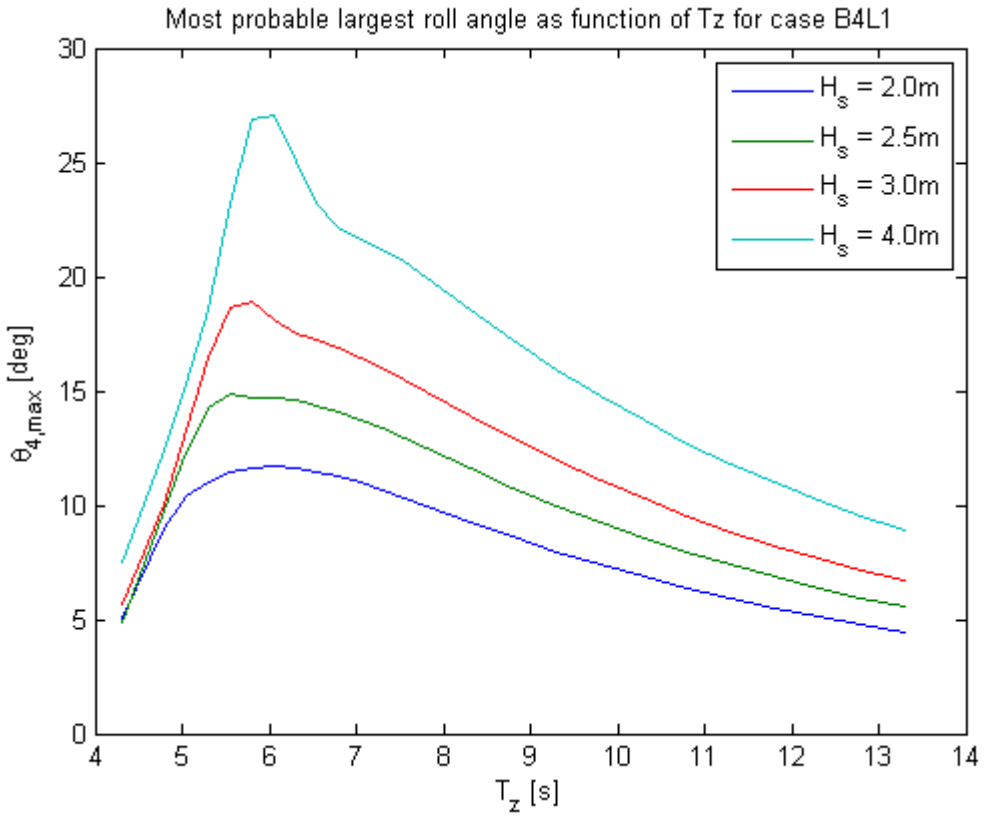

Figure 9-17: Maximum roll angle, case B4L1

The extreme roll angle is still relatively high, reaching from about 12 degrees for H_s = 2.0 m to about 27 degrees for H_s = 4.0 m. However, this is still significantly lower than for case B3L1 and B3L3.

9.1.4 Case B4L5 – 400 feet barge, 5000 tonne module

H_s [m]	Acceleration component	Units	A1	B1	CAP	CFP	DAP	DFP
2.0	X	m/s^2	0.23	0.48	0.39	0.40	0.61	0.62
	Y	m/s^2	0.84	4.74	3.49	3.40	5.16	5.07
	Z	m/s^2	0.87	0.87	2.48	2.47	2.48	2.47
2.5	X	m/s^2	0.30	0.62	0.51	0.51	0.80	0.81
	Y	m/s^2	1.13	6.00	4.44	4.34	6.52	6.42
	Z	m/s^2	1.09	1.09	3.10	3.09	3.10	3.09
3.0	X	m/s^2	0.36	0.78	0.64	0.64	1.00	1.01
	Y	m/s^2	1.45	7.30	5.43	5.30	7.92	7.79
	Z	m/s^2	1.33	1.33	3.73	3.70	3.73	3.70
4.0	X	m/s^2	0.50	1.11	0.90	0.91	1.42	1.43
	Y	m/s^2	2.22	10.70	8.02	7.83	11.58	11.40
	Z	m/s^2	1.83	1.83	5.28	5.24	5.28	5.24

Table 9-4: Design accelerations, case B4L5

As for the preceding cases, the longitudinal and vertical accelerations in CAP/CFP do not exceed the limits specified by Aker Solutions (section 7.9), while the transverse accelerations exceed the limit already at H_s = 2.0 m. Compared to the preceding case, with a 1000 tonne load, the accelerations in the transverse and vertical directions increase, but this is probably largely due to the increase in grillage height (CAP placed higher) as the global accelerations (A1) are about the same.

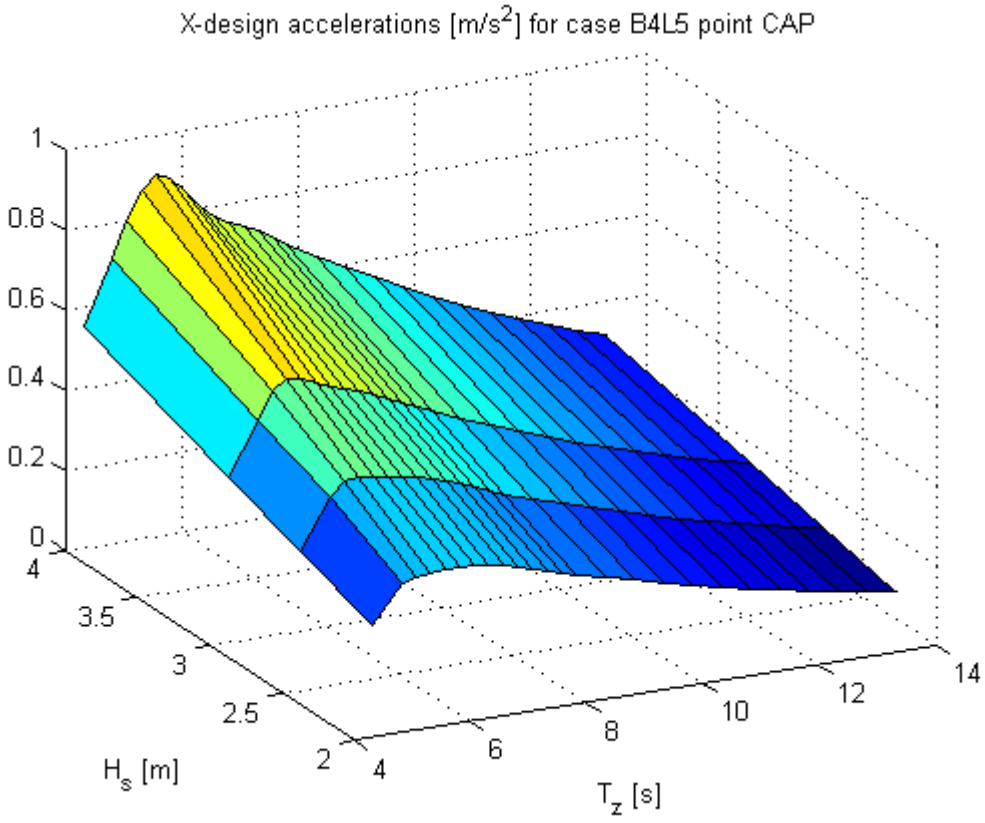

Figure 9-18: X-design accelerations in CAP, case B4L5

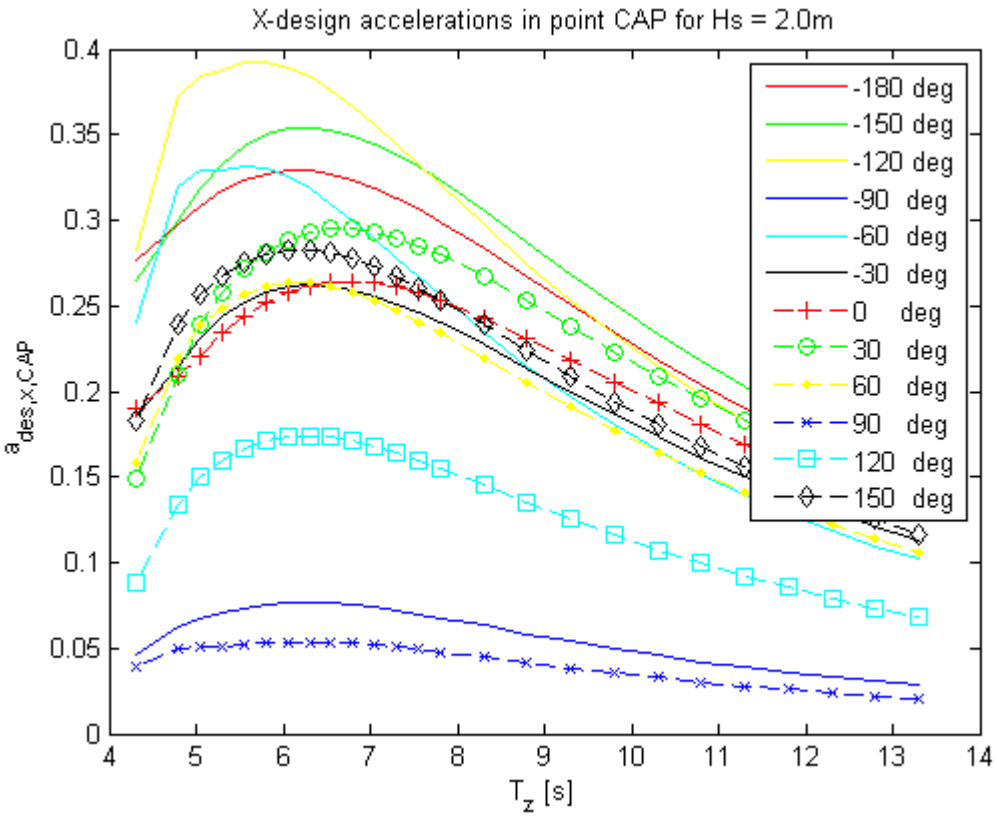

Figure 9-19: X-design accelerations for all waveheadings in CAP, Hs = 2.0 m, case B4L5

The T_z-interval giving maximum longitudinal acceleration (Figure 9-18) is equivalent to a peak period of about 7.6 seconds. In Figure 9-19 we see that the yaw acceleration seem to determine the maximum acceleration in CAP, as the angles from the centre line giving the highest response are quite large.

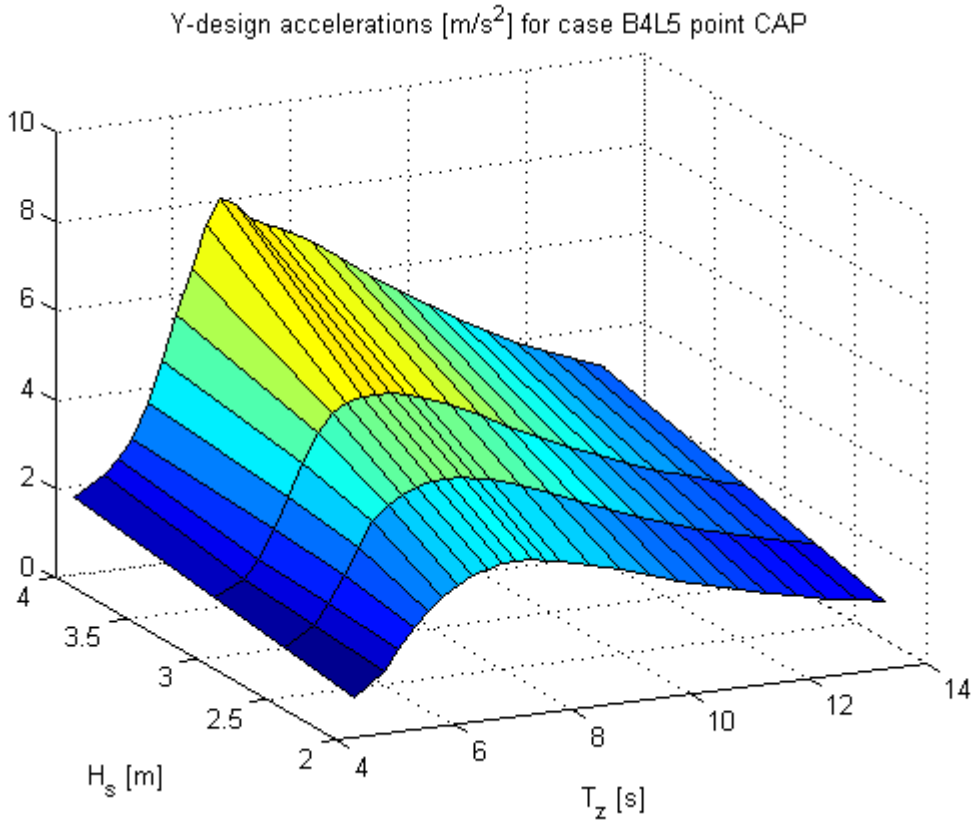

Figure 9-20: Y-design acceleration in CAP, case B4L5

The highest transverse acceleration occurs close to the roll eigenperiod, which in this case is about 9.6 seconds. The peaks of the transverse acceleration are quite smooth for the lower significant wave heights. For H_s = 4.0 m, the peak become more distinct.

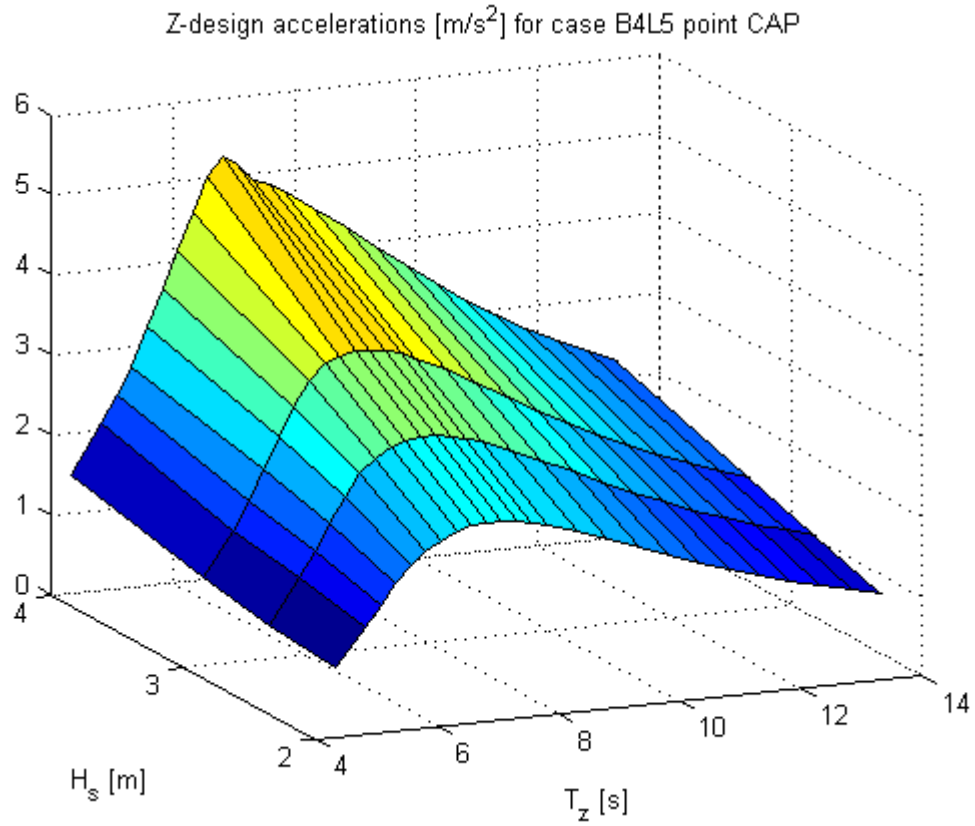

Figure 9-21: Z-design acceleration in CAP, case B4L5

The highest vertical acceleration in CAP occurs at the roll eigenperiod. As for the transverse acceleration, the peak does not become very distinct until the significant wave height reaches 4.0 meters.

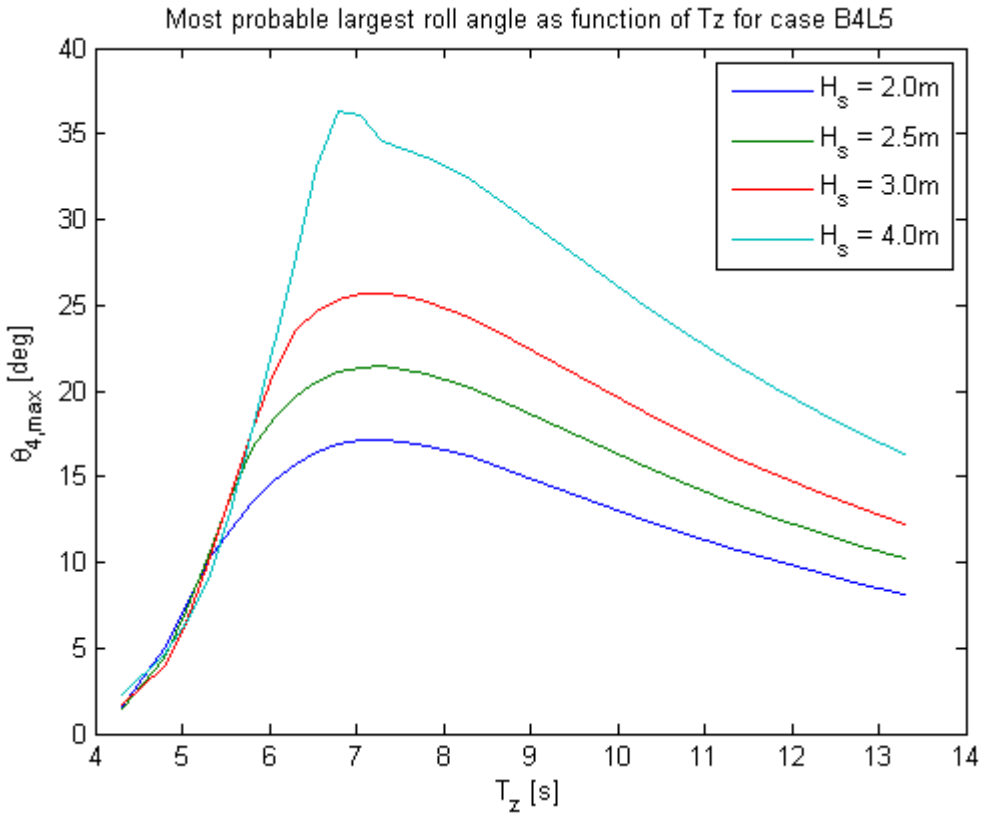

Figure 9-22: Maximum roll angle, case B4L5

As seen in Figure 9-22 and Figure 9-17, the maximum roll angle increases from the case with the lighter load (B4L1). The GM is decreased and this could be the cause of the increase. In general, the roll angles observed are still relatively high, though smaller than for the both the cases for the 300 feet barge (case B3L1 and B3L3).

9.1.5 Case B6L5 – 600 feet barge, 5000 tonne module

H_s [m]	Acceleration component	Units	A1	B1	CAP	CFP	DAP	DFP
2.0	X	m/s^2	0.16	0.33	0.29	0.29	0.47	0.47
	Y	m/s^2	0.57	2.91	2.20	2.16	3.68	3.63
	Z	m/s^2	0.67	0.67	1.62	1.64	1.62	1.64
2.5	X	m/s^2	0.20	0.41	0.36	0.36	0.59	0.59
	Y	m/s^2	0.74	3.67	2.78	2.72	4.63	4.57
	Z	m/s^2	0.84	0.84	2.02	2.05	2.02	2.05
3.0	X	m/s^2	0.24	0.50	0.44	0.44	0.70	0.70
	Y	m/s^2	0.93	4.50	3.38	3.30	5.60	5.53
	Z	m/s^2	1.01	1.01	2.43	2.46	2.43	2.46
4.0	X	m/s^2	0.32	0.68	0.60	0.60	0.96	0.96
	Y	m/s^2	1.36	6.43	4.90	4.79	8.07	7.96
	Z	m/s^2	1.35	1.35	3.44	3.49	3.44	3.49

Table 9-5: Design accelerations, case B6L5

Comparing the accelerations to the criteria (section 7.9), case B6L5 is the first case where the transverse acceleration limit in CAP/CFP is not exceeded for H_s = 2.0 m. For H_s = 2.5 m the

limit is exceeded, though only slightly. Thus, as in the other cases, the transverse acceleration seems to be the limiting criteria, while the longitudinal and vertical accelerations are within the limits even for H_s = 4.0 m.

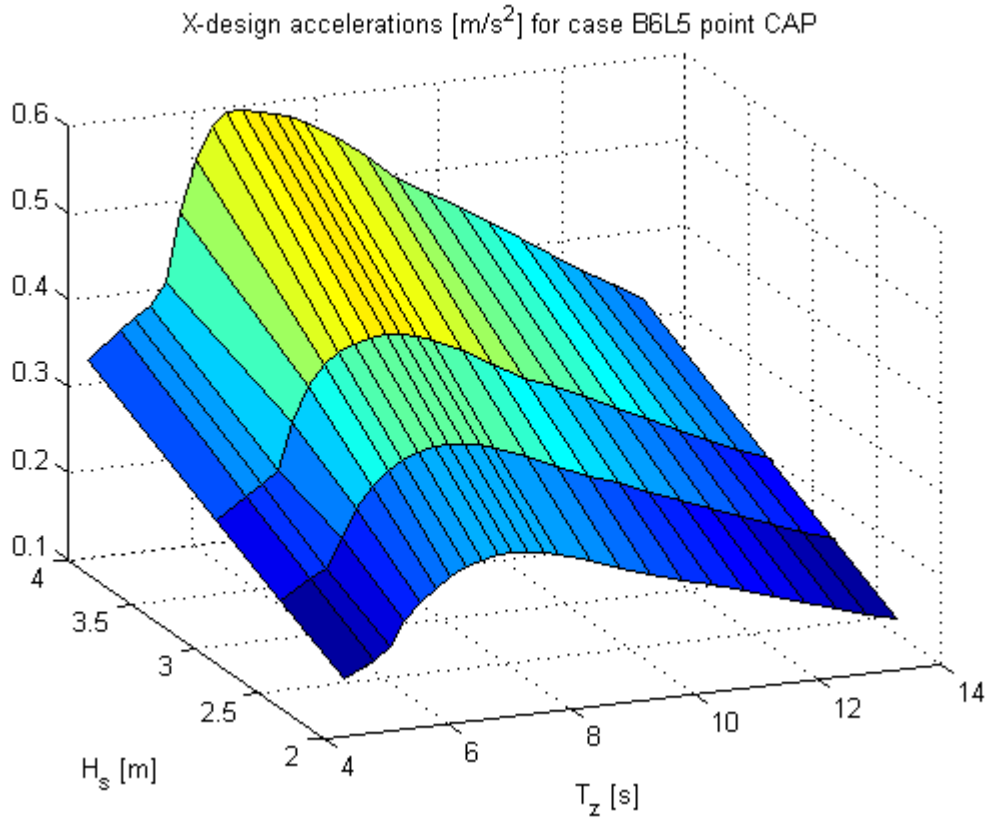

Figure 9-23: X-design acceleration in CAP, case B6L5

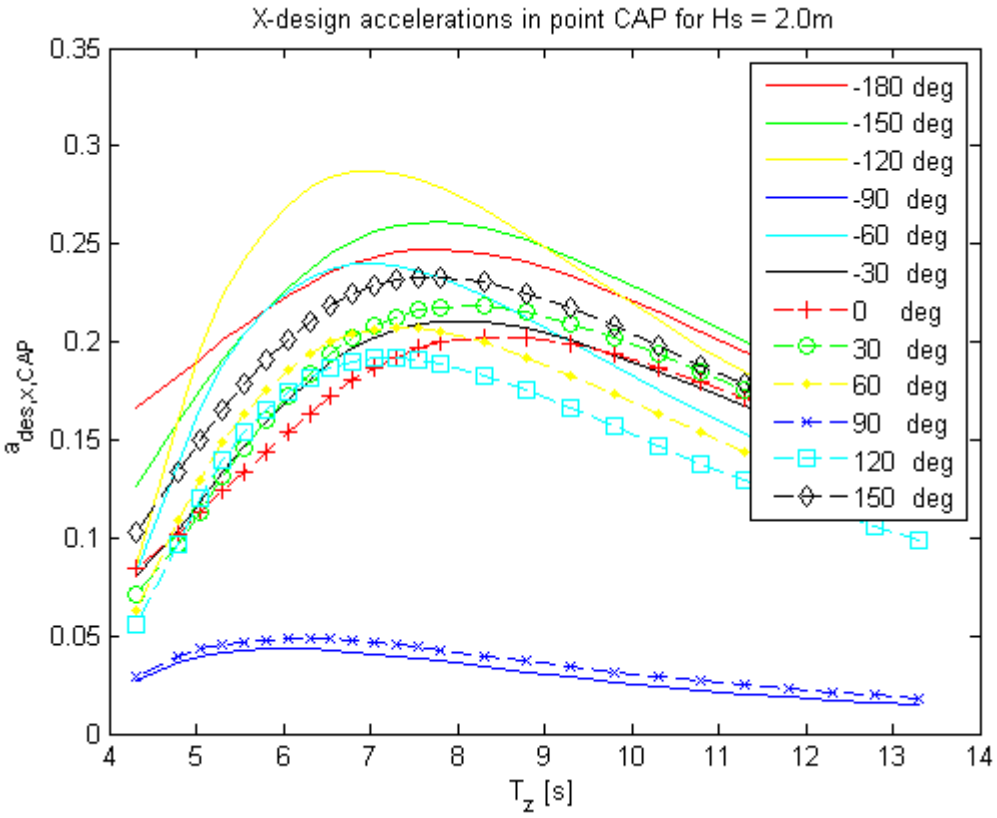

Figure 9-24: X-design acceleration for all waveheadings in CAP, Hs = 2.0 m, case B5L6

As seen from Figure 9-23, the peak of the longitudinal acceleration is not very distinct. It reaches its maximum for a spectral peak period of about 9.4 seconds. A waveheading of -120^{o} gives the highest acceleration (Figure 9-24), suggesting that the yaw acceleration is dominating for the longitudinal acceleration in CAP.

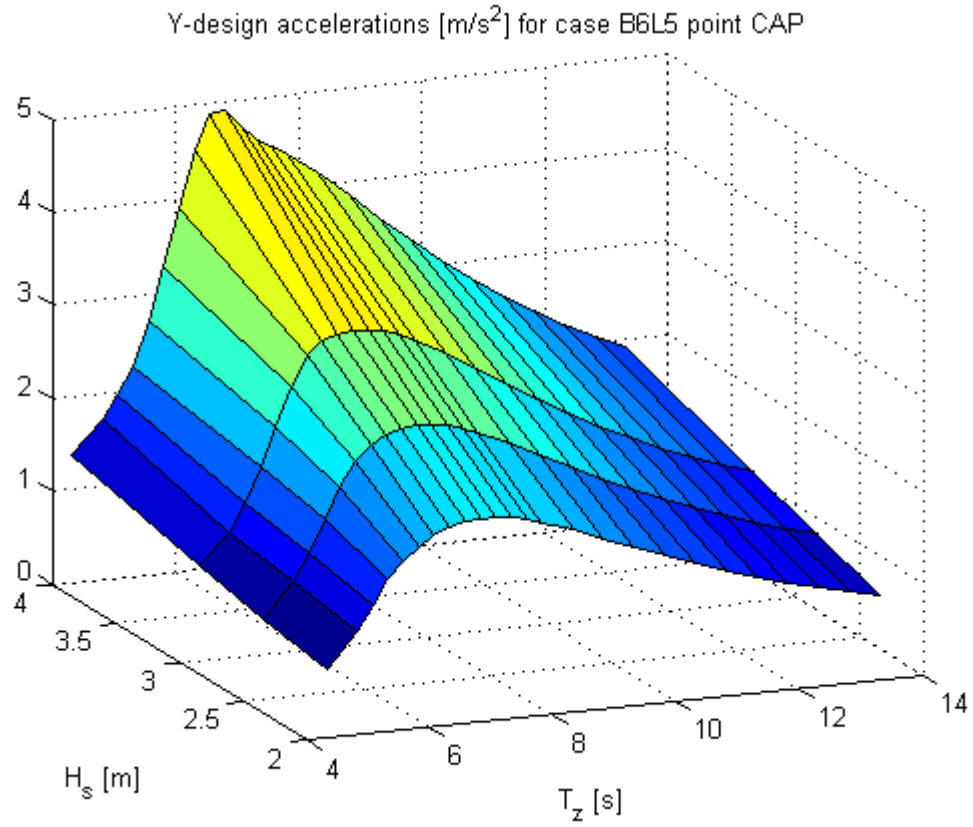

Figure 9-25: Y-design acceleration in CAP, case B6L5

The maximum transverse acceleration occurs in beam seas when the spectral peak period reaches the roll eigenperiod. For this case (B6L5), the roll eigenperiod is about 9.6 seconds.

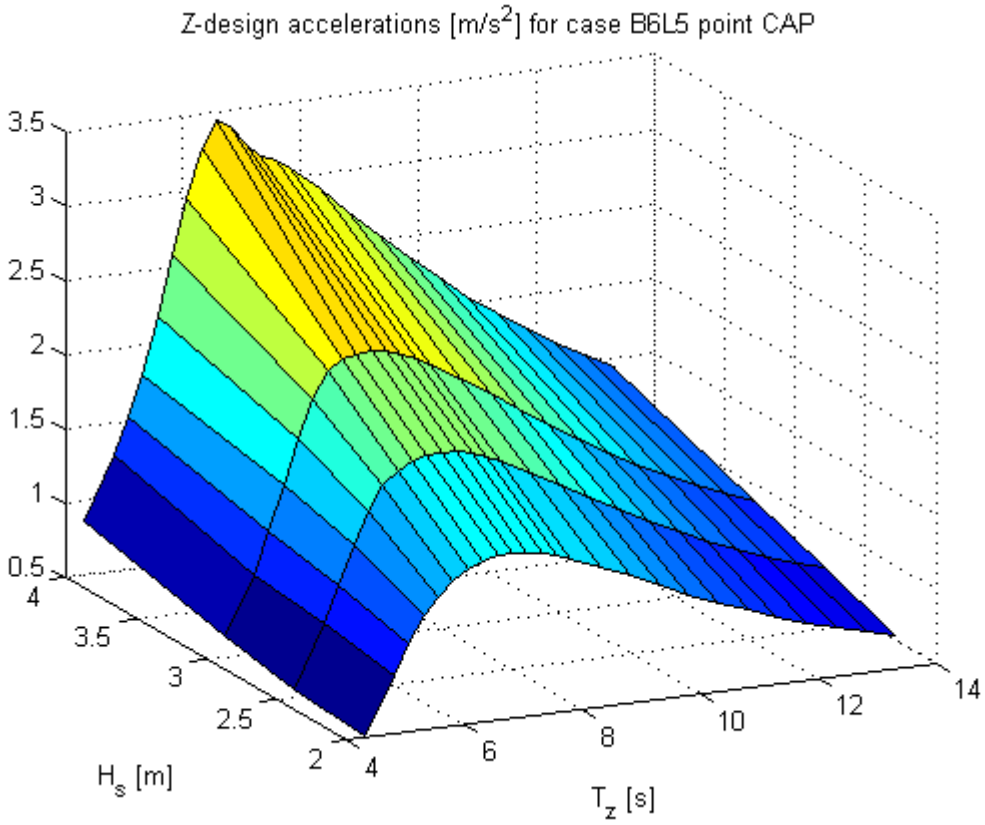

Figure 9-26: Z-design acceleration in CAP, case B6L5

As for the transverse acceleration, the maximum vertical acceleration in CAP occurs at roll resonance.

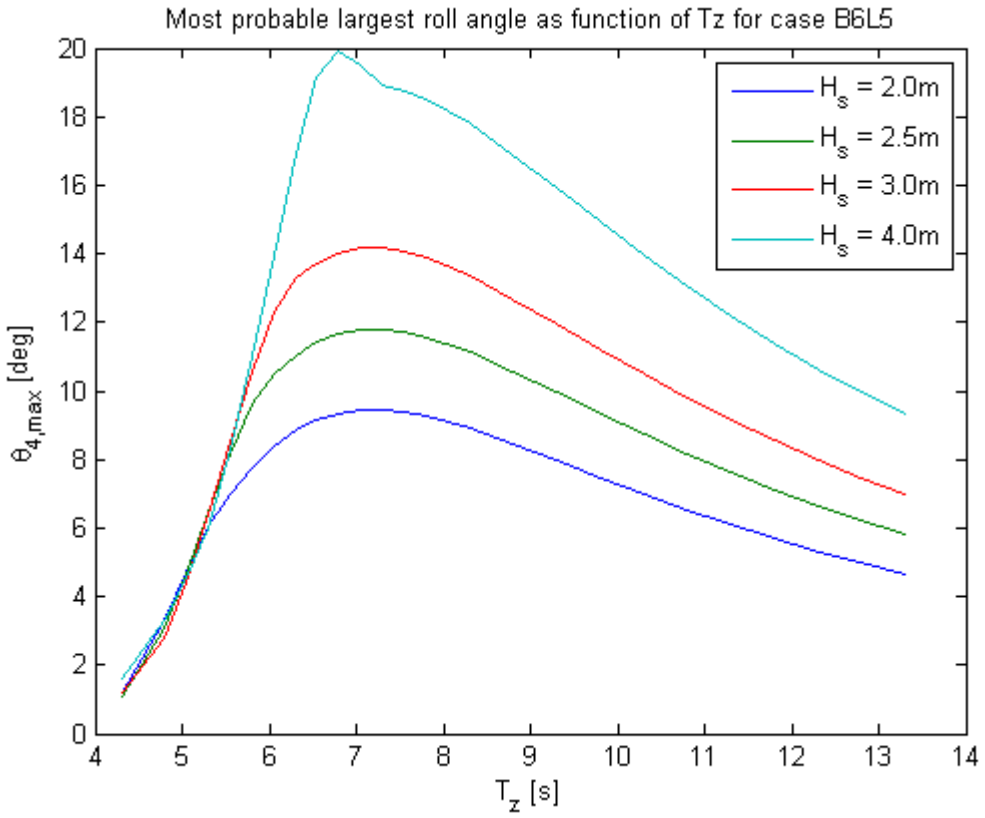

Figure 9-27: Maximum roll angle, case B6L5

The maximum roll angle for case B6L5 is lower than for all the cases with smaller barges, indicating that a larger barge is beneficial for decreasing both roll acceleration and extreme roll angles.

9.1.6 Case B6L8 – 600 feet barge, 8000 tonne module

H_s [m]	Acceleration component	Units	A1	B1	CAP	CFP	DAP	DFP
2.0	X	m/s^2	0.15	0.35	0.29	0.29	0.52	0.52
	Y	m/s^2	0.59	3.61	2.65	2.60	4.61	4.55
	Z	m/s^2	0.67	0.67	1.83	1.83	1.83	1.83
2.5	X	m/s^2	0.19	0.44	0.37	0.37	0.65	0.65
	Y	m/s^2	0.78	4.56	3.36	3.29	5.81	5.74
	Z	m/s^2	0.83	0.83	2.29	2.29	2.29	2.29
3.0	X	m/s^2	0.23	0.54	0.45	0.45	0.78	0.78
	Y	m/s^2	0.99	5.52	4.09	4.00	7.02	6.94
	Z	m/s^2	1.00	1.00	2.74	2.75	2.74	2.75
4.0	X	m/s^2	0.32	0.73	0.61	0.61	1.07	1.07
	Y	m/s^2	1.46	7.50	5.59	5.48	9.50	9.39
	Z	m/s^2	1.34	1.34	3.66	3.68	3.66	3.68

Table 9-6: Design accelerations, case B6L8

For the 8000 load, the accelerations increase slightly compared with the 5000 tonne load (case B6L5), but compared to the rest of the cases, the accelerations are quite low. The limit for

transverse acceleration is still exceeded at H_s = 2.0 m. The longitudinal and vertical accelerations are well within the limits.

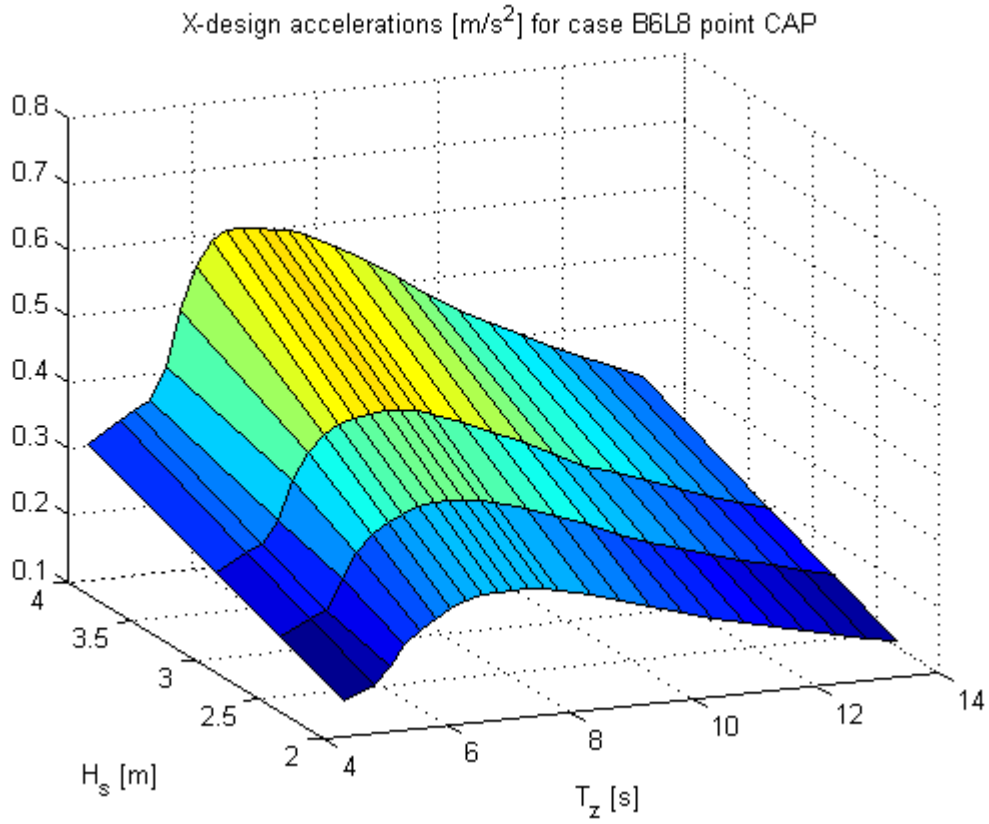

Figure 9-28: X-design acceleration in CAP, case B6L8

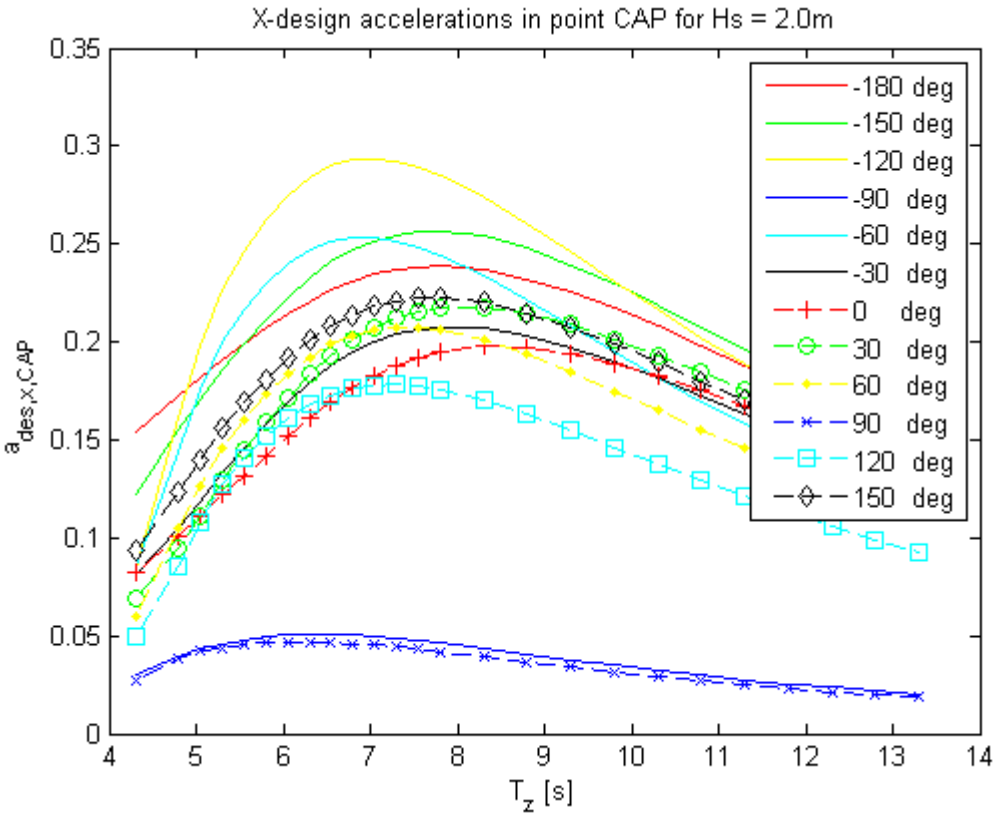

Figure 9-29: X-design acceleration in CAP for all waveheadings, Hs = 2.0 m, case B6L8

The peak of the longitudinal acceleration is, as seen in Figure 9-28, not very distinct, and the acceleration stays at about the maximum value in the interval T_p = 8.5 – 11.0 s. The dominating wave direction is -120^o, suggesting that the longitudinal acceleration in CAP is dominated by the yaw acceleration.

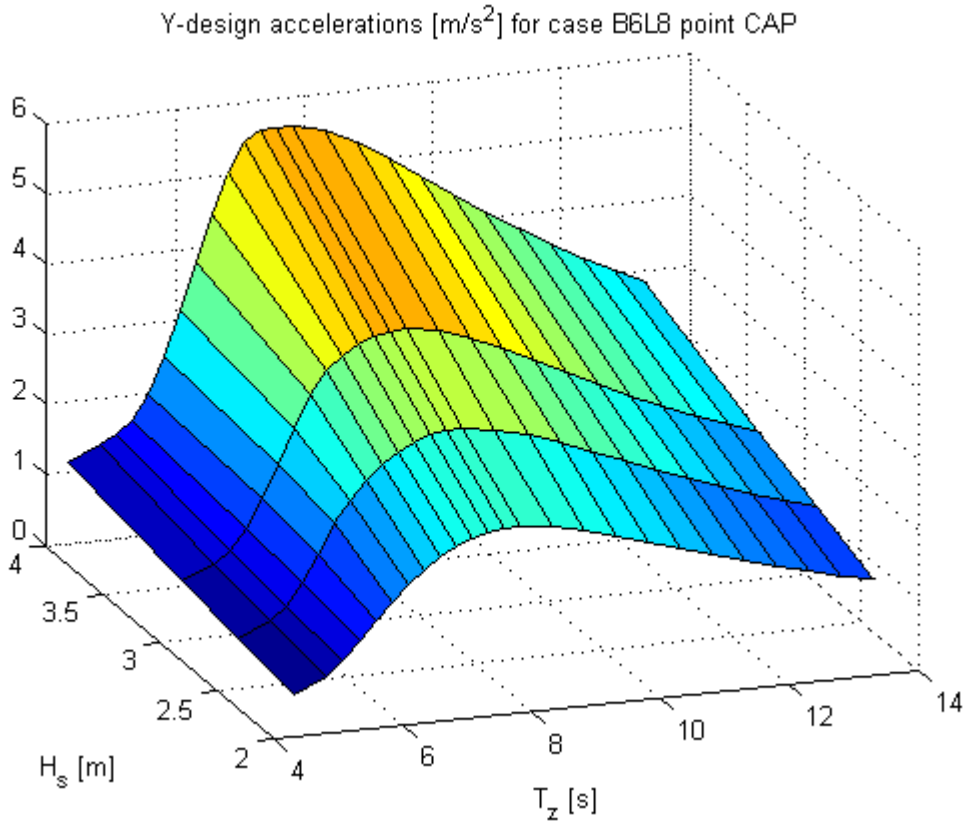

Figure 9-30: Y-design acceleration in CAP, case B6L8

As for the longitudinal acceleration, the transverse acceleration does not have a very distinct peak, and the maximum transverse acceleration can be said to occur in the interval T_p = 9.8 – 11.7 s.

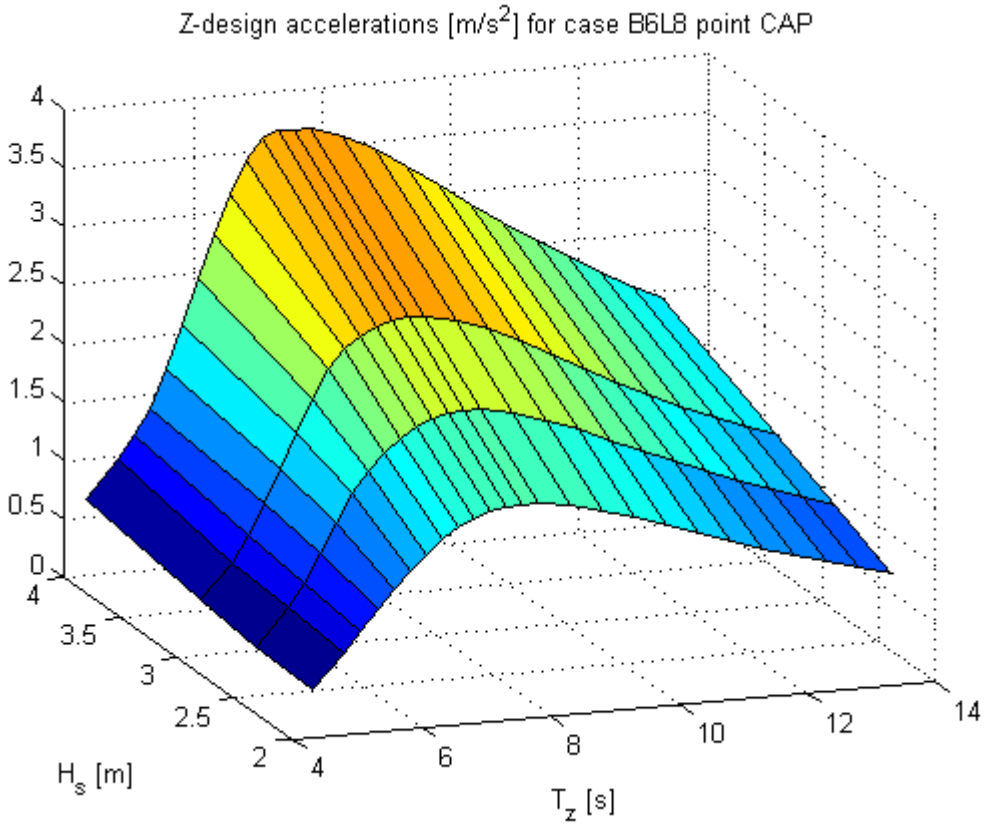

Figure 9-31: Z-design acceleration in CAP, case B6L8

The vertical acceleration is dominated by the roll acceleration, thus the peak value occurs in the same interval as for the transverse acceleration, meaning T_p = 9.8 – 11.7 s.

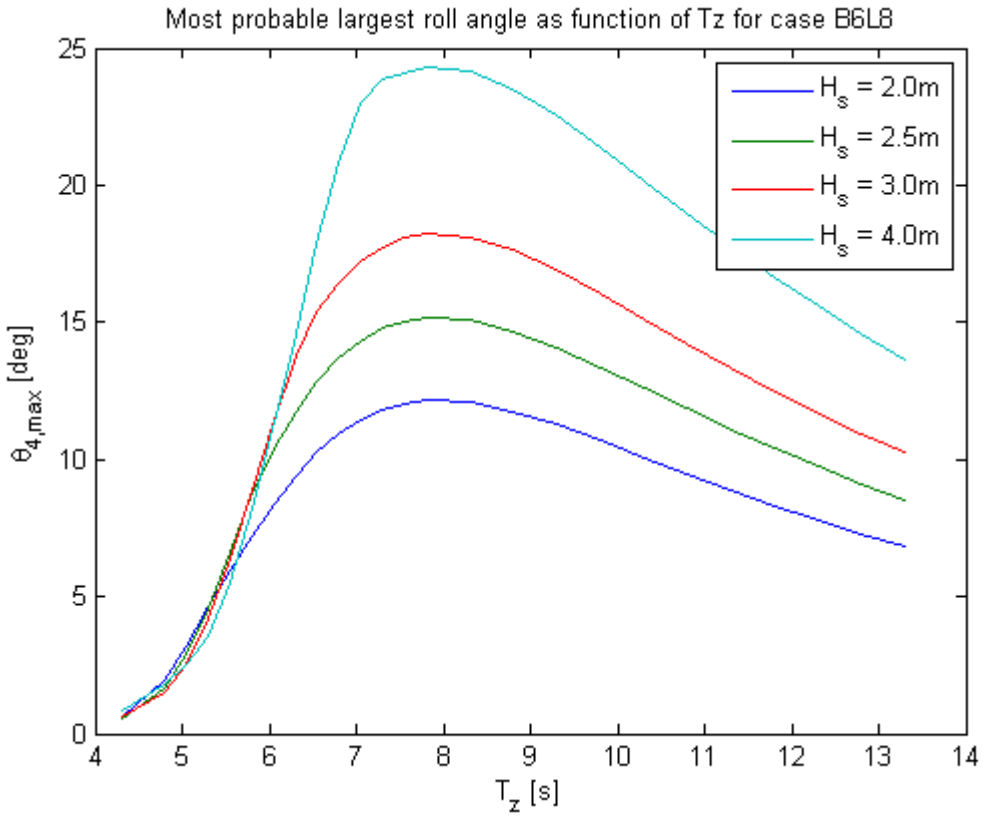

Figure 9-32: Maximum roll angle, case B6L8

The maximum roll angle of the 600 feet barge is higher for the 8000 tonne load than for the 5000 tonne load, which is expected due to the decreased GM. In general however, the roll angle is lower than for the smaller barges.

9.2 Results including viscous roll damping

9.2.1 Case B3L1 – 300 feet, 1000 tonne module

As the roll motions are of little importance for the accelerations in the longitudinal direction, only accelerations in the transverse and the vertical direction are commented in this section (see section 9.1.1 for longitudinal accelerations).

H_s [m]	Acceleration component	Units	A1	B1	CAP	CFP	DAP	DFP
2.0	Y	m/s^2	1.04	4.26	2.91	2.88	5.64	5.61
	Z	m/s^2	1.22	1.22	2.56	2.56	2.56	2.56
2.5	Y	m/s^2	1.48	6.41	4.40	4.36	8.47	8.42
	Z	m/s^2	1.59	1.59	3.18	3.18	3.18	3.18
3.0	Y	m/s^2	1.90	7.95	5.49	5.43	10.47	10.42
	Z	m/s^2	1.96	1.96	3.87	3.88	3.87	3.88
4.0	Y	m/s^2	2.97	12.08	8.44	8.35	15.81	15.73
	Z	m/s^2	2.66	2.66	5.45	5.45	5.45	5.45

Table 9-7: Design accelerations, case B3L1 with VRD

Comparing the Y-accelerations with the criterion of 0.25*g* maximum acceleration, we see that this limit is still exceeded at H_s = 2.0 m, as was the case without the viscous roll damping. The accelerations, both in the transverse and vertical direction, are smaller however.

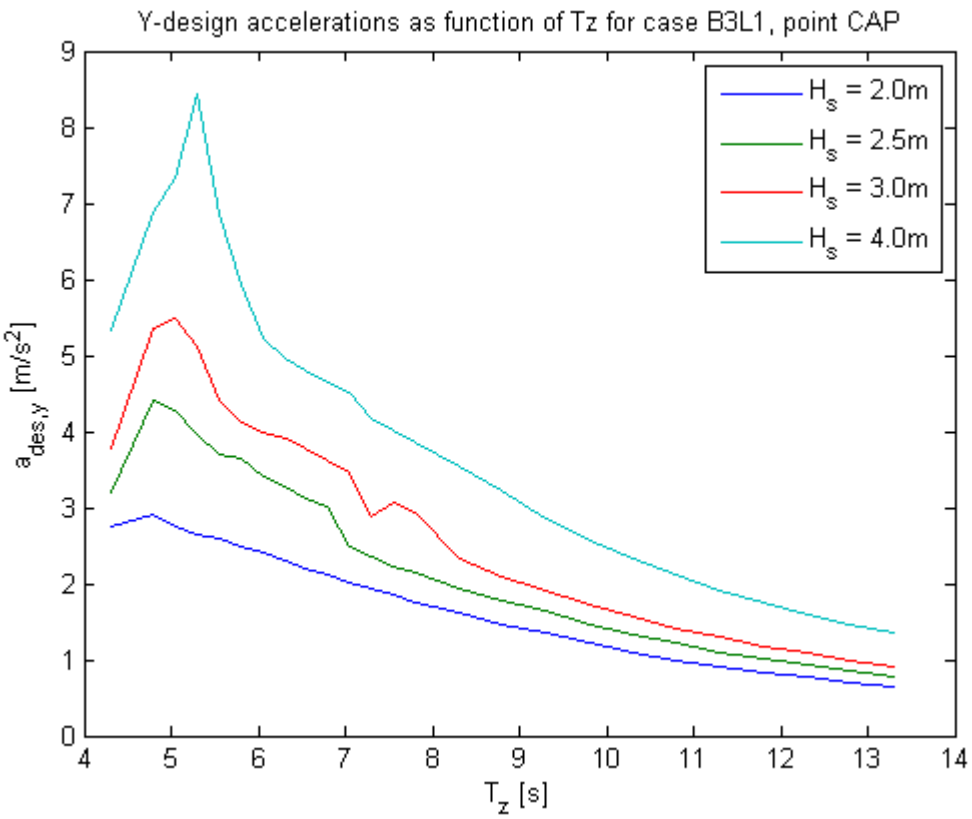

Figure 9-33: Y-design accelerations, case B3L1, point CAP, VRD included

As seen from Figure 9-33, the maximum transverse acceleration in CAP occurs at the roll eigenfrequency, which seems to be unaltered by the viscous roll damping.

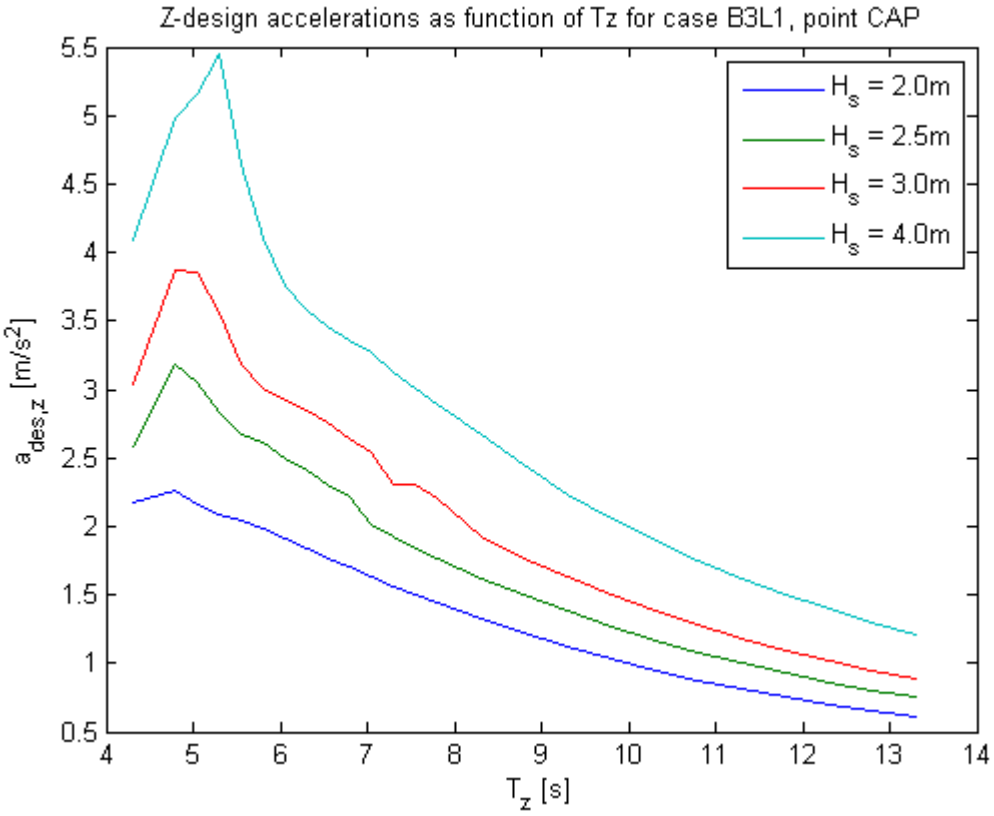

Figure 9-34: Z-design accelerations, case 1, point CAP, VRD included

Same as for the transverse acceleration, the maximum vertical acceleration occurs at the roll eigenfrequency.

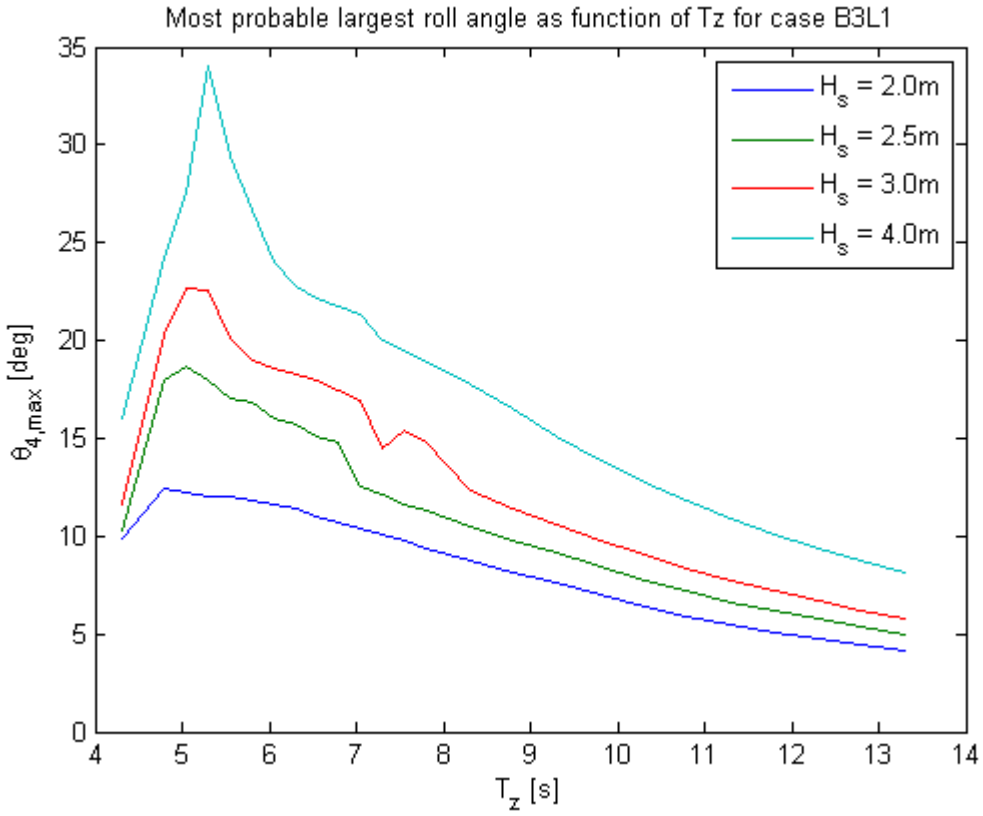

Figure 9-35: Maximum roll angles, case B3L1, point CAP, VRD included

The maximum roll angle for case B3L1 with viscous roll damping is reduced compared to the non-viscous case. However, the roll angle is still relatively high. According to Professor Asle Natskår at NTNU, who has performed model tests on North Sea barges exactly like the 300 feet barge in this case with respect to extreme roll angles, the roll angles seem conservative. This was also the case when the viscous roll damping was included. However, this can only be taken as an indication, and is not conclusive.

Increasing the zero-crossing period towards the roll resonance area, there was a clear change in the roll RAO when the spectral peak period approached the roll resonance period. The absolute peak of the RAO (radians) decreased when entering the resonance area. Within a relatively large area around the resonance period, the peak value of the roll RAO remained decreased and almost constant. When the spectral peak period approached the end of the resonance area, the peak value of the RAO started increasing, and this continued until the relative response was significantly higher than in the resonance area. This indicates that the viscous roll damping has a large effect on roll motion and acceleration in the roll resonance area. A change in significant wave height did not change the RAOs, the governing parameter for change in the roll RAO was the peak period of the wave spectrum. Plots of the roll RAOs for three selected sea states can be seen in Appendix C.

9.3 Considerations

9.3.1 1000 tonne module

Two cases have been analysed with a 1000 tonne module. Some of the reason for this is to compare the design accelerations for the two cases and finding out which case is more beneficial. The way to determine this is to see which case that gives the smallest accelerations. The result of the motion response analysis for the two cases can be seen in Table 9-8.

H_s [m]	Acceleration component	Case B3L1			Case B4L1		
		A1	**B1**	**CAP**	**A1**	**B1**	**CAP**
2.0	X	0.38	0.59	0.38	0.24	0.42	0.33
	Y	1.20	5.85	3.96	0.81	3.53	2.60
	Z	1.22	1.22	2.65	0.88	0.88	1.55
2.5	X	0.48	0.78	0.51	0.30	0.52	0.42
	Y	1.68	7.99	5.45	1.07	4.65	3.44
	Z	1.59	1.59	3.58	1.10	1.10	2.02
3.0	X	0.58	0.97	0.64	0.37	0.65	0.51
	Y	2.22	10.44	7.16	1.37	5.98	4.45
	Z	1.96	1.96	4.46	1.35	1.35	2.53
4.0	X	0.78	1.38	0.91	0.51	0.92	0.72
	Y	3.55	15.29	10.63	2.09	8.79	6.59
	Z	2.66	2.66	6.19	1.85	1.85	3.56

Table 9-8: Case B3L1 and B4L1 compared

As seen from Table 9-8, there is a significant reduction in the maximum accelerations on the 400 feet barge compared to the 300 feet barge. The reduction of the transverse and vertical accelerations is larger than for the longitudinal accelerations. For example, in CAP, the acceleration in the transverse direction for B4L1 is about 60-65% of that of B3L1 for all H_s, while the longitudinal acceleration for case B4L1 is 80-90% of that of case B3L1.

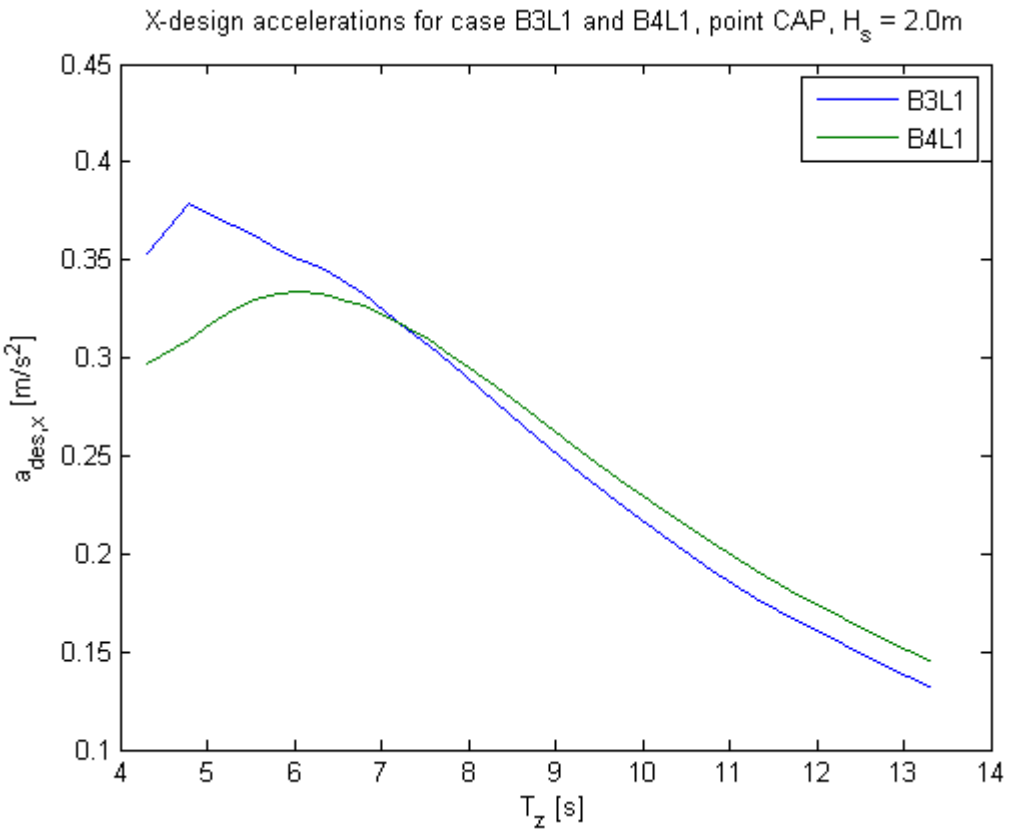

Figure 9-36: Comparison of X-design acceleration for B3L1 and B4L1, Hs = 2.0 m

Looking past the maximum values for the longitudinal acceleration, we see in Figure 9-36 that the reduced acceleration for the 400 feet barge depends strongly on the seastate. As the zero-crossing period increases, the accelerations become more similar until the acceleration becomes larger for the 400 feet barge at about T_z = 7.3 s. For seastates with a higher zero-crossing period, the longitudinal acceleration is always larger for the 400 feet barge.

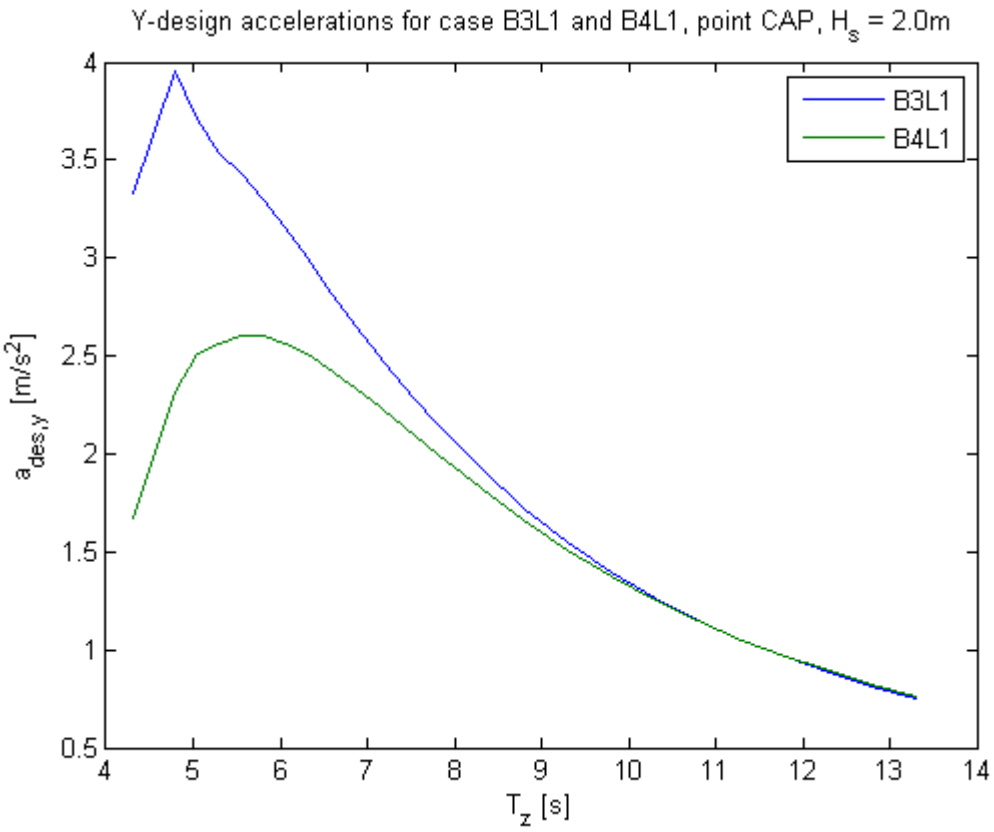

Figure 9-37: Comparison of Y-design acceleration for B3L1 and B4L1, Hs = 2.0 m

As for the longitudinal acceleration, the difference in the transverse acceleration (Figure 9-37) is largest for small zero-crossing periods. As T_z increases, the difference decreases. For $T_z > 9$ s there is virtually no difference between the two barges. For lower T_z however, where the highest accelerations occur, the difference is significant.

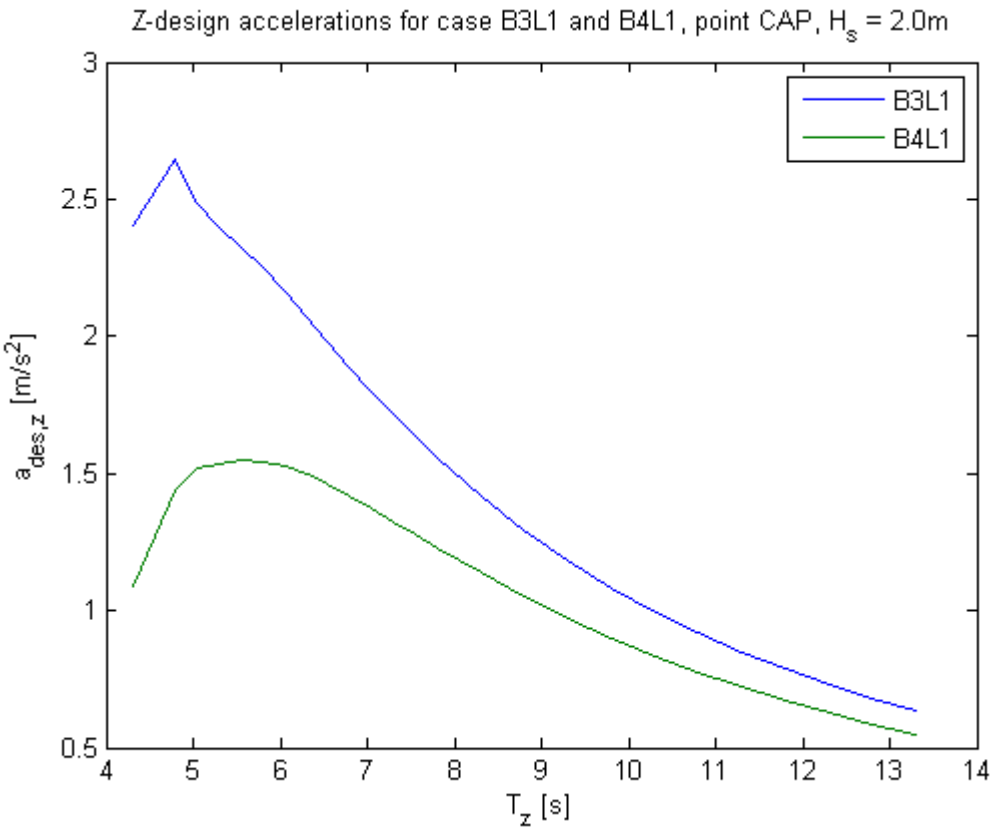

Figure 9-38: Comparison of Z-design acceleration for B3L1 and B4L1, Hs = 2.0 m

The decrease in difference between the two modules with increasing T_z is not as distinct for the vertical acceleration. Although the vertical acceleration decreases faster with T_z for the 300 feet barge after the peak zero-crossing period is passed, the acceleration is always noticeably higher for the 300 feet barge than for the 400 feet barge.

9.3.2 5000 tonne module

Two cases have been analysed with a 5000 tonne module, one case with a 400 feet barge (B4L5) and one case with a 600 feet barge (B6L5). The aim is to determine is to see which case that gives the smallest accelerations, and how big the difference is. The result of the motion response analysis for the two cases can be seen in Table 9-9. None of the cases include viscous roll damping.

H_s [m]	Acceleration component	Units	Case B4L5			Case B6L5		
			A1	B1	CAP	A1	B1	CAP
2.0	X	m/s^2	0.23	0.48	0.39	0.16	0.33	0.29
	Y	m/s^2	0.84	4.74	3.49	0.57	2.91	2.20
	Z	m/s^2	0.87	0.87	2.48	0.67	0.67	1.62
2.5	X	m/s^2	0.30	0.62	0.51	0.20	0.41	0.36
	Y	m/s^2	1.13	6.00	4.44	0.74	3.67	2.78
	Z	m/s^2	1.09	1.09	3.10	0.84	0.84	2.02
3.0	X	m/s^2	0.36	0.78	0.64	0.24	0.50	0.44
	Y	m/s^2	1.45	7.30	5.43	0.93	4.50	3.38
	Z	m/s^2	1.33	1.33	3.73	1.01	1.01	2.43
4.0	X	m/s^2	0.50	1.11	0.90	0.32	0.68	0.60
	Y	m/s^2	2.22	10.70	8.02	1.36	6.43	4.90
	Z	m/s^2	1.83	1.83	5.28	1.35	1.35	3.44

Table 9-9: Case B4L5 and B6L5 compared

As seen from Table 9-9, the increased barge size yields a significant reduction in the maximum accelerations for the same load, as seen in the previous section. The reductions are of the same magnitude. The accelerations in the transverse direction (in all points) on the 600 feet barge are about 60-65% of those on the 400 feet barge, for all H_s. As in the previous section, the longitudinal accelerations do not decrease as much as the transverse accelerations.

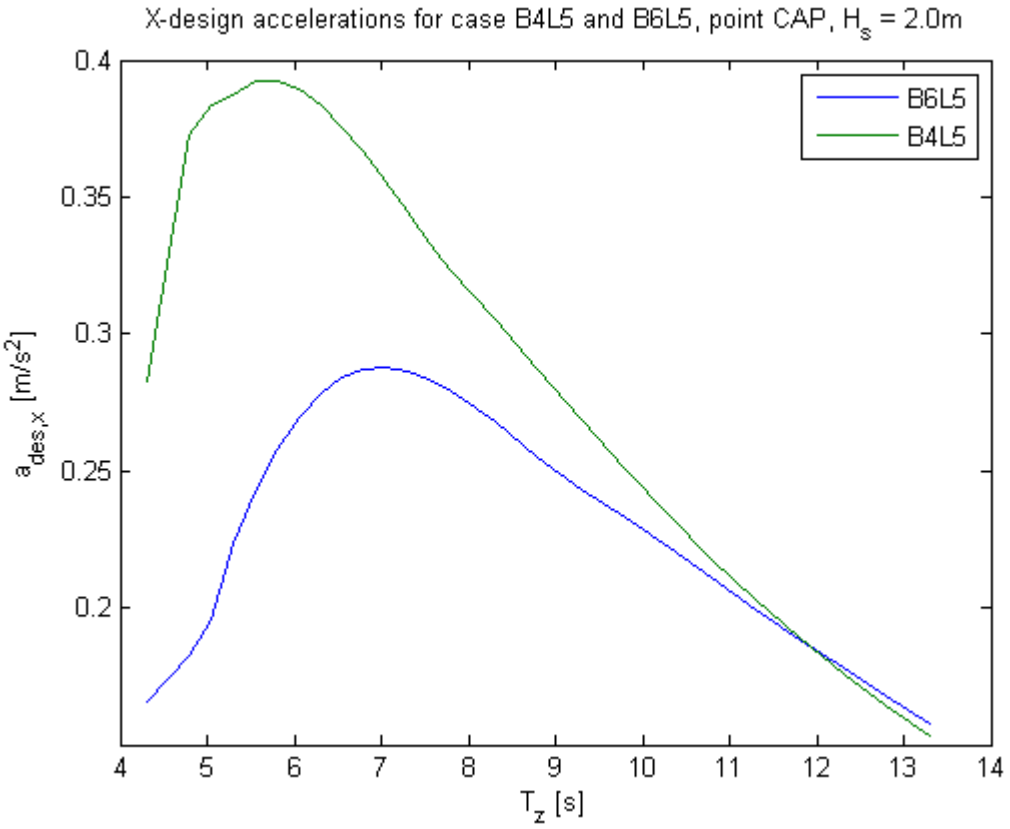

Figure 9-39: Comparison of X-design acceleration in CAP for B4L5 and B6L5, Hs = 2.0 m

Looking at the variation of the longitudinal acceleration with T_z, we see in that the reduced acceleration for the 600 feet barge depends on the seastate as in the previous comparison.

However, the difference is significant up to quite high zero-crossing periods. At about T_z = 12 s, there is no difference between the two barges.

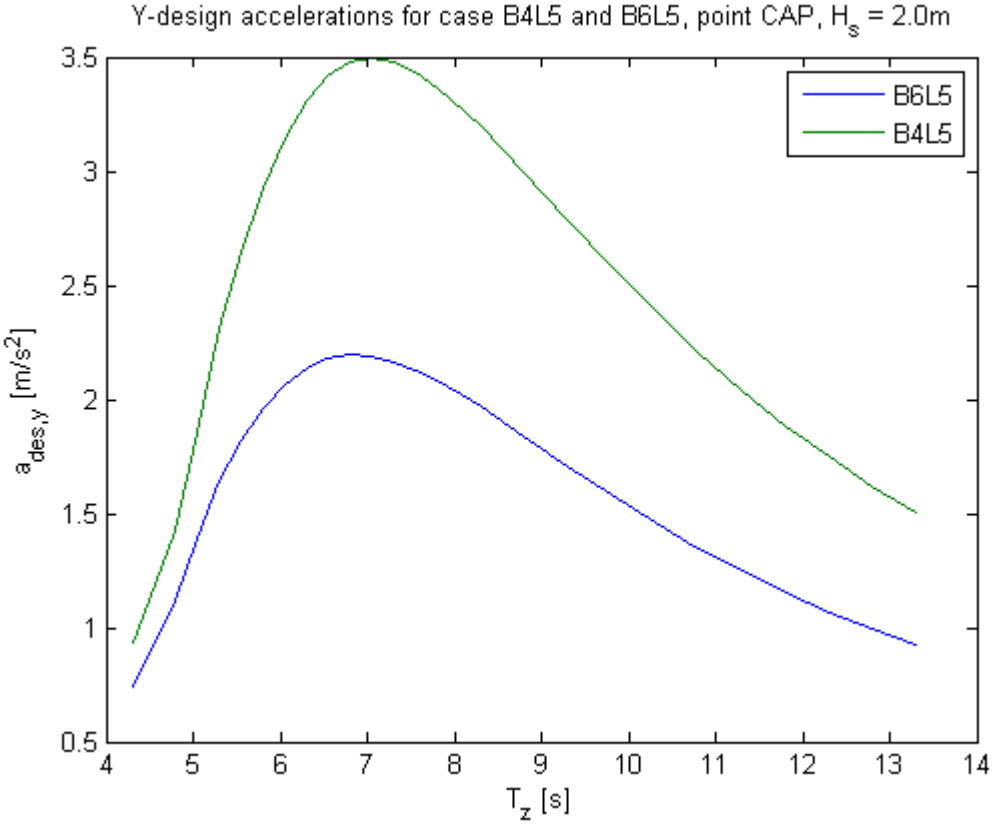

Figure 9-40: Comparison of Y-design acceleration in CAP for B4L5 and B6L5, Hs = 2.0 m

As seen in Figure 9-40, the largest difference is found in the transverse acceleration. The difference is actually smaller for the lowest zero-crossing periods, but even here, the reduction in acceleration for the larger barge is considerable.

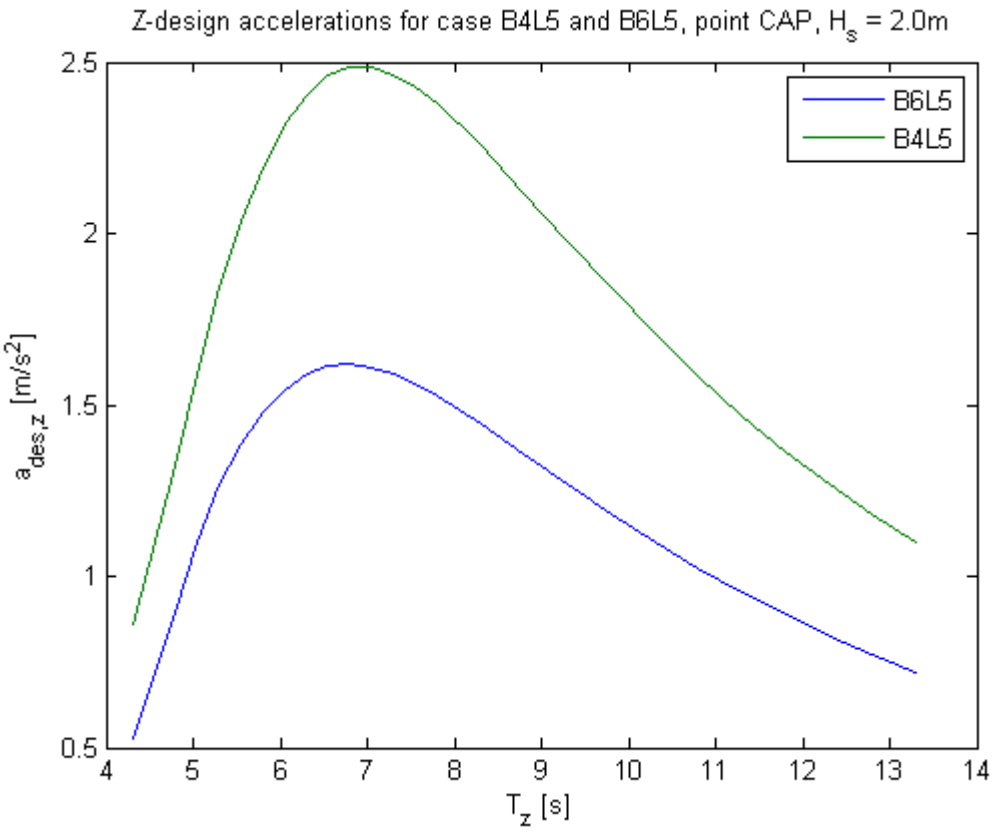

Figure 9-41: Comparison of Z-design acceleration in CAP for B4L5 and B6L5, Hs = 2.0 m

As for the transverse acceleration, the reduction in the vertical acceleration in CAP is significant for the whole wave period interval.

9.3.3 Effect of viscous roll damping

The first case, a 300 feet barge with a 1000 tonne module, has been analysed once more with viscous roll damping included. As the RAO in roll and sway may vary for different seastates when viscous roll damping is included, such analyses can become quite extensive. Thus, analysing the effect of viscous roll damping on case B3L1 may give an estimate of the viscous damping's effect on all the cases. Design accelerations for case B3L1 in the transverse and vertical direction, with and without viscous roll damping, can be seen in Table 9-10.

H_s [m]	Acceleration component	Units	Case B3L1, non-viscous			Case B3L1, with VRD		
			A1	B1	CAP	A1	B1	CAP
2.0	Y	m/s^2	1.20	5.85	3.96	1.04	4.26	2.91
	Z	m/s^2	1.22	1.22	2.65	1.22	1.22	2.56
2.5	Y	m/s^2	1.68	7.99	5.45	1.48	6.41	4.40
	Z	m/s^2	1.59	1.59	3.58	1.59	1.59	3.18
3.0	Y	m/s^2	2.22	10.44	7.16	1.90	7.95	5.49
	Z	m/s^2	1.96	1.96	4.46	1.96	1.96	3.87
4.0	Y	m/s^2	3.55	15.29	10.63	2.97	12.08	8.44
	Z	m/s^2	2.66	2.66	6.19	2.66	2.66	5.45

Table 9-10: Case B3L1, with and without VRD compared

As seen in Table 9-10, there is a significant reduction in both the transverse and vertical accelerations when viscous roll damping is included. In CAP, the transverse acceleration with VRD is 75-80% of that without VRD for all H_s. The vertical acceleration is in the range 86 – 97 % of the non-viscous case.

In point B1, the transverse accelerations with VRD included were about 80% of those without VRD.

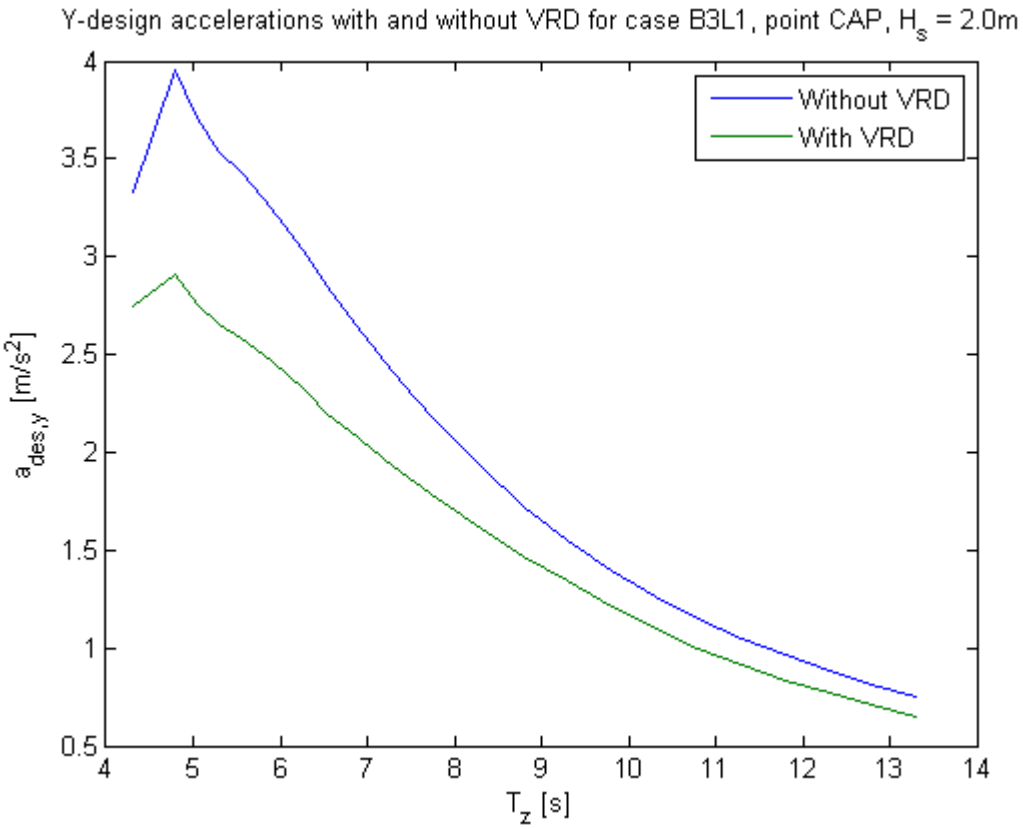

Figure 9-42: Y-design acceleration with and without VRD, point CAP, Hs = 2.0 m, case B3L1

As seen from Figure 9-42 showing the transverse accelerations, the effect of viscous roll damping is larger in the roll resonance area, but it remains significant also outside this area.

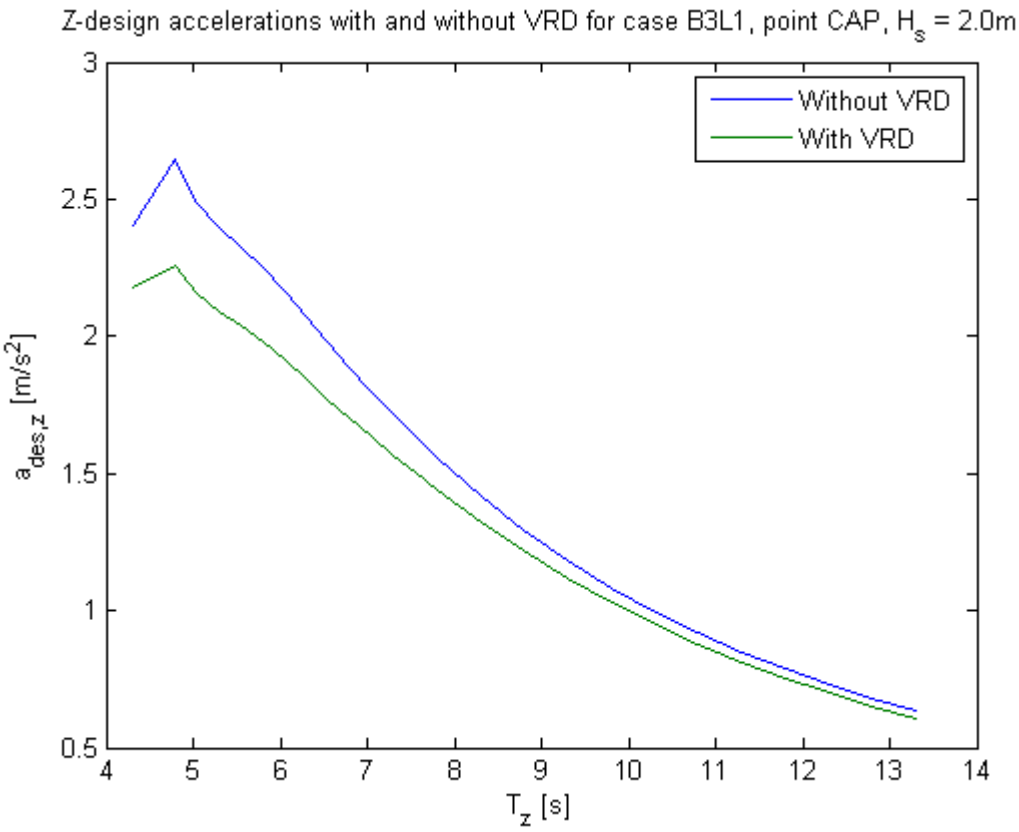

Figure 9-43: Z-design acceleration with and without VRD, point CAP, Hs = 2.0 m, case B3L1

In vertical direction, the same applies for the acceleration as in the transverse direction except the relative reduction in acceleration is smaller.

9.3.4 Effect of metacentric height

As the points of calculation are changed in each case, this effect is difficult to analyse. However, some effects occurred that should be commented.

For the 300 feet barge, the transverse accelerations in CAP are actually smaller with the 3000 tonne load, than with the 1000 tonne load, although the vertical distance from CAP to the centre of rotation is larger with the largest load. As the ballast condition is equal for the two cases, the reduction in acceleration is probably due to the reduction in the metacentric height. This gives a lower stiffness of the system in roll, and thus smoother movements. For the 300 feet barge, there is no increase in the extreme roll angles when the metacentric height is decreased.

For the other two barges, the results are more difficult to interpret. The significant increase in load for the 400 feet barge, from 1000 tonnes to 5000 tonnes makes it difficult to compare. For the 600 feet barge, the accelerations are slightly larger in CAP for the 8000 tonne load than for the 5000 tonne load. The maximum roll angles are larger with the heavier load.

Judging by the cases analysed, it seems that in some cases it can be beneficial to reduce the metacentric height to get smoother roll motions and smaller accelerations. However, it depends largely on the case and presupposes that the stability and extreme roll angles are well within accepted boundaries.

10 Conclusion

Motion response analyses with the aim of finding design accelerations in selected critical points have been performed for six different combinations of barges and platform modules.

One of the cases have further been analysed with viscous roll damping.

The following computer programs have been used in the modelling and calculations:

- Genie – modelling of the barge (hull and ballast tanks)
- HydroD (Wadam) – modelling of environment, hydrodynamic analysis by source technique
- Postresp – Combination of motion characteristics, and transfer of Wadam results to Matlab
- Matlab – Statistical postprocessing and calculation of design accelerations

The main theoretical elements reviewed are

- Potential linear wave theory and the radiation-diffraction problem – foundation of calculations
- Source technique – finding fluid velocity potentials
- Dynamic equilibrium equation – finding motion characteristics
- Short-term statistics – significant and extreme responses for 3 hour sea states

The results of the motion response analysis for each of the six cases have been represented. The results show that the transverse acceleration due to roll acceleration is the limiting factor. The criterion given by Aker Solutions for transverse acceleration is breached in the lowest seastate analysed (H_s = 2.0 m) for most of the cases in beam seas. For the 600 feet barge with a 5000 tonne module (case B6L5), the transverse acceleration criterion is breached at H_s = 2.5 m.

The case including viscous damping showed a clear reduction in transverse and vertical accelerations (roll acceleration). However, the limit for transverse acceleration was still exceeded at H_s = 2.0 m in beam seas.

The comparison between the different barges carrying the same module weight proved that the design accelerations can be significantly reduced by using a larger barge.

11 Further work

11.1 Viscous roll damping

The viscous roll damping gave, as expected, a significant reduction in the roll motion and acceleration for the case tested. The roll acceleration also proved to be the most critical variable limiting the seastate of operation. Using the results for this case, the effect of viscous roll damping can be roughly approximated for the remaining cases by assuming an equivalent reduction ratio compared to the non-viscous results. However, this is an uncertain method as the viscous roll damping term depends heavily on many variables, i.e. cross-section shape and bilge radius. Thus a natural step further would be to include the viscous roll damping for the remaining cases.

11.2 Validating the results

The results obtained in this work without the use of viscous roll damping are clearly conservative. However, the correctness of the viscous roll damping model applied in Wadam is not necessarily satisfying, as the viscous roll damping can be difficult to determine. Few model tests have been performed with a focus on accelerations. In addition, a change in the properties of the barge or the loading condition often makes it difficult to compare with previous model tests. Thus, an alternative could be to perform specific model tests measuring accelerations in simulations of relevant seastates and finding a more correct estimate for the viscous roll damping.

11.3 Optimize metacentric height

All the barges were tested with two different modules. For some barges, when the module weight was increased and the GM reduced, smaller transverse accelerations were observed. This is most likely because of the reduced roll restoring due to reduced GM. Thus, an alternative can be to investigate the effect on accelerations when reducing the ballast, leading to a decreased roll restoring moment. However, larger roll angles were often observed as another consequence. This should only be done as long as the criteria for maximum roll angles and stability are satisfied by a good margin.

11.4 Non-linear effects in high sea states

In linear theory, hydrodynamic forces are only calculated up to the mean waterline. The effect of the hydrodynamic forces between the actual water surface and the actual waterline is unknown, and could produce either higher or lower accelerations.

12 Bibliography

Aker Solutions v/ Gunnar Gjerde “Riser Balcony & Piperacks - Barge transport, Motion response analysis”, 1999

Faltinsen, O.M. “Sea loads on ships and offshore structures”, 1990

Langen, I. & Sigbjørnsson, R. ”Dynamic analysis of structures” (excerpt)

Pettersen, Bjørnar “Marin Teknikk 3 – Hydrodynamikk”, 2007

Havelock, T.H. “The damping of the heaving and pitching motions of a ship”, 1942

Havelock, T.H. “Waves due to floating sphere making periodic heaving oscillations”, 1955

Newman, J.N “Algorithms for the free-surface Green function”, 1985

Abramowitz M. & Stegun, I.A. “Handbook of Mathematical Functions with Formulas, Graphs and Mathematical tables”, 1964

D.E. Newland “An introduction to random vibrations, spectral and wavelet analysis”, 1993, 3rd edition (excerpt)

Wehausen, J. & Laitone, E.V. “Surface waves”. In ”Handbuk der Physik, vol. 9”

Tanaka, N. ”A study on the bilge keels”(Part 4: On the eddy making resistance to the rolling of a ship hull), 1960

Kato, H. “Effect of Bilge Keels on the Rolling of Ships”, 1966

Wadam, SESAM user manual, Det Norske Veritas, 2005

HydroD, SESAM user manual, Det Norske Veritas, 2008

Postresp, SESAM user manual, Det Norske Veritas, 2004

DNV product information (www.DNV.com/software)

Interview with Professor Asle Natskår, Department of Marine Technology, NTNU

13 Appendices

APPENDIX A – BARGE DIMENSIONS AND LIGHTSHIP DATA

Appendix A1 – 300 feet barge

Lightship weight, W_{LS}	1830 t
Lightship centre of gravity, COG_{LS}	(1.26 m, 0 m, 3.47 m)
Length, L	91.44 m
Beam, B	27.44 m
Depth, D	6.10 m
Maximum draught, d_{max}	4.85 m
Bilge radius	0.4 m
Radius of gyration about X-axis, K_{xx}	10.09 m
Radius of gyration about Y-axis, K_{yy}	31.43 m
Radius of gyration about Z-axis, K_{zz}	32.87 m
Coupling inertia X- and Z-axis, K_{xz}= K_{zx}	1.79 m *

*Coupling inertia is found from the Genie model

Appendix A2 – 400 feet barge

Lightship weight, W_{LS}	3960 t
Lightship centre of gravity, COG_{LS}	(-1.80 m, 0 m, 4.22 m)
Length, L	122.00 m
Beam, B	36.60 m
Depth, D	7.60 m
Maximum draught, d_{max}	6.00 m
Bilge radius	0.6 m
Radius of gyration about X-axis, K_{xx}	12.97 m
Radius of gyration about Y-axis, K_{yy}	41.40 m
Radius of gyration about Z-axis, K_{zz}	43.16 m
Coupling inertia X- and Z-axis, K_{xz}= K_{zx}	1.29 m *

*Coupling inertia is found from the Genie model

Appendix A3 – 600 feet barge

Lightship weight, W_{LS}	10870 t
Lightship centre of gravity, COG_{LS}	(5.02 m, 0 m, 6.55 m)
Length, L	183.00 m
Beam, B	47.24 m
Depth, D	11.58 m
Maximum draught, d_{max}	-
Bilge radius	1.0 m

APPENDIX B – MOTION RAO'S FOR CASE B3L1, NON-VISCOUS

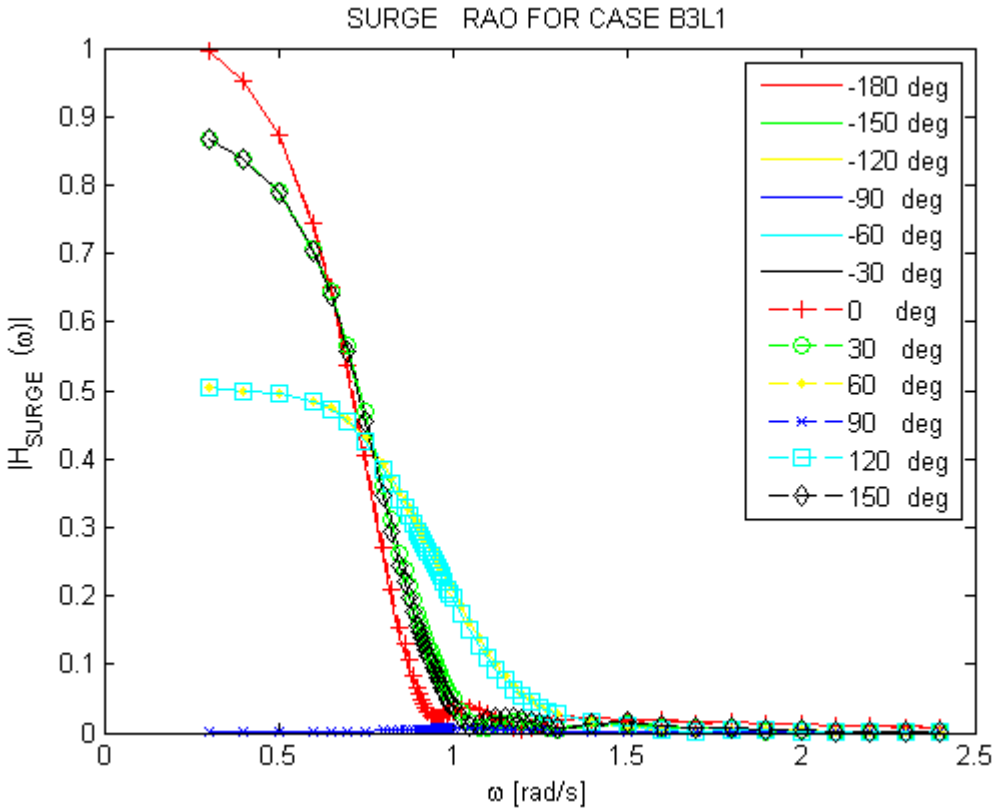

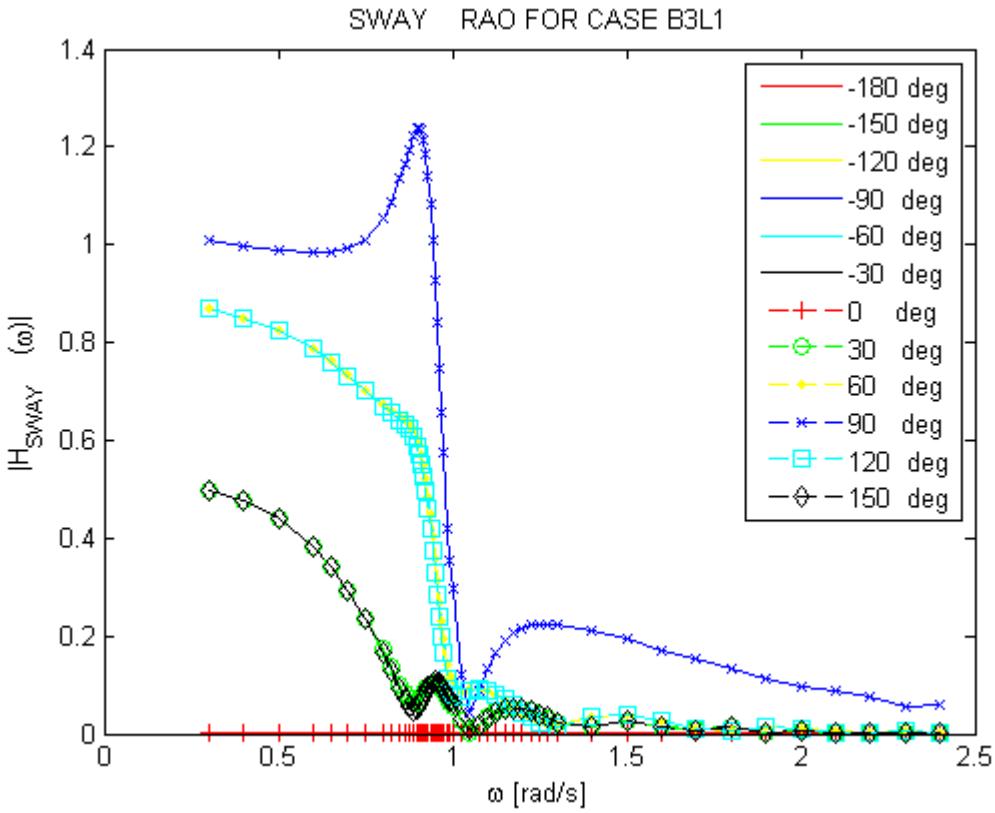

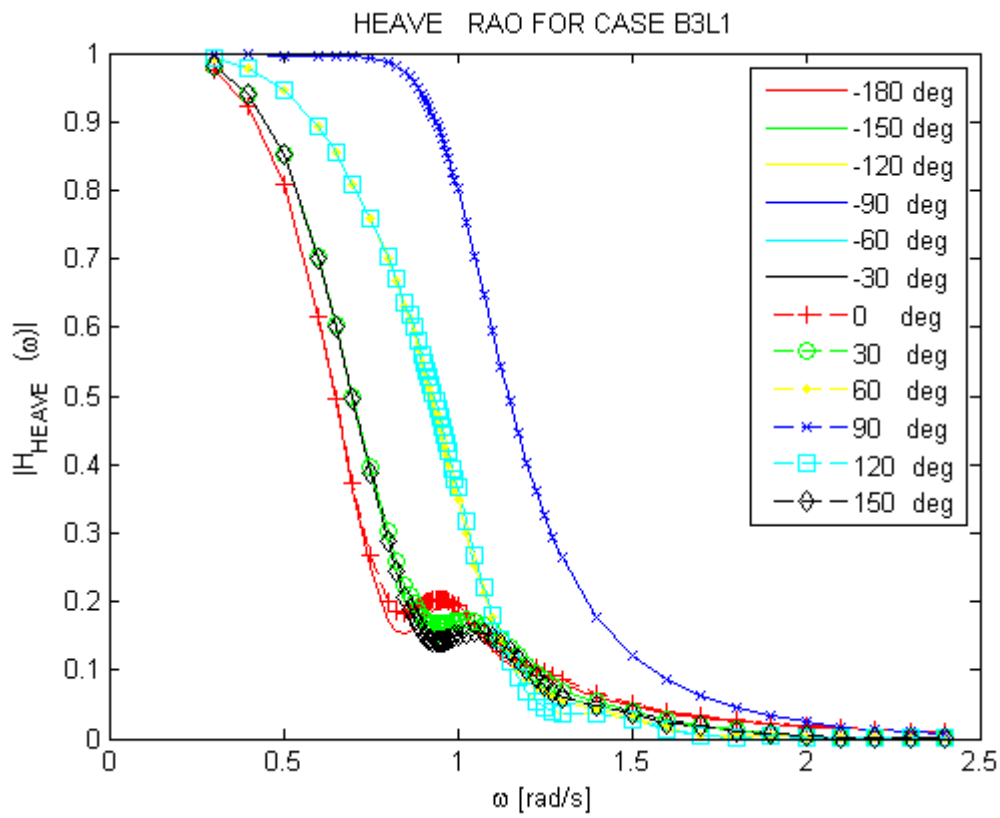
HEAVE RAO FOR CASE B3L1
|H_HEAVE (ω)|
ω [rad/s]
-180 deg
-150 deg
-120 deg
-90 deg
-60 deg
-30 deg
0 deg
30 deg
60 deg
90 deg
120 deg
150 deg

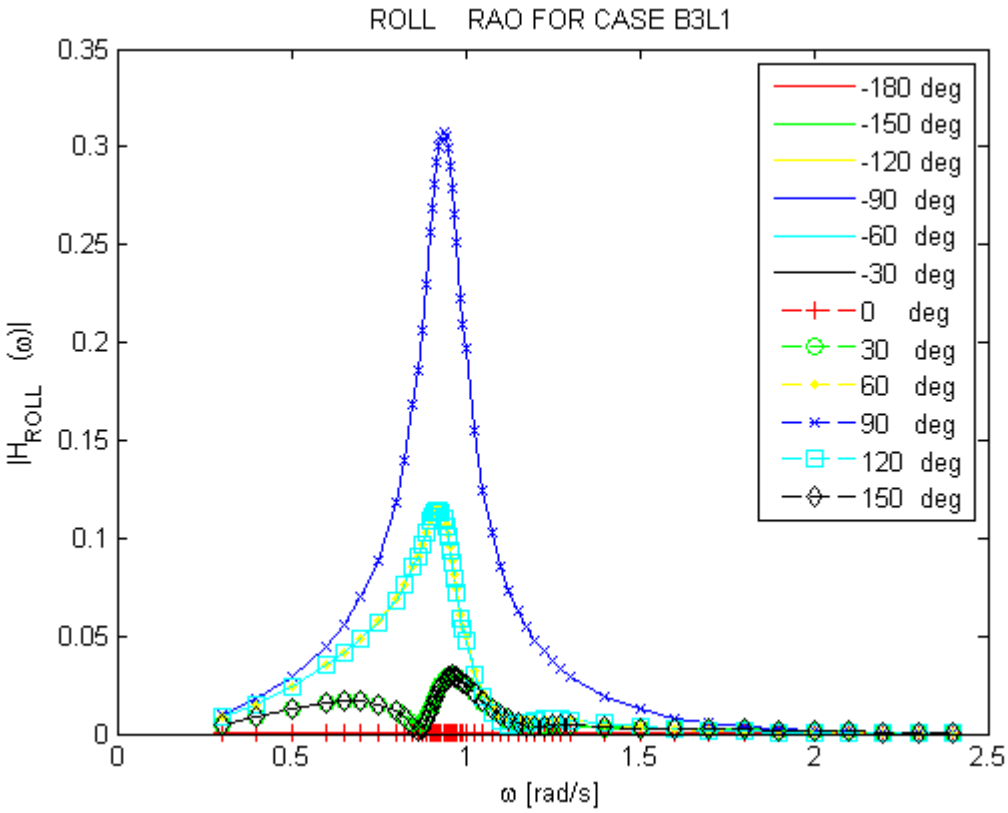
ROLL RAO FOR CASE B3L1
|H_ROLL (ω)|
ω [rad/s]
-180 deg
-150 deg
-120 deg
-90 deg
-60 deg
-30 deg
0 deg
30 deg
60 deg
90 deg
120 deg
150 deg

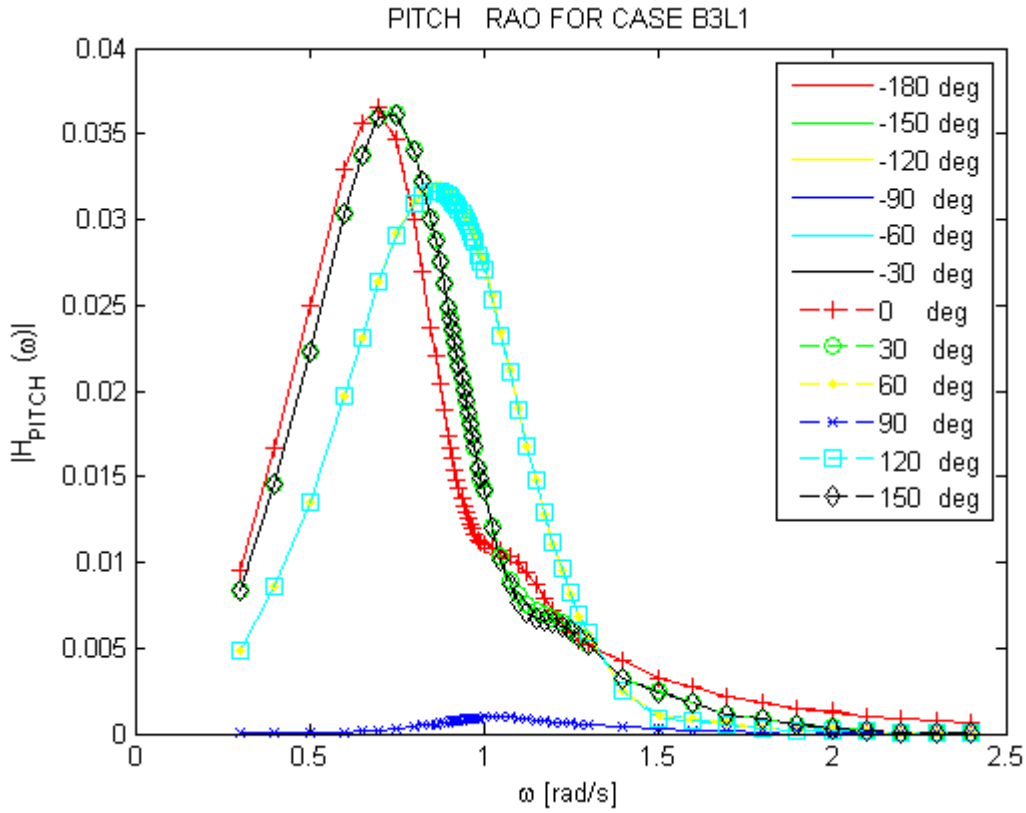
PITCH RAO FOR CASE B3L1
|H_PITCH (ω)|
ω [rad/s]
-180 deg
-150 deg
-120 deg
-90 deg
-60 deg
-30 deg
0 deg
30 deg
60 deg
90 deg
120 deg
150 deg

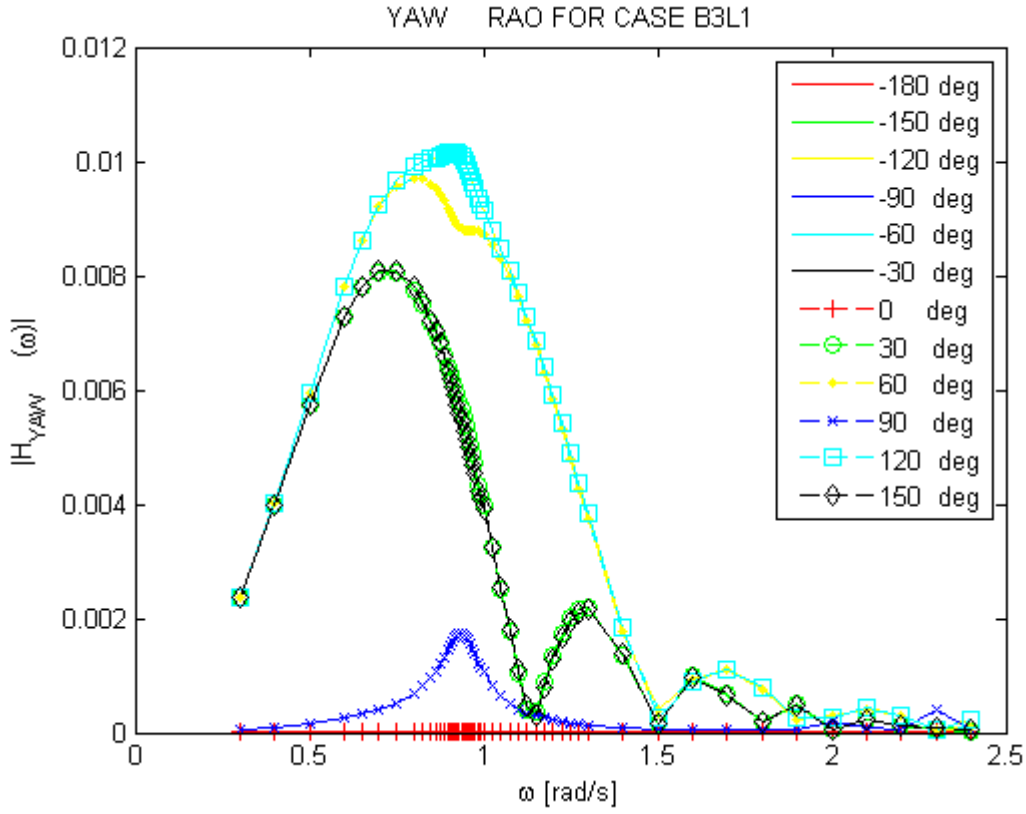
YAW RAO FOR CASE B3L1
|H_YAW (ω)|
ω [rad/s]
-180 deg
-150 deg
-120 deg
-90 deg
-60 deg
-30 deg
0 deg
30 deg
60 deg
90 deg
120 deg
150 deg

APPENDIX C – SELECTED ROLL RAO'S FOR CASE B3L1 INCLUDING VISCOUS ROLL DAMPING

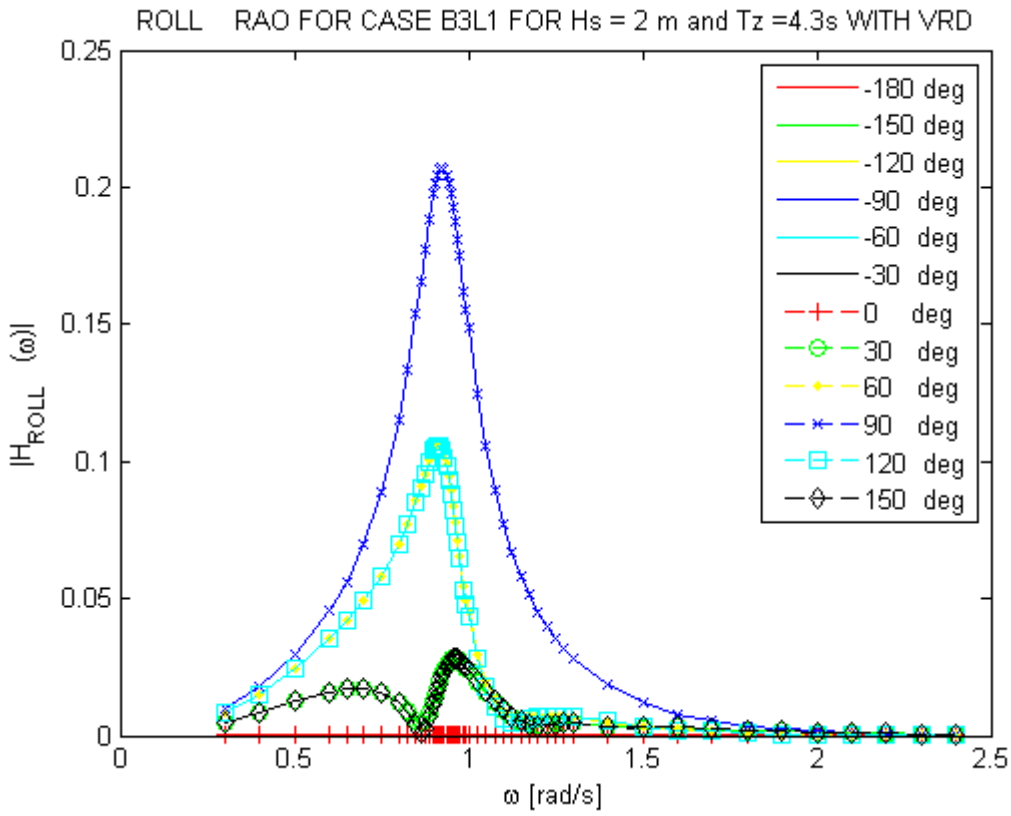

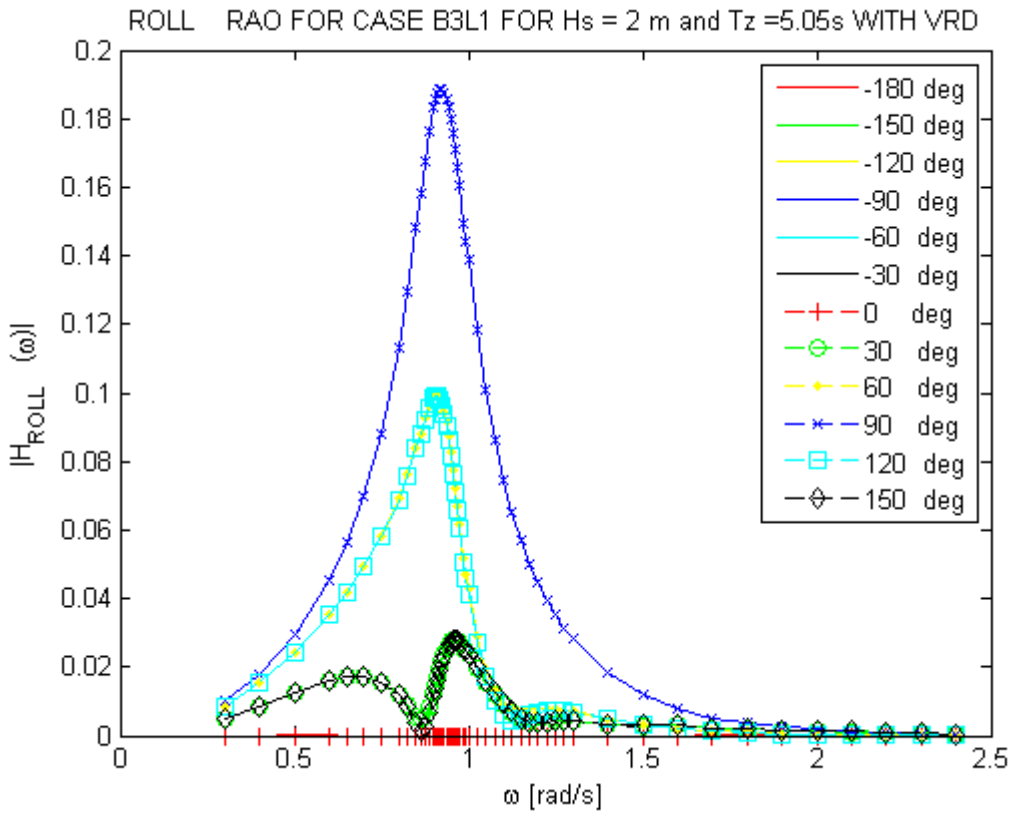
ROLL RAO FOR CASE B3L1 FOR Hs = 2 m and Tz =5.05s WITH VRD
|H_ROLL (ω)|
ω [rad/s]
-180 deg
-150 deg
-120 deg
-90 deg
-60 deg
-30 deg
0 deg
30 deg
60 deg
90 deg
120 deg
150 deg

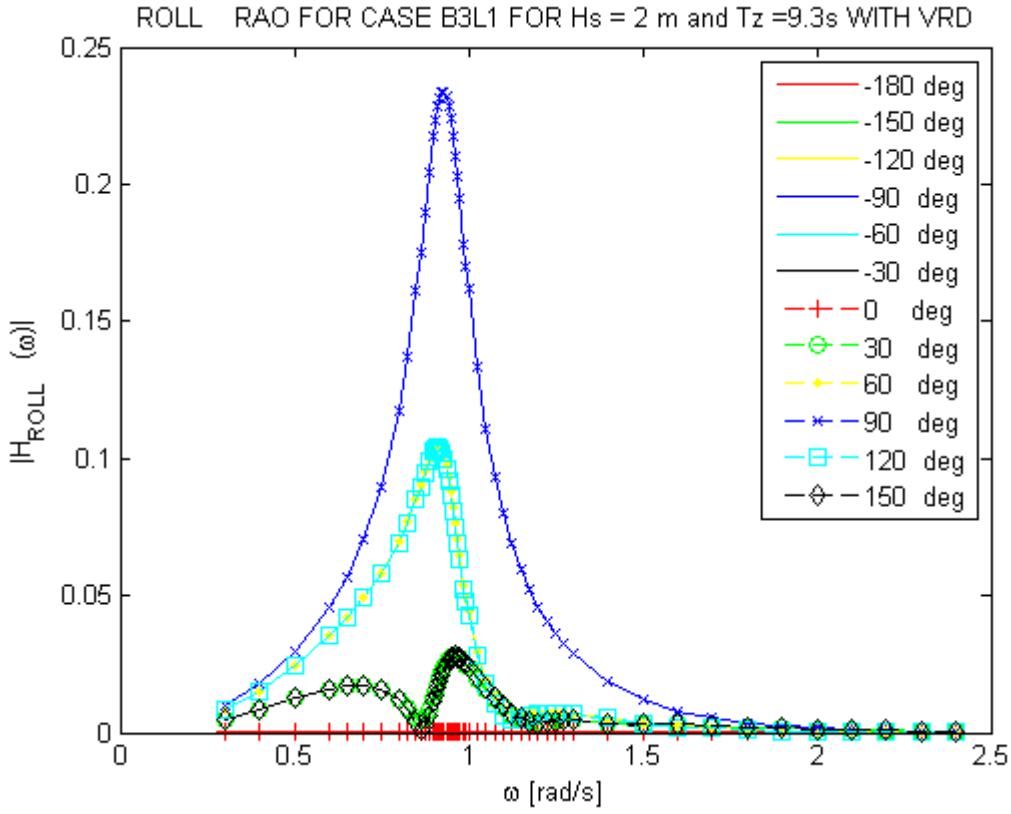
ROLL RAO FOR CASE B3L1 FOR Hs = 2 m and Tz =9.3s WITH VRD
|H_ROLL (ω)|
ω [rad/s]
-180 deg
-150 deg
-120 deg
-90 deg
-60 deg
-30 deg
0 deg
30 deg
60 deg
90 deg
120 deg
150 deg